SANDIA REPORT

SAND2008-1687
Unlimited Release
Printed March 2008

The Application of Taylor Weighting, Digital Phase Shifters, and Digital Attenuators to Phased-Array Antennas

Billy C. Brock

Prepared by
Sandia National Laboratories
Albuquerque, New Mexico 87185 and Livermore, California 94550

Sandia is a multiprogram laboratory operated by Sandia Corporation,
a Lockheed Martin Company, for the United States Department of Energy's
National Nuclear Security Administration under Contract DE-AC04-94AL85000.

Approved for public release; further dissemination unlimited.

Sandia National Laboratories

Issued by Sandia National Laboratories, operated for the United States Department of Energy by Sandia Corporation.

NOTICE: This report was prepared as an account of work sponsored by an agency of the United States Government. Neither the United States Government, nor any agency thereof, nor any of their employees, nor any of their contractors, subcontractors, or their employees, make any warranty, express or implied, or assume any legal liability or responsibility for the accuracy, completeness, or usefulness of any information, apparatus, product, or process disclosed, or represent that its use would not infringe privately owned rights. Reference herein to any specific commercial product, process, or service by trade name, trademark, manufacturer, or otherwise, does not necessarily constitute or imply its endorsement, recommendation, or favoring by the United States Government, any agency thereof, or any of their contractors or subcontractors. The views and opinions expressed herein do not necessarily state or reflect those of the United States Government, any agency thereof, or any of their contractors.

Printed in the United States of America. This report has been reproduced directly from the best available copy.

Available to DOE and DOE contractors from
U.S. Department of Energy
Office of Scientific and Technical Information
P.O. Box 62
Oak Ridge, TN 37831

Telephone: (865) 576-8401
Facsimile: (865) 576-5728
E-Mail: reports@adonis.osti.gov
Online ordering: http://www.osti.gov/bridge

Available to the public from
U.S. Department of Commerce
National Technical Information Service
5285 Port Royal Rd.
Springfield, VA 22161

Telephone: (800) 553-6847
Facsimile: (703) 605-6900
E-Mail: orders@ntis.fedworld.gov
Online order: http://www.ntis.gov/help/ordermethods.asp?loc=7-4-0#online

SAND2008-1687
Unlimited Release
Printed March 2008

The Application of Taylor Weighting, Digital Phase Shifters, and Digital Attenuators to Phased-Array Antennas

Billy C. Brock
SAR Sensor Technologies Department
Sandia National Laboratories
P.O. Box 5800
Albuquerque, NM 87185-0529

Abstract

Application of Taylor weighting (taper) to an antenna aperture can achieve low peak sidelobes, but combining the Taylor weighting with quantized attenuators and phase shifters at each radiating element will impact the performance of a phased-array antenna. An examination of array performance is undertaken from the simple point of view of the characteristics of the array factor. Design rules and guidelines for determining the Taylor-weighting parameters, the number of bits required for the digital phase shifter, and the dynamic range and number of bits required for the digital attenuator are developed. For a radar application, when each element is fed directly from a transmit/receive module, the total power radiated by the array will be reduced as a result of the taper. Consequently, the issue of whether to apply the taper on both transmit and receive configurations, or only on the receive configuration is examined with respect to two-way sidelobe performance.

This Page Intentionally Blank

Contents

List of Figures **7**

1. Introduction and Summary **11**
1.1 Discussion 11
1.2 Graphical Guidelines for Choosing Phase Shifters 13
1.3 Summary of Design Rules for the Taylor Array 14
1.4 Summary of Design Rules for Digital Attenuator 15
1.5 Summary of Guidelines for Transmit Array Illumination 16

2. Switched delay line shifter **17**
2.1 Modulo 2π switched-delay-line phase shifter 18
2.2 Distribution of random phase errors 19

3. Effect of quantized steering phase on array factor **27**
3.1 Periodic phase error 27
3.2 Random phase error 28
3.3 Reduction in directivity due to phase quantization 32
3.4 Contribution to sidelobes due to phase quantization 32
3.5 Effect on steering angle from phase quantization 35

4. Digital attenuator **37**

5. Two-dimensional planar array factor **39**
5.1 Far-field radiation pattern and the array factor 43
5.1.1 Directivity of the array factor 43
5.2 Effect of element weight errors on array factor 45

6. Uniformly illuminated array **47**
6.1 Odd array 47
6.2 Even array 49
6.3 Comparison of the even and odd uniform arrays 50

7. The Taylor array **53**
7.1 Continuous line source 53
7.1.1 Connection between Taylor and Tchebyscheff illumination 56
7.2 Rectangular arrays with Taylor illumination 63
7.2.1 Odd array 63
7.2.2 Even array 65
7.2.3 Consequences of discrete illumination function 66
7.2.4 Summary of Design Rules for Taylor Array 71
7.3 Effect of amplitude quantization on the Taylor array 72
7.3.1 Summary of Design Rules for Digital Attenuator 75
7.4 Design example 77

8. Issue of tapered illumination on transmit **81**
8.1 Taylor illumination for transmit array 81
8.1.1 Rectangular array 81
8.1.2 Truncated array 85
8.2 Uniform illumination of transmit array 93
8.2.1 Rectangular aperture array 93
8.2.1.1 Split-uniform illumination of transmit array (linear phase adjustment) 96
8.2.1.2 Sinusoidal phase adjustment 99
8.2.1.3 Quadratic phase adjustment 103
8.2.2 Circular aperture 107

9. References **117**

Appendix I – Jacobi's Theta Functions **119**

Appendix II – Directivity of the array factor **121**

Appendix III – Definition of beamwidth for off-normal scan **127**

This Page Intentionally Blank

List of Figures

Figure 1 A sixteen-element row with a wide-bandwidth phase-shift feed configuration.....17
Figure 2 Digitized phase as a function of required phase for 3-bit, 4-bit, and 5-bit time-delay phase shifters.....19
Figure 3 Phase-shifter phase error as a function of exact steering phase, for 3-bit, 4-bit, and 5-bit phase shifters. 19
Figure 4 Normalized histogram for one million draws from a zero-mean Gaussian distribution with standard deviation of 22.5˚. 21
Figure 5 Normalized histogram for the 3-bit phase-shifter error when the input is the set of one million random draws associated with the histogram in Figure 4. 21
Figure 6 Normalized histogram for one million draws from a zero-mean Gaussian distribution with standard deviation of 45˚. 22
Figure 7 Normalized histogram for the 3-bit phase-shifter error when the input is the set of one million random draws associated with the histogram in Figure 6. 22
Figure 8 Normalized histogram for one million draws, modulo 180, from a zero-mean Gaussian distribution with standard deviation of 360˚. 23
Figure 9 Normalized histogram for the 3-bit phase-shifter error when the input is the set of one million random draws associated with the histogram in Figure 8. 23
Figure 10 Probability density for the output of a 3-bit phase shifter when the input is a zero-mean Gaussian with two different values for standard deviation, $\sigma_{\delta\varphi}$ 25
Figure 11 Ratio of center value of probability density to the edge value ($\delta\varphi = \pi/2^b$) for four different values for the number of bits, b.....25
Figure 12 Periodic phase error across array containing 201 elements with half-wavelength spacing, steered $1°$ from broadside with 3-bit phase shifters.....29
Figure 13 Normalized array factor for the 201-element array, steered to $\theta = 1°$ with 3-bit phase shifters.....29
Figure 14 Example of phase error across array containing 201 elements with half-wavelength spacing, steered $1°$ from broadside with 3-bit phase shifters, as Figure 12, but with zero-mean Gaussian random insertion phase having a standard deviation of 0.5 radian (28.6˚). 30
Figure 15 Array factor for the 201-element array, steered to $\theta = 1°$ with 3-bit phase shifters (same as Figure 13), but with a random insertion phase for each element, resulting in the phase error plotted in Figure 14. 30
Figure 16 Average quantization-sidelobe level as a function of the number of elements in an array, for several numbers of bits in phase shifter. 33
Figure 17 The rms pointing error (in percent of beamwidth) as a function of number of elements in a linear array, for several sizes of phase shifter. 36
Figure 18 Diagram of an N-bit digital attenuator, using switched attenuator sections with matched phase delays.....37
Figure 19 Attenuation errors for (a) 3-bit 20 dB attenuator and (b) 4-bit 6 dB attenuator. 38
Figure 20 Two-dimensional planar-array geometry when the number of elements in each row is odd, and the number of rows is odd.....40
Figure 21 Two-dimensional planar-array geometry when the number of elements in each row is even, and the number of rows is even.....40
Figure 22 Normalized array factor in the $\phi = 0$ plane for odd array (solid curve) and even array (dashed curve) for $N = 10$ (21 elements and 20 elements respectively), with constant element spacing.....51

Figure 23 Normalized array factor in the $\phi = 0$ plane for odd array (solid curve) and even array (dashed curve) for $N = 10$ (21 elements and 20 elements respectively), with constant array size. 51
Figure 24 Array factor for a Taylor-weighted continuous linear distribution with $\bar{n} = 10$, and $SLL = -60$ dB 54
Figure 25 Comparison of array factor for a uniform linear source (dashed) with the array factor for a Taylor-weighted continuous linear distribution with $\bar{n} = 5$, and $SLL = -40$ dB (solid). 55
Figure 26 Taylor array factor for $\bar{n} = 10$ and $SLL_{dB} = -30$, showing the far-sidelobe peak envelope given by (7.12). 56
Figure 27 Comparison of Tchebyscheff array factor (blue) and Taylor ($\bar{n} = 5$) array factor (red) for -40 dB sidelobes. 57
Figure 28 Comparison of Tchebyscheff array factor (blue) and Taylor ($\bar{n} = 35$) array factor (red) for -40 dB sidelobes. 57
Figure 29 Values of u_{3dB} as a function of sidelobe level. 58
Figure 30 θ_{3dB} as a function of half-length, a, for $\bar{n} = 10$ and $SLL_{dB} = -40$. 59
Figure 31 θ_{3dB} as a function of sidelobe level with half-length $a = 10\lambda$, and $\bar{n} = 10$. 60
Figure 32 θ_{3dB} as a function of order, $\bar{n}$, for $SLL_{dB} = -40$ and $a = 10$ wavelengths 60
Figure 33 Taylor illumination function, $W(\xi)$, for $SLL_{dB} = -30$, and three different values of $\bar{n}$ 61
Figure 34 Illumination function, $W(\xi)$, viewed as a function of continuous $\bar{n}$ at $\xi = 1$. 62
Figure 35 Recommended range for $\bar{n}$ as a function of sidelobe level. 63
Figure 36 Two equal size Taylor array factors with $\bar{n} = 3$ and $SLL_{dB} = -30$. The blue curve is a continuous line source (no aliasing), and the red curve is a discrete-element array, with mild aliasing. 67
Figure 37 Two equal size, discrete, Taylor array factors with $\bar{n} = 3$ and $SLL_{dB} = -30$, illustrating the increased sidelobe level due to aliasing. 67
Figure 38 Minimum value of N for given design sidelobe level and Taylor order, for (a) $\varepsilon_{alias} = 0.5$ dB, and (b) $\varepsilon_{alias} = 3$ dB 69
Figure 39 Attenuator range for one-dimensional taper as a function of design sidelobe level. 73
Figure 40 Normalized directivity for design example with optimum number of elements to avoid aliasing and practical number of elements. 78
Figure 41 Comparison of normalized directivity for design example with 9-bit attenuator and 5-bit attenuator. 79
Figure 42 Comparison of sidelobe region for directivity pattern of design example with 9-bit attenuator and continuous (ideal) attenuator. 79
Figure 43 Transmitter efficiency for the linear Taylor-weighted array. 82
Figure 44 Transmitter efficiency for the two-dimensional Taylor-weighted array. 83
Figure 45 Two-way antenna pattern with Taylor illumination with -20 dB one-way design sidelobes and $\bar{n} = 2$. 84
Figure 46 Normalized two-way array factor for a two-dimensional even array with a Taylor illumination, $SLL = -20$ dB, $\bar{n} = 2$, for both transmit and receive. 84
Figure 47 Two-way antenna patterns with Taylor illumination with several sets of design parameters. 85
Figure 48 Weights for a two-dimensional odd array with a Taylor illumination, $SLL = -45$ dB, $\bar{n} = 5$ without truncation. 87
Figure 49 Weights for a two-dimensional odd array with a Taylor illumination, $SLL = -45$ dB, $\bar{n} = 5$, and truncated to -12 dB 88

Figure 50 Normalized array factor for a two-dimensional odd array with a Taylor illumination, $SLL = -45$ dB, $\bar{n} = 5$, and truncated to -12 dB, with a nearly circular aperture. 89
Figure 51 Weights for a two-dimensional odd array with a Taylor illumination, $SLL = -45$ dB, $\bar{n} = 5$, truncated to -15 dB. 90
Figure 52 Normalized array factor for a two-dimensional odd array with a Taylor illumination, $SLL = -45$ dB, $\bar{n} = 5$, and truncated to -15 dB 91
Figure 53 Directivity of uniformly illuminated transmit array (blue) and Taylor receive array (red), normalized to peak of receiver array. 94
Figure 54 Normalized two-way directivity for uniform transmit array with Taylor receive array. 94
Figure 55 Normalized two-way directivity for uniform transmit array with $N_{tx} = 7$ combined with Taylor receive array with $N_{rx} = 13$. 96
Figure 56 Two linear, uniformly illuminated arrays. 96
Figure 57 Comparison of two-way patterns using the split-uniform transmit array and the reduced-size transmit array. 98
Figure 58 Relative phase for two-way pattern using the split-uniform transmit array.....98
Figure 59 Comparison of one-way patterns of the split-uniform transmit array and the reduced-size transmit array. 99
Figure 60 The Anger function, both $\mathbf{J}_\nu(\zeta)$ and $\mathbf{J}_\nu(-\zeta)$ as functions of ν, for several values of ζ. 100
Figure 61 Normalized two-way antenna pattern when the transmit array has sinusoidal phase adjustment with $\zeta = 0.258$, and the receive array uses a Taylor distribtution with $\bar{n} = 2$ and $SLL = -30$ dB. Note that $u = \frac{2a}{\lambda}\sin\theta$. 102
Figure 62 A symmetric linear combination of two Anger functions, $\frac{1}{2}\mathbf{J}_\nu(-\zeta) + \frac{1}{2}\mathbf{J}_\nu(\zeta)$. 103
Figure 63 One-way array factor with uniform illumination and quadratic phase adjustment for several values of parameter ξ. 105
Figure 64 Two-way antenna pattern with uniform illumination and quadratic phase adjustment for several values of ξ for the transmit array, and a –40 dB sidelobe Taylor illumination for the receive array. 105
Figure 65 Two-way array factor with quadratic-phase-adjustment parameter $\xi = \sqrt{6} \simeq 2.45$. 106
Figure 66 Relative phase of the two-way array factor with quadratic-phase-adjustment parameter $\xi = \sqrt{6} \simeq 2.45$. 106
Figure 67 Comparison of normalized array factor for uniform illumination in full rectangular aperture and circular apertures (along a primary axis of the array). 108
Figure 68 Normalized array factor for a two-dimensional odd array with a uniform illumination in a truncated, nearly circular aperture corresponding to the example in Figure 49.....108
Figure 69 Normalized two-way array factor for a two-dimensional, odd array with a uniform illumination for transmit, and Taylor illumination for receive, $SLL = -45$ dB, $\bar{n} = 5$, with the aperture truncated at -12 dB (nearly circular). 109
Figure 70 Weights and aperture shape for the truncated odd array with $N_{rwo} = N_{col} = 13$, $\bar{n} = 2$, and $SLL = -20$ dB 110
Figure 71 Normalized two-way array factor for a two-dimensional, truncated, odd array with a uniform illumination for transmit, and Taylor illumination for receive, $SLL = -20$ dB, $\bar{n} = 2$ 110
Figure 72 Weights for a two-dimensional odd array with a Taylor illumination, $SLL = -34$ dB, $\bar{n} = 4$, truncated to a circular aperture. 112

Figure 73 Normalized two-way array factor for a two-dimensional, circular, odd array with a uniform illumination for transmit, and Taylor illumination for receive, $SLL = -34\ \text{dB}$, $\bar{n} = 4$ 113
Figure 74 Weights for a two-dimensional odd array with a Taylor illumination, $SLL = -47\ \text{dB}$, $\bar{n} = 2$, truncated to a circular aperture. 114
Figure 75 Normalized two-way array factor for a two-dimensional, circular, odd array with a uniform illumination for transmit, and Taylor illumination for receive, $SLL = -47\ \text{dB}$, $\bar{n} = 2$ 115
Figure 76 Diagram showing the planes in which the beamwidth can be measured when the beam is scanned away from the normal vector. 128

1. Introduction and Summary

1.1 Discussion

The design of a phased-array antenna is a complex task. Not only must an impedance-matched element be designed, but several additional issues must be addressed, such as illumination taper, resolution of the attenuator used to achieve the taper, and the resolution of the beam-steering phase shifters. This report develops design rules and guidelines for determining:

- the number of bits required for the digital phase shifter,
- the dynamic range and number of bits required for the digital attenuator,

and

- the parameters of an appropriate Taylor illumination.

In addition, the issue of whether to taper the illumination for transmit applications is examined.

In this report, the term *odd array* refers to an array with an odd number of elements in each of an odd number of rows, while the term *even array* refers to an even number of elements in each of an even number of rows. In reality, there is very little difference between these arrays, but the formulations have subtle differences, and both are addressed for completeness. Mixed even and odd arrays are not explicitly addressed. Even arrays are usually preferred for the simplification in RF power division and distribution, while odd arrays favor more elegant formulation for the array factor.

It will be shown that the number of bits required for the digital phase shifter in a large, low-sidelobe array is usually determined by the sidelobe-level specification, rather than by the required beam-pointing accuracy or steering increments. In a large array, only a few bits are required to achieve pointing resolution that is much smaller than the beamwidth, while more bits are required to achieve low sidelobe levels. It is also seen that random phase errors are usually much more desirable than the periodic steering-phase error that would be present if all the paths in the array were perfectly phase-matched. Periodic phase errors produce quantization lobes, while random phase errors increase the error-sidelobe level. In this case, the error-sidelobe level is determined by the resolution of the phase shifter. However, to avoid quantization lobes, it is necessary that the insertion-phase contributions in the paths from the transmitter or receiver to each of the radiating antenna elements be uncorrelated between elements, and be no smaller than some minimum size. This ensures that the phase errors will be random, not periodic. This minimum-error size is derived, and it is shown that the minimum error causes the final phase error at each array element to be uniformly distributed between ± half of the value of the least significant bit of the phase shifter. Of course, the presence of random phase errors in the paths within the array implies a requirement to calibrate the array, in order to determine a correcting phase offset for each element. Thus, it is necessary that a high-performance phased-array antenna be carefully calibrated after assembly. This calibration should be a standard part of the characterization of the assembled array.

While much of the analysis of the phase-shifter requirements can be accomplished without reference to the array's illumination function, such is not the case for the digital attenuator. Aside from correcting gain errors in the transmit/receive (T/R) modules, the purpose of the digital attenuator is to provide the illumination taper necessary to meet sidelobe requirements. As with the phase shifter, it is desirable that amplitude errors be random, rather than deterministic. In the presence of suitable random gain errors in the T/R modules, the error in the quantized amplitude taper will be random, uniform, and determined by the resolution of the attenuator. The required dynamic range of the digital attenuator will be determined by the amplitude taper, which is determined by the required sidelobe level. The characteristics of the amplitude taper set the level of the deterministic sidelobes, and the resolution of the attenuator determines

the random sidelobe level. Thus, the specification of the required sidelobe level will determine both the required amplitude taper and the characteristics of the digital attenuator.

In order to provide specific design rules, an amplitude taper must be specified. The Taylor illumination [1] is chosen because it can be analyzed, while leaving the sidelobe level as a design parameter. In addition, it provides a near-optimum beamwidth for a given peak-sidelobe level. This statement should not be construed to mean that the Taylor illumination is the *optimum taper* for a phased-array antenna. Tapers that produce broader main beams will produce lower integrated sidelobes than the Taylor illumination, which may be important in some applications. Some applications may require specially shaped beams. Determining the optimum illumination requires detailed knowledge of the application, and therefore cannot be addressed in a general way. Nevertheless, it should be understood that the choice of the digital attenuator specification is dependent in detail on the illumination function. Thus, the design rules and guidelines described below apply *only* to the Taylor-illuminated array. Similar rules could be developed for other illumination functions, and a separate study could be justified to examine which illumination function is optimum for each of various applications.

The issue of whether to taper the illumination of the transmit array impacts both the peak-sidelobe level of the two-way antenna pattern and the transmitter efficiency. Sometimes, the power amplifier in a T/R module will be operated in a nonlinear region in order to achieve high efficiency. In such a situation, the attenuator would necessarily be placed between the T/R module and the antenna element, lowering the transmitter efficiency and increasing the power dissipated by the array. On the other hand, if the power amplifier is operated in a linear gain region, then the attenuator should be placed between the source and the T/R module's power amplifier to maximize transmit efficiency. However, in the receive array, a linear, low-noise amplifier can, and should, always be placed between the element and the attenuator, to minimize the effect of the taper on the noise figure of the receiver. For a rectangular array, specified two-way sidelobe levels can be achieved with an appropriate taper for the receive array and uniform illumination for the transmit array, if only a portion of the array is used to transmit. This approach can significantly reduce the power dissipated by the array, but as with transmit-array tapering, it reduces the peak power available from the transmitter. Using the full rectangular array with uniform illumination for the transmitter will provide the maximum peak transmit power, at the price of a higher first sidelobe in the two-way antenna pattern. Truncating the rectangular array to a circular array, or at least eliminating elements in the corner regions, can improve array transmit efficiency and reduce array cost, while allowing the transmit array to be uniformly illuminated. These issues are examined in some detail.

It is concluded from this study that random phase and amplitude errors in the T/R modules are actually desirable to ensure that the errors due to quantization are randomized and are not periodic across the array. This is fortunate, since it would be difficult to manufacture the T/R modules otherwise. However, this is not to say that the T/R module performance and the array construction can be haphazard. Minimum required random-error levels are determined to ensure that the errors at the array face follow a uniform distribution. These required minimum error levels are not large. The point is, though, that if tolerances are too tight, the errors across the array will be quantized according to the size of the least significant bit, but will not be uniform and random. Non-random quantized errors will adversely affect the array performance. This is a situation where reasonable module-to-module variation is not only tolerable; it is desirable.

This study is not exhaustive, and additional similar studies, which do not address the specifics of the antenna element, would be useful. These include studies of optimum illumination functions for different applications, density tapering of the elements to achieve low sidelobes, and the extension of these ideas to conformal, non-planar arrays. In addition, further examination of circular and elliptical apertures would be useful.

In order to make it unnecessary for the reader to delve into the details, the design rules and guidelines are summarized and repeated in this section. However, this is not a complete summary of the useful information buried in the detailed discussion. In particular, Appendix II derives closed-form sums for the directivity of the array factor, and Appendix III defines a simple method for defining beamwidths when the beam is steered away from broadside.

1.2 Graphical Guidelines for Choosing Phase Shifters

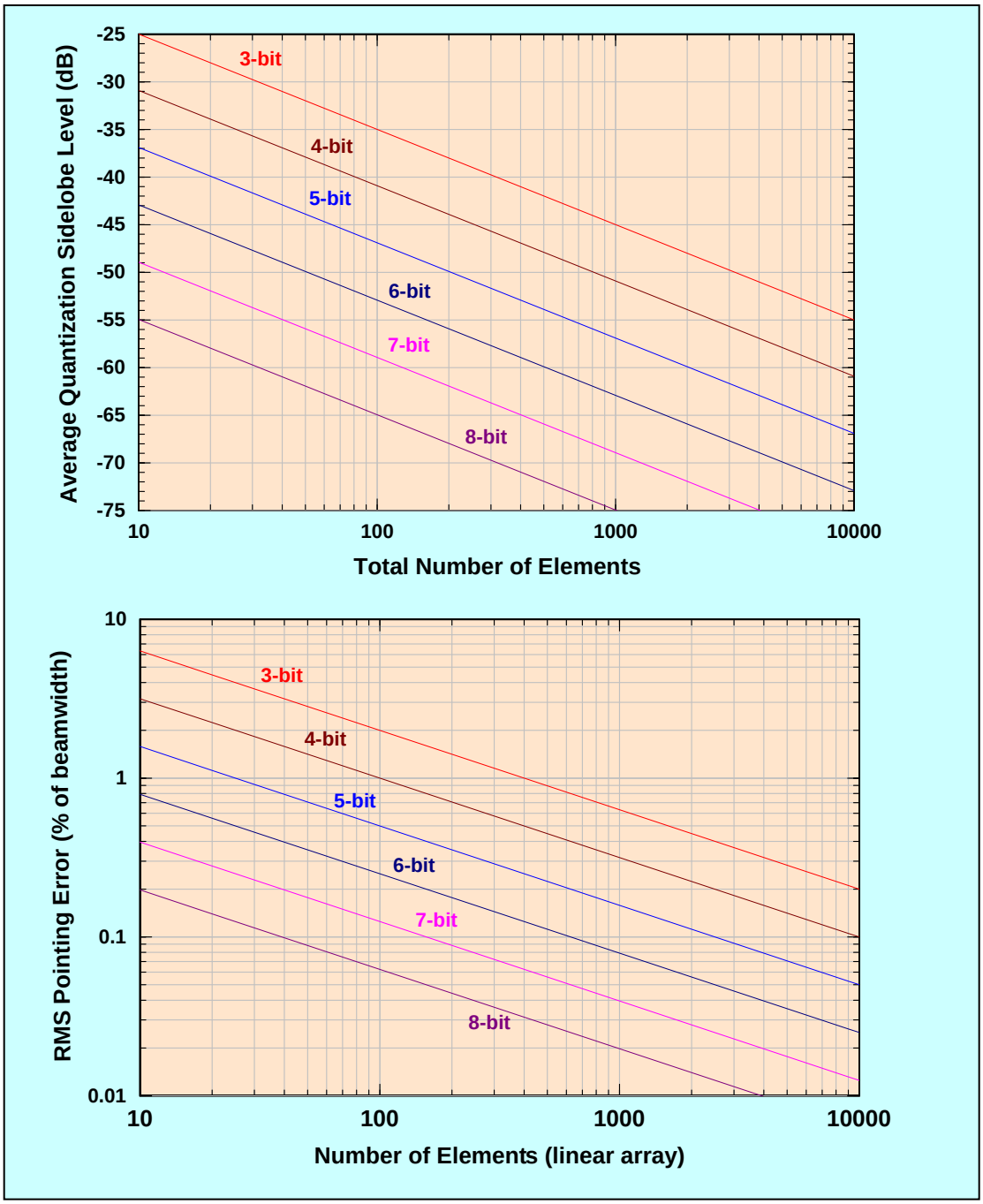

1.3 Summary of Design Rules for the Taylor Array

Specification: θ_{3dB} half beam width

SLL_{dB} sidelobe level $\left(SLL_{dB} < 0\right)$

ε_{dB} sidelobe degradation due to aliasing ($\varepsilon_{dB} > 0$)

Compute:

Taylor parameter:
$$A = \frac{1}{\pi}\cosh^{-1}\left(10^{\frac{-SLL_{dB}}{20}}\right) = \frac{1}{\pi}\ln\left(10^{\frac{-SLL_{dB}}{20}} + \sqrt{10^{\frac{-SLL_{dB}}{10}} - 1}\right)$$

Taylor order:
$$\mathrm{rnd}\left(\left(\frac{SLL_{dB}}{22.8}\right)^2 - \frac{SLL_{dB}}{36.3} + 0.759\right) \le \bar{n} \le \mathrm{floor}\left(\frac{1}{2} + 2A^2\right)$$

Taylor parameter:
$$\sigma_p^2 = \frac{\bar{n}^2}{A^2 + \left(\bar{n} - \frac{1}{2}\right)^2}$$

Taylor coefficients:
$$F_m = \frac{(-1)^{m+1}}{2\prod_{\substack{n=1\\ n\neq m}}^{\bar{n}-1}\left(1 - \frac{m^2}{n^2}\right)}\prod_{n=1}^{\bar{n}-1}\left[1 - \frac{m^2}{\sigma_p^2\left[A^2 + \left(n - \frac{1}{2}\right)^2\right]}\right],\ 1 \le m \le \bar{n} - 1$$

Minimum N to avoid aliasing in sidelobe region:
$$N \ge \bar{n} + \frac{1}{\pi(10^{\varepsilon_{dB}/20} - 1)}\cosh(\pi \mathrm{A})\prod_{n=1}^{\bar{n}-1}\left[\frac{n^2}{\sigma_p^2\left(A^2 + \left(n - \frac{1}{2}\right)^2\right)}\right]$$

Iterate:
$$u_{3dB,0} = 0.55$$
$$u_{3\,dB,i+1} \approx u_{3\,dB,i} - \left(F\left(u_{3\,dB,i}\right) - \frac{1}{\sqrt{2}}\right)\Big/\left.\frac{\partial F}{\partial u}\right|_{u = u_{3\,dB,i}}$$
$$F(u) = \sum_{m=-(\bar{n}-1)}^{\bar{n}-1} F_m \frac{\sin\pi(u+m)}{\pi(u+m)}$$
$$\frac{\partial F(u)}{\partial u} = \sum_{m=-(\bar{n}-1)}^{\bar{n}-1} F_m \frac{\pi(u+m)\cos\pi(u+m) - \sin\pi(u+m)}{\pi(u+m)^2}$$

Compute half width of array:
$$a = \frac{\lambda u_{3\,dB}}{2\sin\theta_{3\,dB}}$$

Odd array $\left(2N + 1 \text{ elements}\right)$: $\quad element\ spacing = \dfrac{a}{N}$

Element weights
$$A_n = 1 + 2\sum_{p=1}^{\bar{n}_{row}-1} F_p(\alpha,\sigma)\cos\left(\frac{\pi}{N}np\right)$$

Even array $2N$ elements: $\quad element\ spacing = \dfrac{2a}{2N-1}$

Element weights
$$A_n = 1 + 2\sum_{p=1}^{\bar{n}_{row}-1} F_p(\alpha,\sigma)\cos\left(\frac{\pi}{N - \frac{1}{2}}\left(|n| - \frac{1}{2}\right)p\right)$$

1.4 Summary of Design Rules for Digital Attenuator

Specification: Quantization errors produce no more than $\pm\delta$ dB effect on the side lobe level

Side lobe level: $SLL_{dB,elevation}$, $SLL_{dB,azimuth}$ in decibels $\left(SLL_{dB} < 0\right)$

Unit-to-unit gain variation of T/R modules: $\pm\Delta g_{T/R}$ in decibels

Compute:

Required taper ranges (in decibels):

$$a_{row} = -\left(8 + 0.63 \cdot SLL_{dB,\,azimuth} - 0.0014 \cdot SLL_{dB,\,azimuth}^2\right)$$

$$a_{col} = -\left(8 + 0.63 \cdot SLL_{dB,\,elevation} - 0.0014 \cdot SLL_{dB,\,elevation}^2\right)$$

Required attenuator range: $a_{range} = \left|\Delta g_{T/R}\right| + a_{row} + a_{col}$ in decibels

Note: $a_{range} > 0$

Tolerable error- sidelobe level: $\gamma = 20 \cdot \log\left(\dfrac{10^{\delta/10} - 1}{10^{\delta/10} + 1}\right)$ in decibels

Range of tolerable error: $$\alpha \le \frac{20\sqrt{3}}{\ln(10)} 10^{\frac{\min\left(SLL_{dB,elevation}, SLL_{dB,azimuth}\right) + \gamma}{20}} \frac{\left|\sum_{n,m} A_{n,m}\right|}{\sqrt{\sum_{n,m} \left|A_{n,m}\right|^2}}$$

Number of bits: $$b = \text{ceiling}\left[\frac{1}{\ln 2} \ln\left(1 + \frac{a_{range}}{2\alpha}\right)\right]$$

1.5 Summary of Guidelines for Transmit Array Illumination

Reduced-size uniform transmit array:

- Most efficient approach
- Reduced peak transmit power
- Pick transmit array size according to:

$$N_{tx} = \text{ceiling}\left(\frac{N_{rx} - \frac{1}{2}}{\bar{n}_{rx}\sqrt{\dfrac{\alpha^2 + \frac{1}{4}}{\alpha^2 + \left(\bar{n}_{rx} - \frac{1}{2}\right)^2}}} \right) \text{ for even array}$$

$$\alpha \cong \frac{1}{\pi}\cosh^{-1}\left(10^{\frac{-SLL_{rx,dB}}{20}}\right) = \frac{1}{\pi}\ln\left(10^{\frac{-SLL_{rx,dB}}{20}} + \sqrt{10^{\frac{-SLL_{rx,dB}}{10}} - 1}\right)$$

Full-size uniform array:

- Highest peak transmitter power
- High efficiency
- Rectangular array:
  - Large first sidelobe in two-way pattern
- Truncate array to circular aperture:
  - Reduces first sidelobe in two-way pattern
  - Increases sidelobe level for receive (Taylor) array

Taylor illumination for transmit array:

- Lowest achievable two-way sidelobes for given mainlobe width
- Reduced peak transmitter power for specified peak element power
- Efficiency can be reduced for some T/R module architectures

Phase adjustment with uniform illumination

- Not recommended
- Poor on-target power efficiency
- Nonlinear phase response in main lobe of two-way pattern.

2. Switched delay line shifter

In order to achieve wide-bandwidth performance, it has been shown that varying the time delay to the elements, rather than using true phase shift, is necessary [2]. When the array dimensions exceed a few wavelengths, and the array must scan to large angles, the total insertion phase for some of the elements will need to exceed 2π radians, in order to maintain wide-bandwidth performance. If the largest array dimension is L, and the required maximum scan angle (measured from the normal to the array face) is $\theta_{\max}$, then the required total insertion phase difference between elements on one edge and elements on the opposite edge is

$$\Delta\varphi = 2\pi \frac{L}{\lambda} \sin\theta_{\max} \tag{2.1}$$

at wavelength $\lambda = c/f$, with c the speed of light and f the cyclical frequency. For example, suppose $\theta_{\max} = \pi/4$ and $L = 2\lambda$, then $\Delta\varphi = 2\pi\sqrt{2}$. As shown in [2], using modulo 2π phase shifters (even if implemented as delay-line phase shifters) will reduce the usable bandwidth of the array. Nevertheless, fine control of the beam position will at least require phase shifters at each element with a range of $\{0, 2\pi\}$. A typical wide-bandwidth phased array with large scan-angle requirements would be fed in a sub-array configuration, similar to the 16-element row illustrated in Figure 1. If the element spacing of the three-tiered configuration in Figure 1 is $\lambda/4$, switched delay-line shifters with the band-center phase shown in the figure would provide wide-bandwidth scanning out to $\theta \approx \pm 48°$. For the wide-bandwidth array, λ refers to the wavelength of the highest frequency contained in the signal.

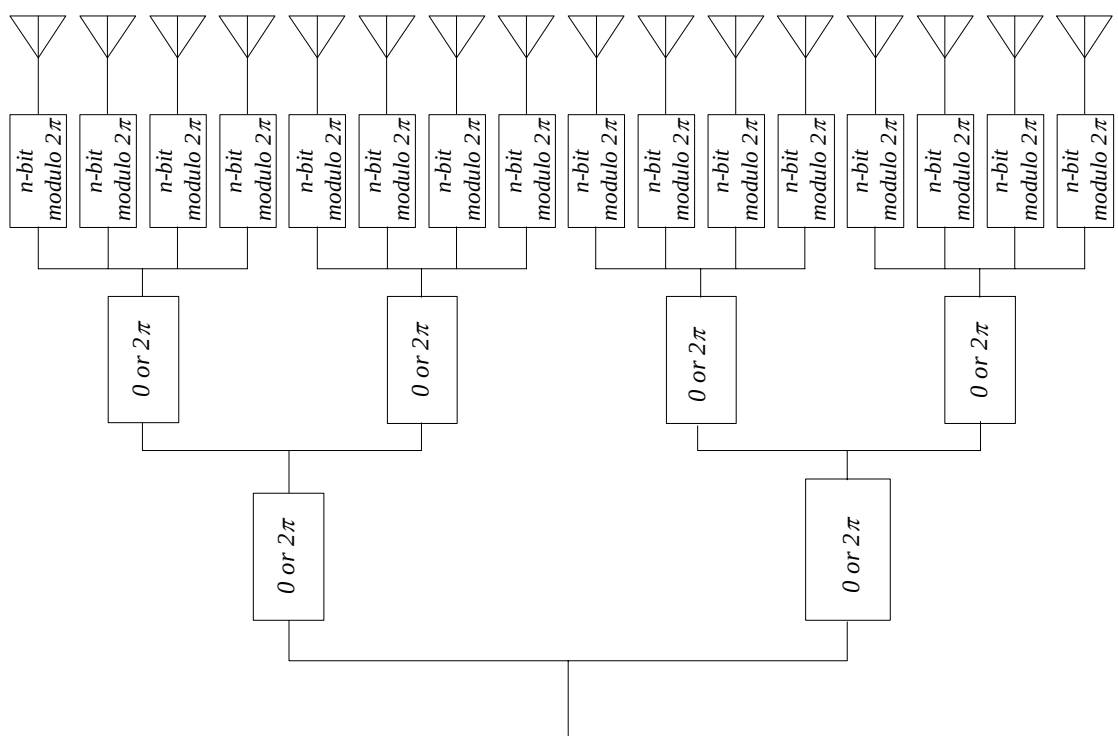

Figure 1 A sixteen-element row with a wide-bandwidth phase-shift feed configuration.

2.1 Modulo 2π switched-delay-line phase shifter

The switched delay line with *b* bits will have 2^b states so the phase for a $\{0, 2\pi\}$ phase shifter will be modeled as

$$\varphi_n(f) \equiv 2\pi \frac{f}{f_\lambda} \frac{n}{2^b}, n \in \{0, 1, \cdots 2^b - 1\}, \tag{2.2}$$

where f_λ is the frequency at which the switched delay line can provide $\left(1 - \frac{1}{2^b}\right) 2\pi$ of phase with all bits set. For φ the exact desired phase at $f = f_\lambda$, the required state of the phase shifter can be modeled as

$$\varphi_b(\varphi) \equiv \frac{2\pi}{2^b} \frac{f}{f_\lambda} \mathrm{rnd}\left(\frac{2^b}{2\pi}\varphi\right), 0 \le \varphi < 2\pi, \tag{2.3}$$

where, *b* is the number of bits in the phase shifter, and the rounding function, $\mathrm{rnd}(x)$, is

$$\mathrm{rnd}(x) = n, \text{ the integer nearest } x \text{ so that } |n - x| \le \frac{1}{2}. \tag{2.4}$$

The phase function in (2.3) allows both a zero state and a 2π state, for a total of $2^b + 1$ states. This extra state would be supplied by the 1-bit (0 or 2π) switched-line shifter in the second tier, as illustrated in Figure 1. Consistent with the true-time-delay philosophy, the analysis that follows assumes this configuration.

The digitized phase as a function of the desired phase (at $f = f_\lambda$) is plotted in Figure 2 for three phase shifters (3-bit, 4-bit, and 5-bit). The phase-shifter error is the difference between the set phase and the actual desired phase,

$$\delta\varphi_b(\varphi) \equiv \varphi_b(\varphi) - \varphi = \frac{2\pi}{2^b} \frac{f}{f_\lambda} \mathrm{rnd}\left(\frac{2^b}{2\pi}\varphi\right) - \varphi, \tag{2.5}$$

which is plotted in Figure 3 for $f = f_\lambda$ and several different numbers of bits in the phase shifter.

The phase error is a periodic function, with period $2\pi/2^b$, and can be described as follows:

$$\begin{aligned} &\delta\varphi_b(\varphi) = -\varphi \text{ for } -\frac{\pi}{2^b} \le \varphi < \frac{\pi}{2^b} \\ &\delta\varphi_b\left(\varphi \pm \frac{2\pi}{2^b}\right) = \delta\varphi_b(\varphi) \end{aligned}. \tag{2.6}$$

There are 2^b periods within the interval $0 \le \varphi \le 2\pi$. The mean phase error is obviously zero,

$$\delta\overline{\varphi}_b = \frac{1}{2\pi}\int_0^{2\pi} \delta\varphi_b d\varphi = \sum_{r=1}^{2^b} \frac{1}{2\pi} \int_{-\pi/2^b}^{\pi/2^b} x dx = 0. \tag{2.7}$$

The rms phase error is

$$\delta\varphi_{b,rms} = \sqrt{\frac{1}{2\pi}\int_0^{2\pi} \delta\varphi_b^2 d\varphi} = \sqrt{\sum_{r=1}^{2^b} \frac{1}{2\pi} \int_{-\pi/2^b}^{\pi/2^b} x^2 dx} = \frac{\pi}{2^b\sqrt{3}}. \tag{2.8}$$

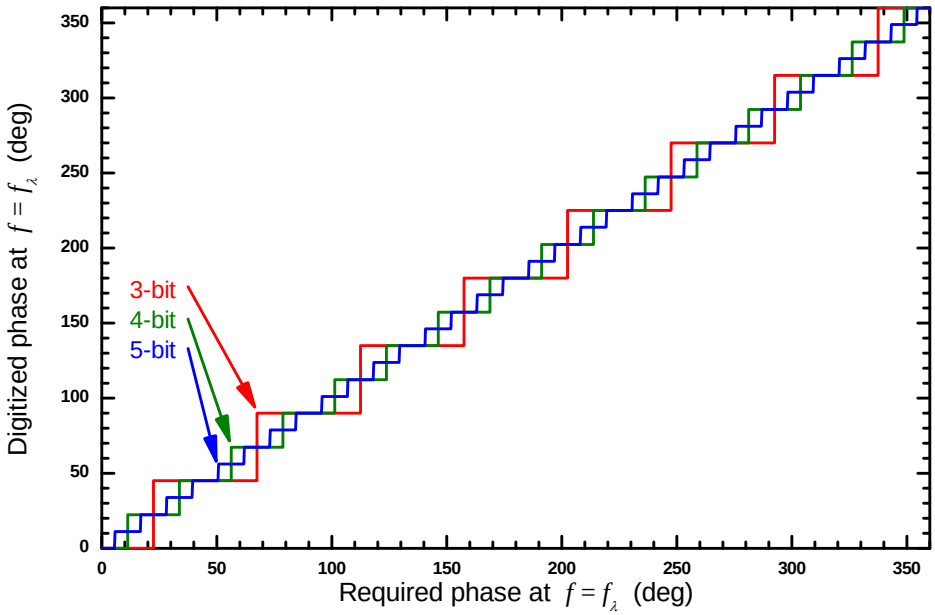

Figure 2 Digitized phase as a function of required phase for 3-bit, 4-bit, and 5-bit time-delay phase shifters

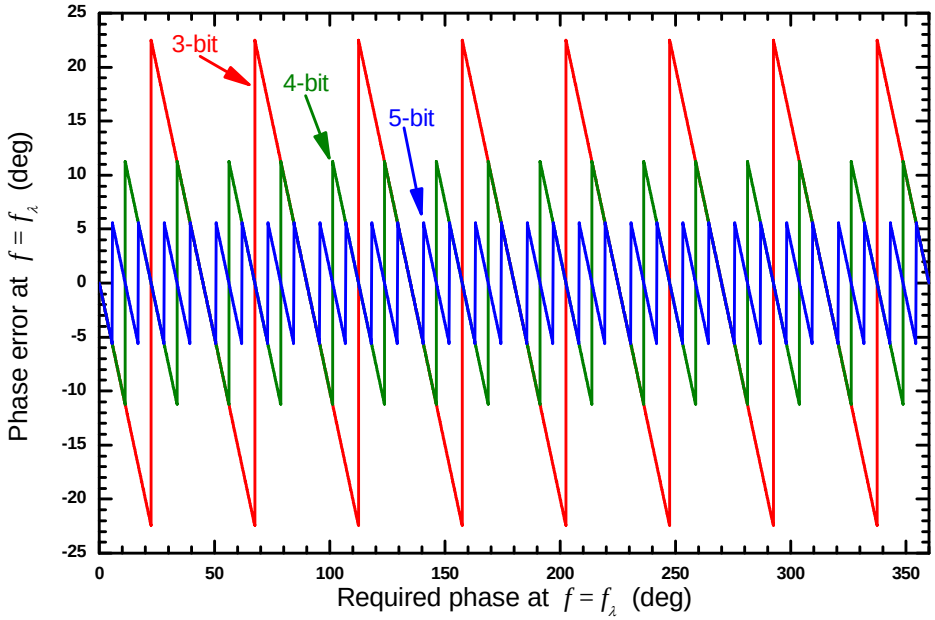

Figure 3 Phase-shifter phase error as a function of exact steering phase, for 3-bit, 4-bit, and 5-bit phase shifters.

2.2 Distribution of random phase errors

When the input to the phase shifter is a zero-mean Gaussian random variable with a standard deviation at least half the least significant bit, the error associated with the output of the phase shifter will be essentially uniformly distributed. The validity of this claim can be demonstrated by using the relative-frequency approach for determining an approximate probability density.

In this case, histograms are computed and normalized so that they have unit area. Thus, they represent the approximate probability densities for the respective random variables. Figure 4 shows the normalized histogram for a set of one million random draws from a zero-mean Gaussian distribution having a standard deviation of 22.5˚, half the least significant bit of a 3-bit phase shifter. The distribution of the errors, when this same set of angles is approximated with a 3-bit phase shifter, is plotted in Figure 5. The approximate probability density has slight curvature, but is nearly flat, indicating that the errors are essentially uniformly distributed.

Figure 6 shows the normalized histogram for a set of one million random draws from a zero-mean Gaussian distribution having a larger standard deviation of 45˚. The normalized histogram for the error associated with a 3-bit phase shifter is illustrated in Figure 7, given the same set of random draws. This distribution is even flatter, and the errors are even more uniformly distributed than in Figure 5.

If the standard deviation of the phase-shifter input becomes large enough, a significant number of the draws can lie outside the range $-180° \le \delta\varphi < 180°$. When the input is mapped to the range $-180° \le \delta\varphi < 180°$ through the modulo function, the distribution appears different from the original Gaussian. This effect is illustrated in Figure 8 for the case when the standard deviation is 360˚. However, the error distribution for the output of the phase shifter still is essentially uniform, as indicated for this example in Figure 9. Note that the modulo function is defined

$$\mathrm{mod}_p(a) \equiv a - p\,\mathrm{int}\left(\frac{a}{p}\right), \tag{2.9}$$

where

$$\mathrm{int}(x) \equiv \mathrm{sgn}(x)\,n, \text{ where } n \in \textit{Integers}, \text{ such that } n \le |x| < n+1. \tag{2.10}$$

These definitions, by the way, match the definitions of the equivalent functions in Fortran 95.

While the error distribution from the phase shifter is essentially uniform, it is not precisely uniform. The degree to which it deviates from uniformity is small, and can be determined by computing the probability density of the phase shifter error from the statistics of the phase shifter input. The error of a digital phase shifter is periodic, as described by (2.6),

$$\delta\varphi_b\left(\varphi \pm \frac{2\pi}{2^b}\right) = \delta\varphi_b(\varphi).$$

The input to the phase shifter is assumed zero-mean Gaussian with standard deviation $\sigma_{\delta\varphi}$. The choice of zero mean is for convenience, and does not limit the generality; by choosing a new phase reference, any phase distribution can be converted to a zero-mean distribution.

The probability that the error at the output of the phase shifter is between $\delta\varphi - \Delta/2$ and $\delta\varphi + \Delta/2$ is

$$P\left(\delta\varphi - \frac{\Delta}{2}, \delta\varphi + \frac{\Delta}{2}\right) = \frac{1}{\sqrt{2\pi}\sigma_{\delta\varphi}} \sum_{n=-\infty}^{\infty} \int_{\delta\varphi-\frac{\Delta}{2}}^{\delta\varphi+\frac{\Delta}{2}} e^{-\left(x+n\frac{2\pi}{2^b}\right)^2 \Big/ 2\sigma_{\delta\varphi}^2} dx. \tag{2.11}$$

Note that the summation is extended from $n = -\infty$ to $n = \infty$. This accounts for the periodicity of the error function and the tails of the input distribution, allowing the input to the phase shifter, φ, to extend beyond the range $-\pi \le \varphi < \pi$.

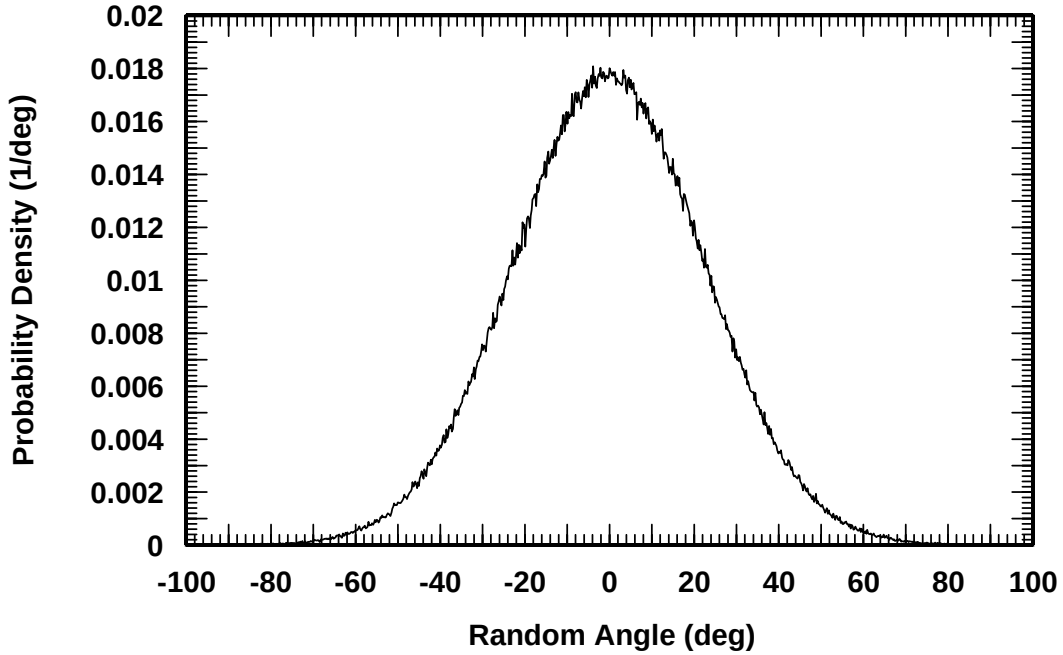

Figure 4 Normalized histogram for one million draws from a zero-mean Gaussian distribution with standard deviation of 22.5˚.

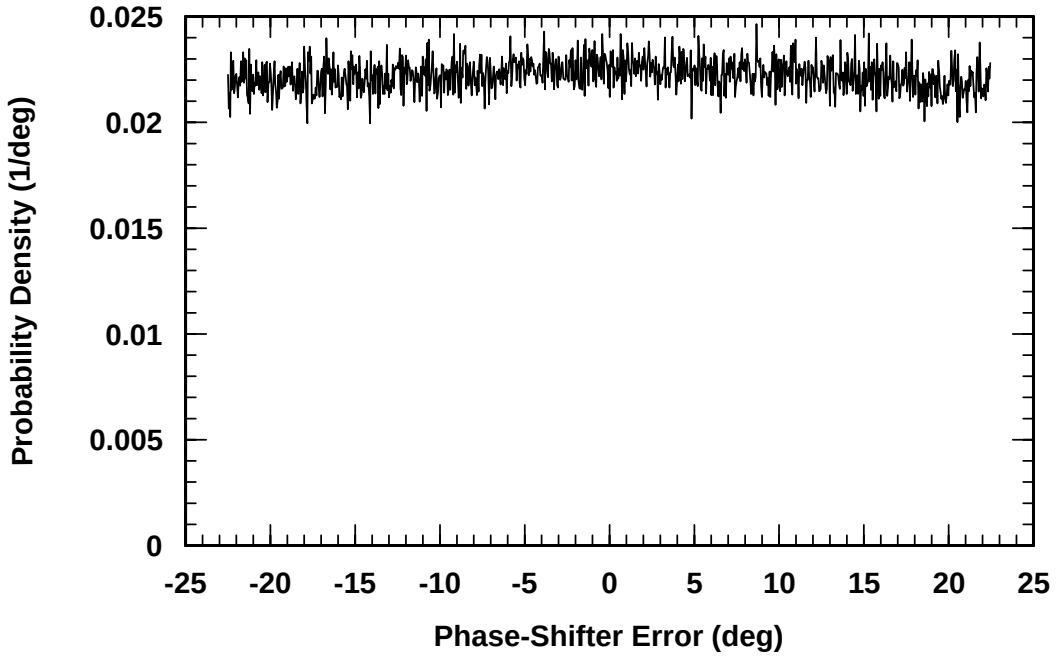

Figure 5 Normalized histogram for the 3-bit phase-shifter error when the input is the set of one million random draws associated with the histogram in Figure 4.

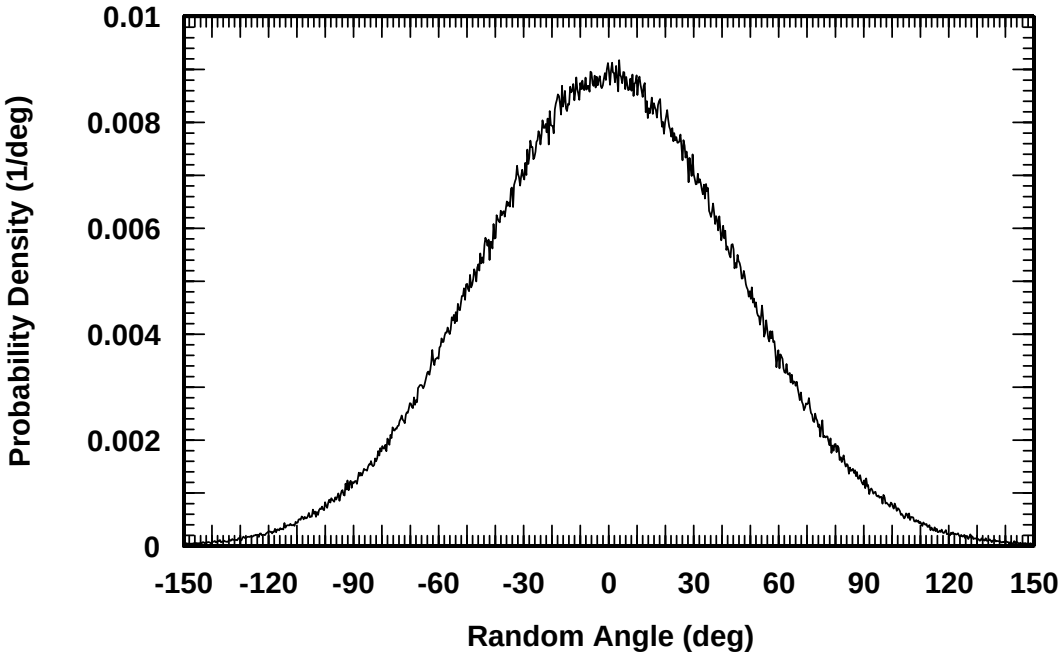

Figure 6 Normalized histogram for one million draws from a zero-mean Gaussian distribution with standard deviation of 45˚.

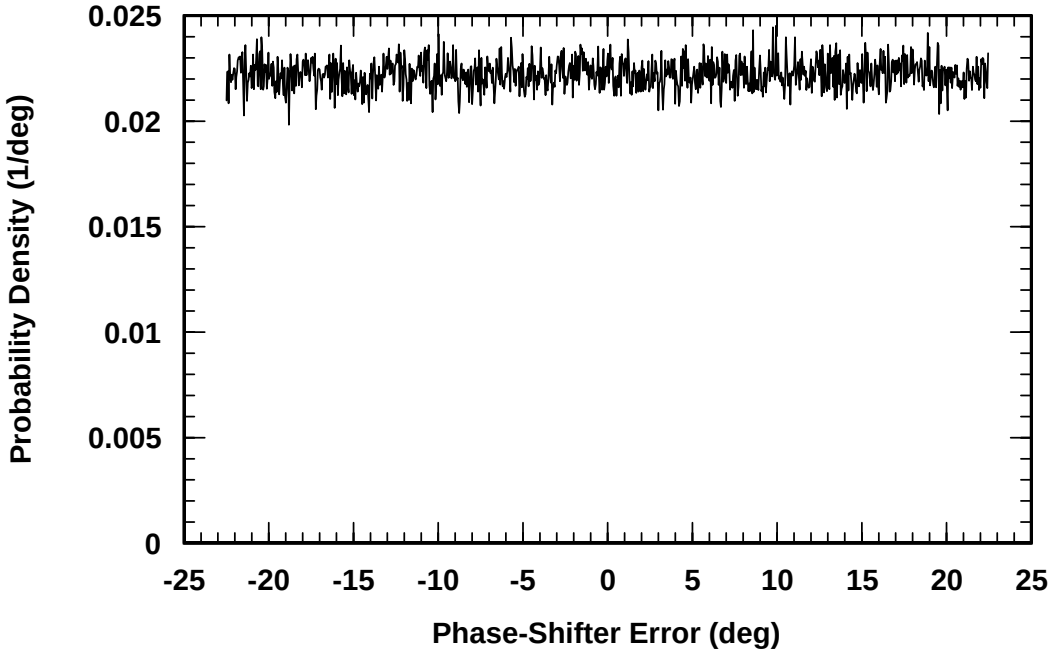

Figure 7 Normalized histogram for the 3-bit phase-shifter error when the input is the set of one million random draws associated with the histogram in Figure 6.

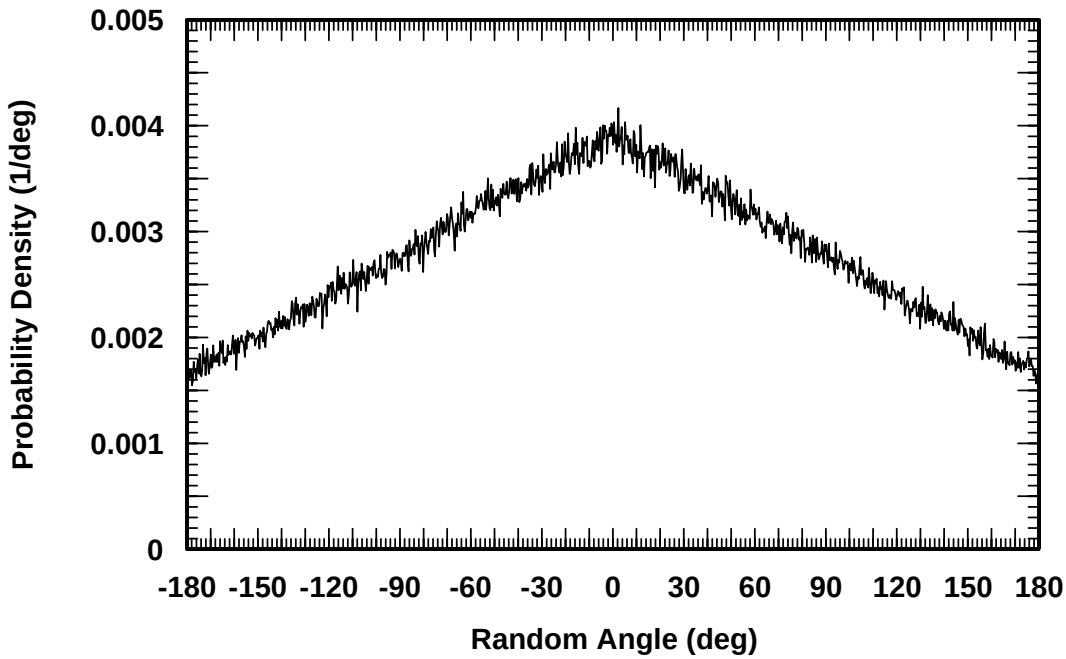

Figure 8 Normalized histogram for one million draws, modulo 180, from a zero-mean Gaussian distribution with standard deviation of 360˚.

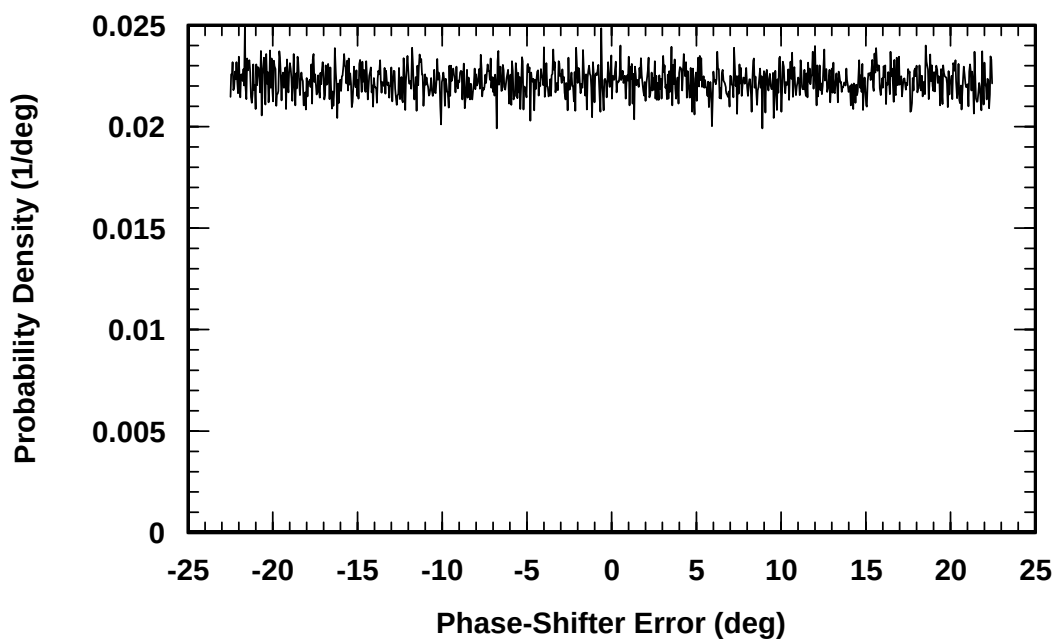

Figure 9 Normalized histogram for the 3-bit phase-shifter error when the input is the set of one million random draws associated with the histogram in Figure 8.

The probability density is

$$p(\delta\varphi) = \frac{1}{\sqrt{2\pi}\sigma_{\delta\varphi}} \sum_{n=-\infty}^{\infty} e^{-\left(\delta\varphi + n\frac{2\pi}{2^b}\right)^2 \Big/ 2\sigma_{\delta\varphi}^2} . \tag{2.12}$$

The summation in (2.12) cannot be performed in closed form for all values of $\delta\varphi$. However, at the center and edges of the error distribution, $\delta\varphi = 0$ and $\delta\varphi = \pi/2^b$, it can be summed in terms of theta functions [3, 4, 5, Appendix I],

$$p(0) = \frac{1}{\sqrt{2\pi}\sigma_{\delta\varphi}} \vartheta_3\left(0, \exp\left(-\frac{\pi^2}{2^{2b-1}\sigma_{\delta\varphi}^2}\right)\right), \tag{2.13}$$

and

$$p\left(\frac{\pi}{2^b}\right) = \frac{1}{\sqrt{2\pi}\sigma_{\delta\varphi}} \vartheta_2\left(0, \exp\left(-\frac{\pi^2}{2^{2b-1}\sigma_{\delta\varphi}^2}\right)\right). \tag{2.14}$$

The exact probability density (2.12) for the output of a 3-bit phase shifter is plotted in Figure 10 for three values of the standard deviation, $\sigma_{\delta\varphi}$, of the input. When the standard deviation is one-half of the least significant bit (22.5˚ in this case), the distribution is nearly flat. Thus, when the standard deviation is large, the error at the output is essentially uniformly distributed. A measure of the uniformity of the output distribution is the ratio of the probability density at $\delta\varphi = 0$ (the center) to the probability density at $\delta\varphi = \pi/2^b$ (the edge). As this ratio approaches unity, the distribution more closely approaches the uniform distribution. Figure 11 plots the ratio of the edge value to the center value for four different size phase shifters (number of bits). There is an obvious threshold in the standard deviation below which the assumption of a uniform distribution is no longer good, and as the number of bits increases, the delineation of the threshold becomes sharper.

The ratio of the probability density at $\delta\varphi = 0$ (the center) to the probability density at $\delta\varphi = \pi/2^b$ (the edge) can be approximated with

$$\frac{p(0)}{p\left(\frac{\pi}{2^b}\right)} = \frac{1.0002 + 0.43165x + 0.11894x^2 + 0.0090399x^3}{1 + 0.42774x + 0.10886x^2 + 0.0029426x^3}, \tag{2.15}$$

where

$$x = \ln q = -\frac{\pi^2}{2^{2b-1}\sigma_{\delta\varphi}^2} . \tag{2.16}$$

The approximation (2.15) is accurate to better than $\pm 0.1\%$ for $0.01 \le q \le 1$. For the range $10^{-15} \le q \le 0.01$, use

$$\frac{p(0)}{p\left(\frac{\pi}{2^b}\right)} = \frac{2.2770 + 0.16917x + 0.0043476\mathrm{x}^2 + 0.000038445\mathrm{x}^3}{1 - 0.30670x - 0.0044575x^2 - 0.0023463x^3}, \tag{2.17}$$

which has an accuracy better than $\pm 0.5\%$.

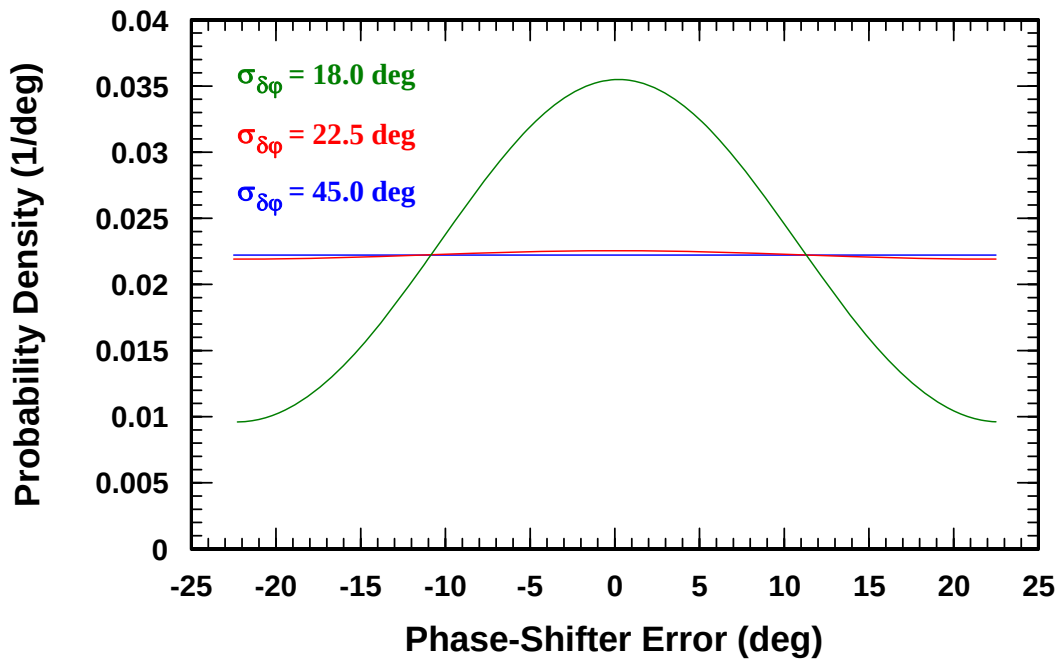

Figure 10 Probability density for the output of a 3-bit phase shifter when the input is a zero-mean Gaussian with two different values for standard deviation, $\sigma_{\delta\varphi}$.

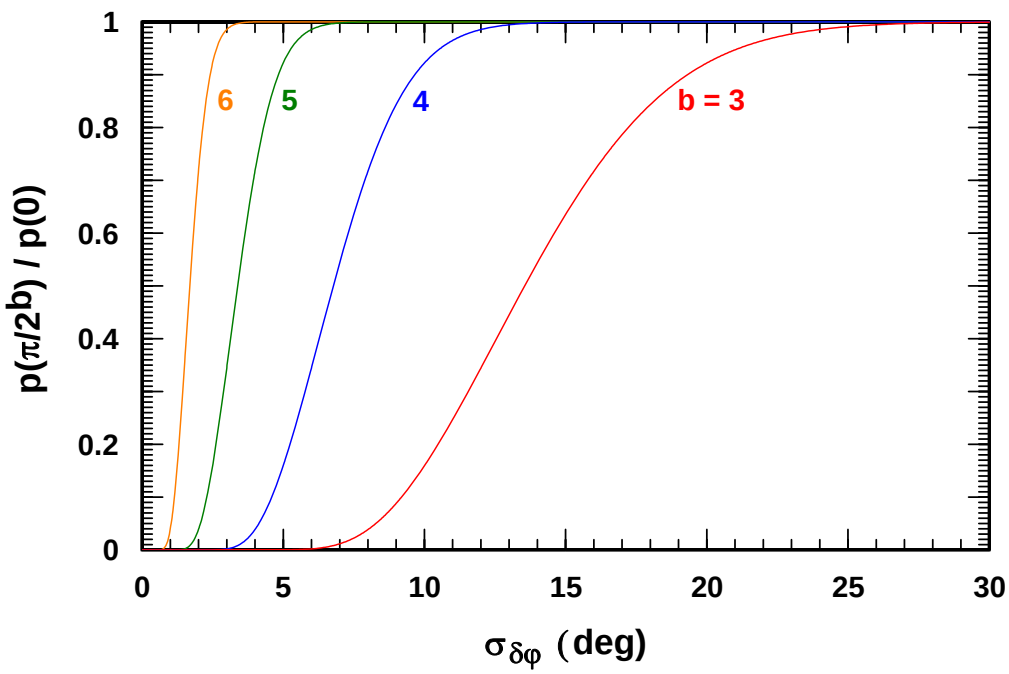

Figure 11 Ratio of center value of probability density to the edge value ($\delta\varphi = \pi/2^b$ *) for four different values for the number of bits, b.*

This Page Intentionally Blank

3. Effect of quantized steering phase on array factor

In order to examine the effect of the quantized steering phase, a linear array will be examined. Suppose we have a uniformly illuminated odd array, with $2N+1$ elements, element spacing Δs, steering phases ξ_n, and random insertion phases $\Delta\psi_n$ at each element. The random insertion phases, $\Delta\psi_n$, may be incorporated intentionally into the array's feed network, or may arise from the tolerances and errors introduced during manufacture. For convenience, it is assumed that the frequency is $f = f_\lambda$. The array factor is

$$S(\theta) = 1 + 2\sum_{n=1}^{N} \cos\left(nk\Delta s \sin\theta - \xi_n + \Delta\psi_n\right). \tag{3.1}$$

The quantization phase error is the difference between the quantized phase and the exact phase,

$$\delta\xi_n = \delta\varphi_b\left(nk\Delta s\sin\theta_0 + \Delta\psi_n\right) = \frac{2\pi}{2^b}\mathrm{rnd}\left(\frac{2^b}{2\pi}\left(nk\Delta s\sin\theta_0 + \Delta\psi_n\right)\right) - \left(nk\Delta s\sin\theta_0 + \Delta\psi_n\right) \tag{3.2}$$

It will be convenient to write the steering phase as the exact phase plus the error,

$$\xi_n = nk\Delta s\sin\theta_0 + \Delta\psi_n + \delta\xi_n. \tag{3.3}$$

The quantization phase error will range between minus and plus one half of the least significant bit of the phase shifter,

$$-\frac{\pi}{2^b} \le \delta\xi_n \le \frac{\pi}{2^b}. \tag{3.4}$$

3.1 Periodic phase error

When there is no insertion phase difference between the element phases, $\Delta\psi_n = 0$, and the phase error is due solely to quantization by the phase shifter. The phase error is

$$\begin{aligned}\delta\xi_n &= \frac{2\pi}{2^b}\left[\mathrm{rnd}\left(n\frac{2^b}{2\pi}k\Delta s\sin\theta_0\right) - n\frac{2^b}{2\pi}k\Delta s\sin\theta_0\right] \\ &= \frac{2\pi}{2^b}\left[\mathrm{rnd}\left(n2^b\frac{\Delta s}{\lambda}\sin\theta_0\right) - n2^b\frac{\Delta s}{\lambda}\sin\theta_0\right]\end{aligned}, \tag{3.5}$$

which is periodic across the array. The number of cycles of error across the array depends on the angle θ_0, to which the array is steered. For p error cycle across the array,

$$\theta_0 = \sin^{-1}\left(\frac{p}{2N}\frac{\lambda}{\Delta s}2^{-b}\right), \tag{3.6}$$

and the worst error occurs at elements $\pm n_q$

$$n_q = \pm(2q+1)\frac{N}{p},\ q = 0,1,\cdots\frac{p-1}{2}. \tag{3.7}$$

For $-n_0 \le n \le n_0$, the phase error is

$$\delta\xi_n = -n\frac{p}{2N}\frac{2\pi}{2^b},\ -n_0 \le n \le n_0, \tag{3.8}$$

and for $-n_{q+1} \le n \le -n_q$ or $n_q \le n \le n_{q+1}$

$$\delta\xi_n = \begin{cases} \left(\dfrac{N}{p} - n_{q+1} - n\right)\dfrac{p}{2N}\dfrac{2\pi}{2^b}, & -\min\left(N, n_{q+1}\right) \le n \le -n_q \\ \left(\dfrac{N}{p} + n_q - n\right)\dfrac{p}{2N}\dfrac{2\pi}{2^b}, & n_q \le n \le \min\left(N, n_{q+1}\right) \end{cases} . \tag{3.9}$$

When the insertion phase term is zero (no random phase), the phase error is periodic with the form (3.8) and (3.9). Using the periodicity, the error term can be written as

$$\begin{aligned} S_{err}(\theta) = &-\sum_{n=1}^{n_0}\left(-n\frac{p}{2N}\frac{2\pi}{2^b}\right)^2 \cos\left(nk\Delta s\left(\sin\theta - \sin\theta_0\right)\right) \\ &- \sum_{n=n_0+1}^{n_1}\left(\left(\frac{N}{p} + n_q - n\right)\frac{p}{2N}\frac{2\pi}{2^b}\right)^2 \cos\left(nk\Delta s\left(\sin\theta - \sin\theta_0\right)\right) - \cdots \\ &+2\sum_{n=1}^{n_0} -n\frac{p}{2N}\frac{2\pi}{2^b}\sin\left(nk\Delta s\left(\sin\theta - \sin\theta_0\right)\right) \\ &+2\sum_{n=n_0+1}^{n_1}\left(\frac{N}{p} + n_q - n\right)\frac{p}{2N}\frac{2\pi}{2^b}\sin\left(nk\Delta s\left(\sin\theta - \sin\theta_0\right)\right) + \cdots \end{aligned} \tag{3.10}$$

Suppose an array contains $2N+1 = 201$ elements in a row with $\lambda/2$ spacing. The array is uniformly illuminated, with no random insertion phase, and has 3-bit phase shifters for steering. This will produce a periodic phase error across the array, when it is steered from broadside. For example, steering the array $1°$ from broadside introduces the periodic phase error illustrated in Figure 12. The periodic phase error produces spurious sidelobes (quantization lobes), as illustrated in Figure 13. The quantization lobes vary with scan angle, and they can be reduced by increasing the number of bits in the phase shifter. The peak phase error is $\frac{1}{2}$ of the phase of the least-significant bit in the phase shifter.

3.2 Random phase error

If the array is built with random insertion phases for each element, the phase error will no longer be periodic over the array, but will be randomized. For the example of 201 elements with $\lambda/2$ spacing, if the insertion phases, $\Delta\psi_n$, are taken from a zero-mean Gaussian distribution with standard deviation 0.5 radian, the phase error across the array face will appear similar to that plotted in Figure 14. As illustrated in Figure 15, the randomization of the error essentially eliminates the quantization lobes. This example demonstrates that it will be advantageous to ensure that the phase errors are randomized.

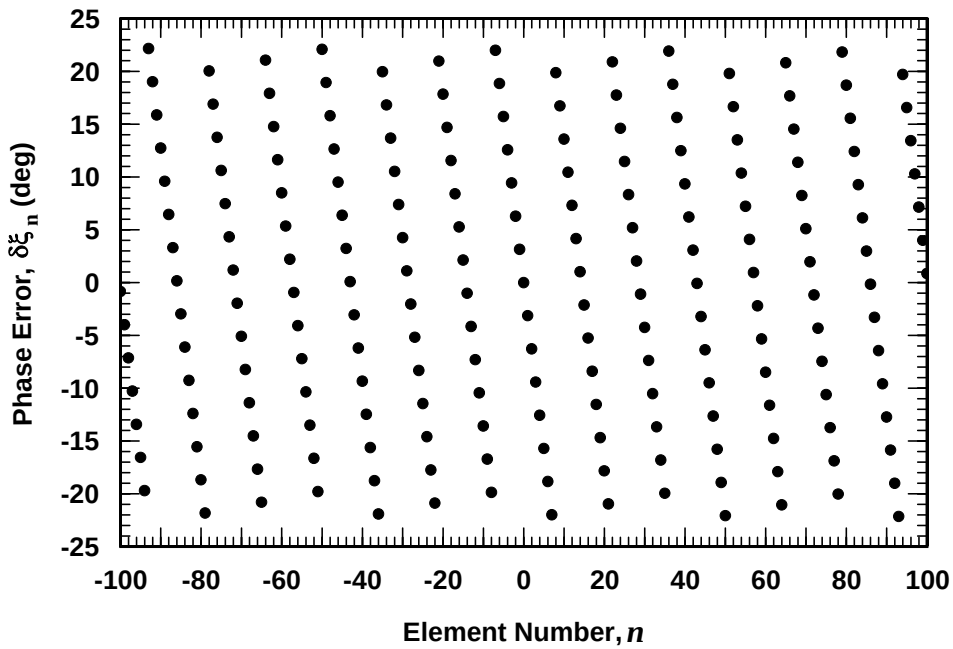

Figure 12 Periodic phase error across array containing 201 elements with half-wavelength spacing, steered $1°$ *from broadside with 3-bit phase shifters.*

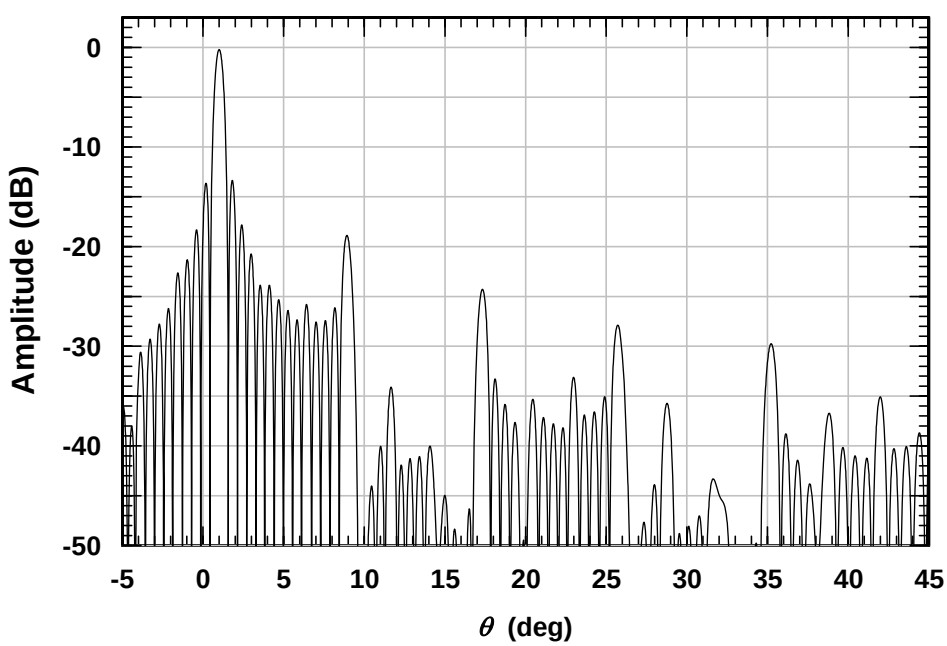

Figure 13 Normalized array factor for the 201-element array, steered to $\theta = 1°$ *with 3-bit phase shifters.*

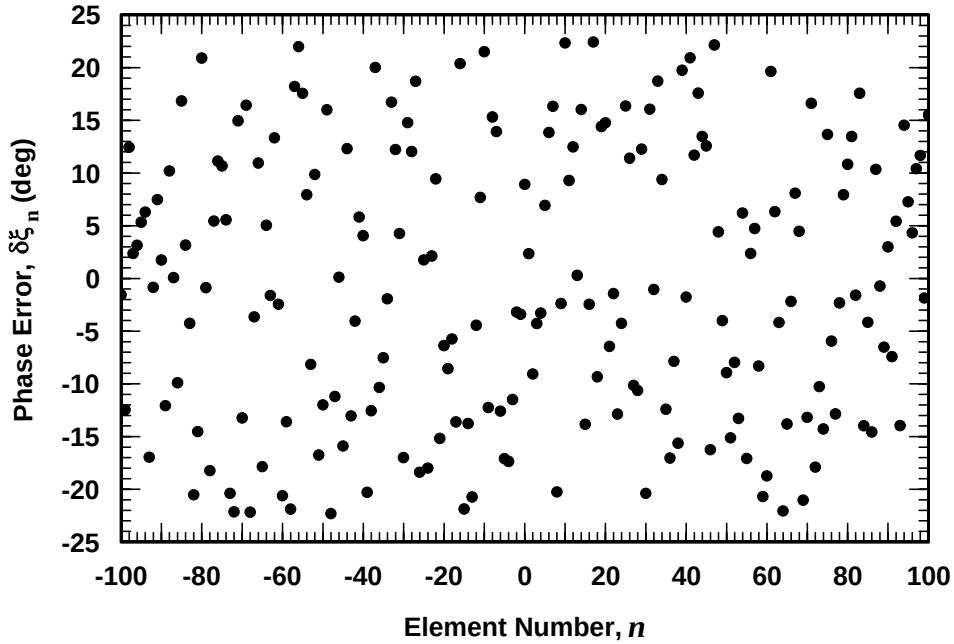

Figure 14 Example of phase error across array containing 201 elements with half-wavelength spacing, steered $1°$ *from broadside with 3-bit phase shifters, as Figure 12, but with zero-mean Gaussian random insertion phase having a standard deviation of 0.5 radian (28.6˚).*

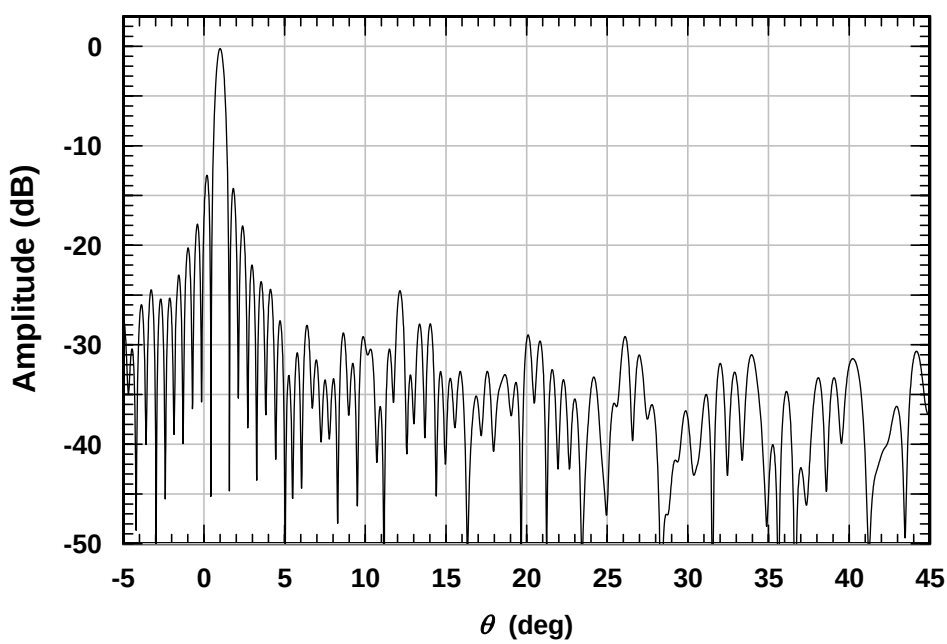

Figure 15 Array factor for the 201-element array, steered to $\theta = 1°$ *with 3-bit phase shifters (same as Figure 13), but with a random insertion phase for each element, resulting in the phase error plotted in Figure 14.*

Writing the array factor in terms of the element phase errors, $\delta\xi_n$,

$$
\begin{aligned}
S(\theta) &= 1 + 2\sum_{n=1}^{N} \cos\left(nk\Delta s\left(\sin\theta - \sin\theta_0\right) - \delta\xi_n\right) \\
&= 1 + 2\sum_{n=1}^{N} \cos\left(nk\Delta s\left(\sin\theta - \sin\theta_0\right)\right)\cos\left(\delta\xi_n\right) \\
&\quad + 2\sum_{n=1}^{N} \sin\left(nk\Delta s\left(\sin\theta - \sin\theta_0\right)\right)\sin\left(\delta\xi_n\right) \\
&= 1 + 2\sum_{n=1}^{N} \cos\left(nk\Delta s\left(\sin\theta - \sin\theta_0\right)\right)\left(1 - \frac{1}{2}\delta\xi_n^2 + \frac{1}{24}\delta\xi_n^4 + \cdots\right) \\
&\quad + 2\sum_{n=1}^{N} \sin\left(nk\Delta s\left(\sin\theta - \sin\theta_0\right)\right)\left(\delta\xi_n - \frac{1}{6}\delta\xi_n^3 + \cdots\right)
\end{aligned}
\quad . \tag{3.11}
$$

The array factor can be written

$$
S(\theta) = \frac{\sin\left(\left(2N+1\right)\frac{k}{2}\Delta s\left(\sin\theta - \sin\theta_0\right)\right)}{\sin\left(\frac{k}{2}\Delta s\left(\sin\theta - \sin\theta_0\right)\right)} + S_{err}(\theta) . \tag{3.12}
$$

where an array factor error is defined

$$
\begin{aligned}
S_{err}(\theta) &= -\sum_{n=1}^{N} \delta\xi_n^2\left(1 - \frac{1}{12}\delta\xi_n^2 + \cdots\right)\cos\left(nk\Delta s\left(\sin\theta - \sin\theta_0\right)\right) \\
&\quad + 2\sum_{n=1}^{N} \delta\xi_n\left(1 - \frac{1}{6}\delta\xi_n^2 + \cdots\right)\sin\left(nk\Delta s\left(\sin\theta - \sin\theta_0\right)\right)
\end{aligned}
\tag{3.13}
$$

When the phase error is small, the following second-order approximation can be used,

$$
\begin{aligned}
S_{err}(\theta) &\cong -\sum_{n=1}^{N} \delta\xi_n^2 \cos\left(nk\Delta s\left(\sin\theta - \sin\theta_0\right)\right) + 2\sum_{n=1}^{N} \delta\xi_n \sin\left(nk\Delta s\left(\sin\theta - \sin\theta_0\right)\right) \\
&= -\sum_{n=1}^{N} \delta\xi_n\left[\cos\left(nk\Delta s\left(\sin\theta - \sin\theta_0\right)\right) - 2\delta\xi_n \sin\left(nk\Delta s\left(\sin\theta - \sin\theta_0\right)\right)\right]
\end{aligned}
\quad . \tag{3.14}
$$

When the random insertion phases are measured and accounted for in a calibration procedure, the phase error should be limited to plus or minus half of the least significant phase bit. For three or more bits in the phase shifter, the error in the approximation of the first sum is less than 1.3%, while the error in the approximation of the second sum is less than 2.6%. Assuming the phase errors are uniformly distributed, the expectation of the error term is

$$
\begin{aligned}
E\left[S_{err}(\theta)\right] &= -\sum_{n=1}^{N} \frac{1}{2\left(\pi/2^b\right)} \int_{-\pi/2^b}^{\pi/2^b} \delta\xi_n^2 d\delta\xi_n \cos\left(nk\Delta s\left(\sin\theta - \sin\theta_0\right)\right) \\
&\quad + 2\sum_{n=1}^{N} \frac{1}{2\left(\pi/2^b\right)} \int_{-\pi/2^b}^{\pi/2^b} \delta\xi_n d\delta\xi_n \sin\left(nk\Delta s\left(\sin\theta - \sin\theta_0\right)\right)
\end{aligned}
\quad , \tag{3.15}
$$

so

$$E\left[S_{err}(\theta)\right] = -\frac{1}{3}\frac{\pi^2}{2^{2b}}\sum_{n=1}^{N}\cos\left(nk\Delta s\left(\sin\theta - \sin\theta_0\right)\right)$$

$$= -\left(\delta\varphi_{b,rms}\right)^2 \frac{\sin\left(N\frac{k\Delta s\left(\sin\theta-\sin\theta_0\right)}{2}\right)}{\sin\left(\frac{k\Delta s\left(\sin\theta-\sin\theta_0\right)}{2}\right)}\cos\left(\left(2N+1\right)\frac{k\Delta s\left(\sin\theta-\sin\theta_0\right)}{2}\right), \tag{3.16}$$

where $\delta\varphi_{b,rms}$ is given by (2.8). Recall from section 2.2 that the assumption of uniformly distributed phase errors does not mean that the random insertion phases are uniformly distributed.

3.3 Reduction in directivity due to phase quantization

At $\theta = \theta_0$, with $\Delta s = \lambda/2$, the array factor is

$$S\left(\theta=\theta_0\right) = \left(2N+1\right)\left(1-\left(\delta\varphi_{b,rms}\right)^2\frac{N}{2N+1}\right). \tag{3.17}$$

The directivity is

$$D(\theta) = \frac{4\pi}{\Omega_S}\left|S(\theta)\right|^2, \tag{3.18}$$

where the beam solid angle is

$$\Omega_S = \int_0^{\pi}\int_0^{2\pi}\left|S(\theta)\right|^2 d\phi\sin\theta d\theta. \tag{3.19}$$

The normalized directivity for $\Delta s = \lambda/2$ is

$$d\left(\theta=\theta_0\right) = \left(\frac{S\left(\theta=\theta_0\right)}{\left(2N+1\right)}\right)^2 \cong \left(1-\left(\delta\varphi_{b,rms}\right)^2\frac{N}{2N+1}\right)^2$$
$$\simeq 1-\delta\varphi_{b,rms}^2 = 1-\frac{1}{3}\frac{\pi^2}{2^{2b}}. \tag{3.20}$$

The reduction in directivity (in decibels) is approximately

$$\Delta D \approx -4.34\delta\varphi_{b,rms}^2 = -\frac{14.3}{2^{2b}}\ \text{dB}. \tag{3.21}$$

For a 3-bit phase shifter, $\Delta D \approx -0.22$ dB, while a 4-bit phase shifter reduces the directivity by only $\Delta D \simeq -0.06$ dB. Thus, the reduction in directivity is minimal when at least 3 bits are used for the phase shifter.

3.4 Contribution to sidelobes due to phase quantization

The energy lost from the main beam is redistributed into the sidelobes. Assuming this energy is distributed uniformly among the elements with random phase, then a particular point in space will have an additional sidelobe directivity contribution,

$$\Delta D_{SL}(\theta) = \sum_{n=-N}^{N} d_n(\theta)\delta\varphi_{b,rms}^2 \tag{3.22}$$

where $d_n(\theta)$ is the element directivity in the direction θ. If the element directivity is approximated as the same from element to element and constant over the region of interest, the average sidelobe directivity due to phase quantization, relative to the main beam directivity, is

$$SLL_{phase\ quantization} = \frac{\delta\varphi_{b,rms}^2}{(2N+1)\left(1-\delta\varphi_{b,rms}^2\right)} = \frac{\frac{1}{3}\frac{\pi^2}{2^{2b}}}{(2N+1)\left(1-\frac{1}{3}\frac{\pi^2}{2^{2b}}\right)}. \tag{3.23}$$

Although the average sidelobe directivity due to phase quantization has been derived for a linear array, the same argument holds for an areal array, in which case the integer $2N+1$ becomes the total number of elements in the array.

The average sidelobe level due to phase quantization is illustrated in Figure 16 as a function of the total number of elements in an array, for several numbers of bits in the phase shifter.

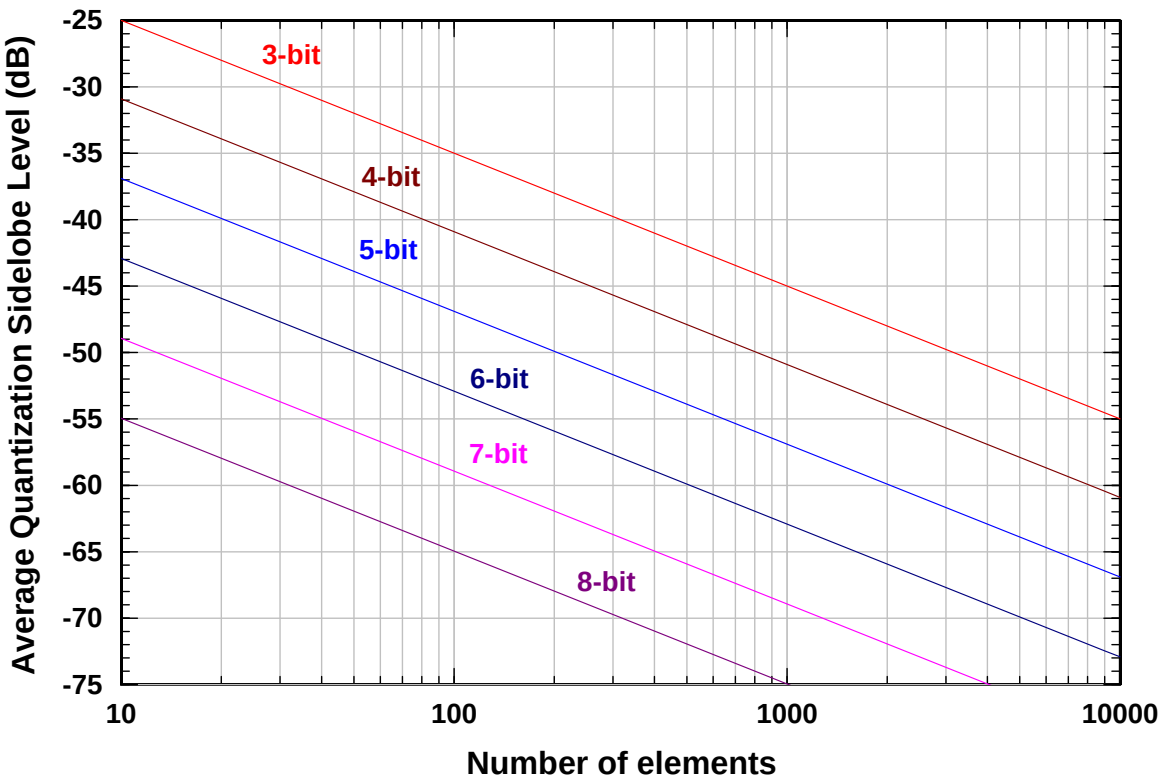

Figure 16 Average quantization-sidelobe level as a function of the number of elements in an array, for several numbers of bits in phase shifter.

This Page Intentionally Blank

3.5 Effect on steering angle from phase quantization

The expectation function for the array factor can be written

$$E\left[S(\theta)\right]=\frac{\sin\left(\left(2N+1\right)\frac{k}{2}\Delta s\left(\sin\theta-\sin\theta_0\right)\right)}{\sin\left(\frac{k}{2}\Delta s\left(\sin\theta-\sin\theta_0\right)\right)}\cdot$$
$$\left(1-\frac{1}{2}\left(\delta\varphi_{b,rms}\right)^2\sin\left(N\frac{k\Delta s\left(\sin\theta-\sin\theta_0\right)}{2}\right)\frac{\cos\left(\left(2N+1\right)\frac{k\Delta s\left(\sin\theta-\sin\theta_0\right)}{2}\right)}{\sin\left(\left(2N+1\right)\frac{k}{2}\Delta s\left(\sin\theta-\sin\theta_0\right)\right)}\right)\cdot \tag{3.24}$$

To second order in $\left(\sin\theta-\sin\theta_0\right)$, the peak of the main lobe of the expected array factor occurs at $\theta=\theta_0$, independent of the rms phase error, $\delta\xi_{b,rms}$, and the number of elements in the array. Thus, on average, the pointing error is essentially independent of the number of bits in the phase shifter.

The derivative of the array factor with respect to angle θ is

$$\frac{\partial}{\partial\theta}S(\theta)=2k\Delta s\cos(\theta)\sum_{n=1}^{N}n\sin\left(nk\Delta s\left(\sin\theta-\sin\theta_0\right)-\delta\xi_n\right). \tag{3.25}$$

The main peak of the array pattern will occur when $\frac{\partial}{\partial\theta}S(\theta)=0$, and should occur near $\theta=\theta_0$. Thus, at the peak,

$$\sum_{n=1}^{N}\left(n^2k\Delta s\left(\sin\theta-\sin\theta_0\right)-n\delta\xi_n\right)\cong 0, \tag{3.26}$$

which has the approximate solution

$$\theta\cong\theta_0+\frac{1}{\cos\theta_0}\frac{6}{k\Delta s\left(2N+1\right)\left(N+1\right)N}\sum_{n=1}^{N}n\delta\xi_n. \tag{3.27}$$

When the phase errors are random and uncorrelated from element to element, the rms pointing error is

$$\begin{aligned}\delta\theta_{rms}&=\frac{1}{\cos\theta_0}\frac{6}{k\Delta s\left(2N+1\right)\left(N+1\right)N}\sqrt{\sum_{n=1}^{N}n^2\frac{2^b}{2\pi}\int_{-\pi/2^b}^{\pi/2^b}\delta\xi_n^2\,d\delta\xi_n}\\&=\frac{\sqrt{2}}{k\Delta s\cos\theta_0\sqrt{N\left(N+1\right)\left(2N+1\right)}}\frac{\pi}{2^b}\end{aligned}. \tag{3.28}$$

For a uniformly illuminated odd array, the 3–dB beamwidth is approximately (see section 6)

$$\Delta\theta_{3dB}=2\theta_{3dB}\cong\frac{0.443}{\sqrt{N\left(N+1\right)}}\frac{\lambda}{\Delta s}, \tag{3.29}$$

so the rms pointing error in beamwidths is

$$\frac{\delta\theta_{rms}}{\Delta\theta_{3dB}}\cong\frac{1.60}{2^b\sqrt{\left(2N+1\right)}}. \tag{3.30}$$

When a 3-bit phase shifter is used with $2N+1=201$ elements, the rms pointing error is about 1.4% of the beamwidth. The rms pointing error, measured in beamwidths, is plotted in Figure 17, as a function of total number of elements in a linear array, for several numbers of bits in the phase shifter.

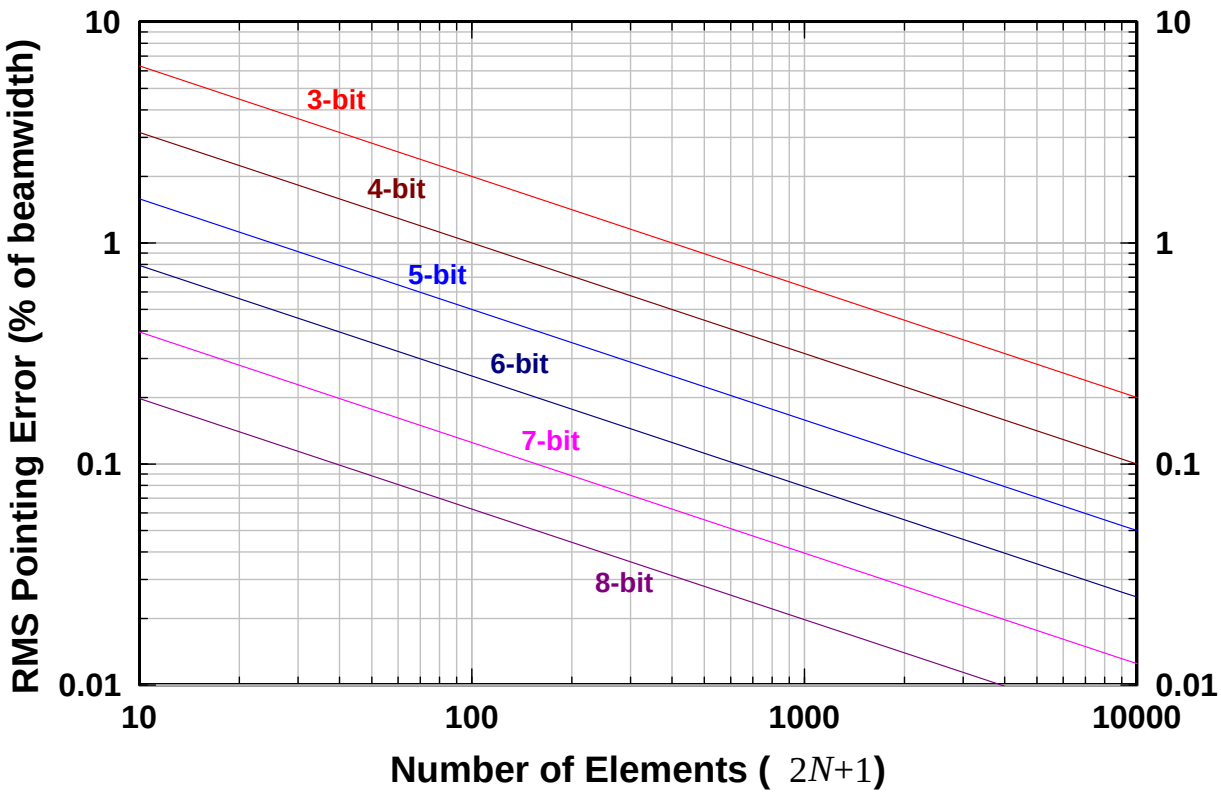

Figure 17 The rms pointing error (in percent of beamwidth) as a function of number of elements in a linear array, for several sizes of phase shifter.

4. Digital attenuator

It is assumed that the gain of the T/R modules will be controlled by a digital (quantized) attenuator, and that the maximum gain for each module will vary from unit to unit. A model of a *b*-bit attenuator is shown in the diagram of Figure 18. This model utilizes switched attenuator sections, with the delay matched between the attenuation and through paths for each section. The attenuation is (in decibels)

$$a_b(n) = a_{range}\frac{n}{2^b - 1},\ \ n \in \{0,1,2,\cdots 2^b - 1\}, \tag{4.1}$$

where a_{range} is the maximum attenuation and *b* is the number of bits. Given a desired attenuation, *a*, the attenuator is set to the nearest value

$$a_b(a) = \frac{a_{range}}{2^b - 1}\ \mathrm{rnd}\left(\frac{a}{a_{range}}\left(2^b - 1\right)\right), \tag{4.2}$$

where the rounding function, $\mathrm{rnd}(x)$, is

$$\mathrm{rnd}(x) = n, \text{ the integer nearest } x \text{ so that } |n - x| \le \frac{1}{2}. \tag{4.3}$$

The attenuator error, a_{error}, is the difference between the desired attenuation and the actual value set (in decibels),

$$a_{error} = a - a_b = a - \frac{a_{range}}{2^b - 1}\ \mathrm{rnd}\left(\frac{a}{a_{range}}\left(2^b - 1\right)\right). \tag{4.4}$$

This error will be periodic in the desired attenuation, with a period $a_{range}/\left(2^b - 1\right)$, and

$$-\frac{a_{range}}{2\left(2^b - 1\right)} \le a_{error} \le \frac{a_{range}}{2\left(2^b - 1\right)}. \tag{4.5}$$

The error as a function of attenuation is plotted in Figure 19 for both a 3-bit 20 dB attenuator and a 4-bit 6 dB attenuator.

The quantized attenuator will have an effect on the array's peak sidelobe level. In order to examine this effect, the array factor will be examined. In the next section, the general array factor for a two-dimensional planar array is formulated. The effect of quantization of the element weights is then examined for the Taylor array.

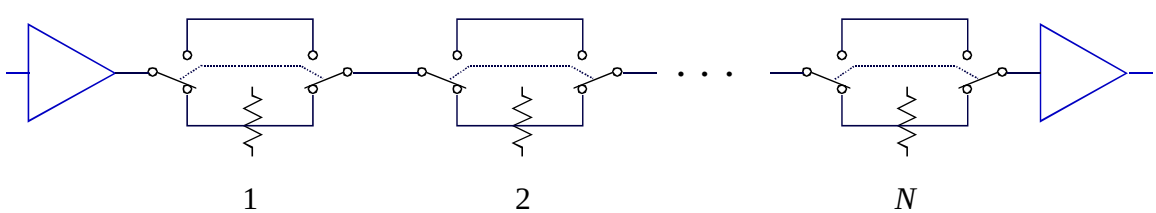

Figure 18 Diagram of an N-bit digital attenuator, using switched attenuator sections with matched phase delays.

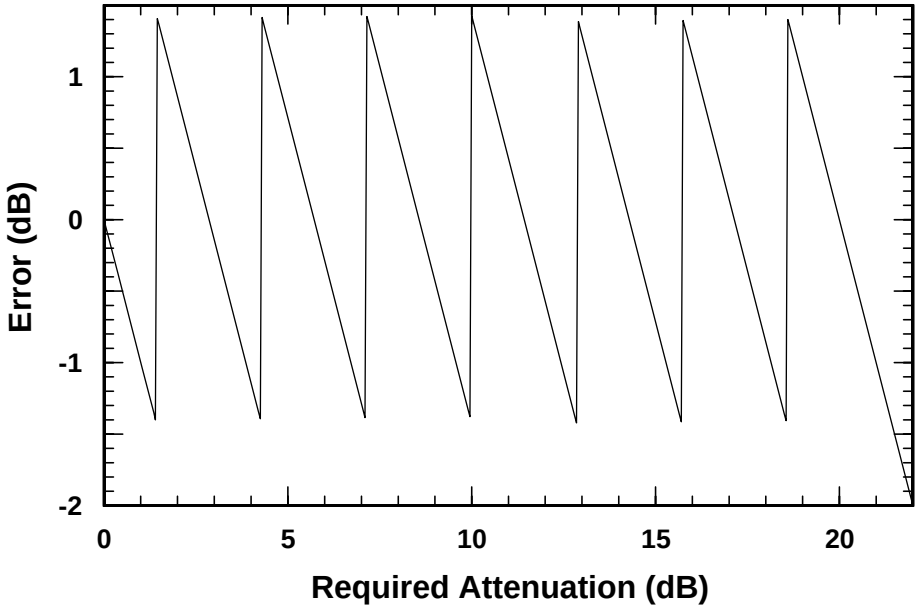

(a)

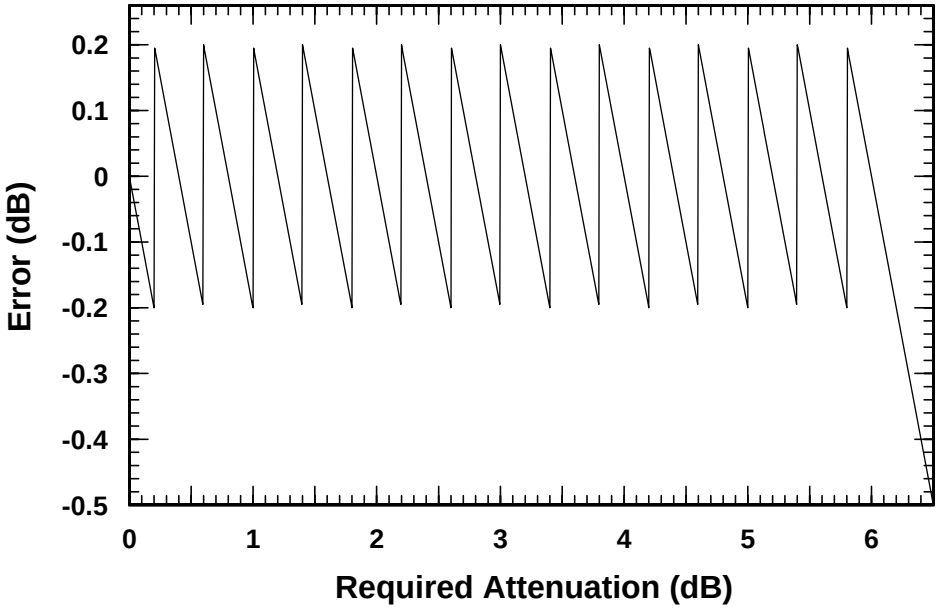

(b)

Figure 19 Attenuation errors for (a) 3-bit 20 dB attenuator and (b) 4-bit 6 dB attenuator.

5. Two-dimensional planar array factor

The following discussion addresses the properties of a two-dimensional planar array that are independent of the element type and element-to-element coupling. Consider a two-dimensional planar array of radiating elements, as illustrated in Figure 20. The array is organized into equally spaced rows of equally spaced elements. However, in the general array, alternating rows can be different. For this discussion, the elements have the same spacing in each row, but the elements in the even-numbered rows have an offset, x_a, from the $\hat{\mathbf{x}}$ axis, while the elements in the odd-numbered rows have an offset x_b. The element spacing within all of the rows is Δx, and the row spacing is Δy. For a rectangular lattice, set $x_a = x_b$. A convenient definition for a triangular lattice sets $x_a = 0$ and $x_b = \Delta x/2$.

For completeness, two types of arrays will be considered:

- the "odd array", which has an odd number of elements in each of an odd number of rows,

and

- the "even array", which has an even number of elements in each of an even number of rows.

The even array is most commonly used in practice, because power dividers are more easily designed with an even number of output ports.

In the odd array, as illustrated in Figure 20, the nth element in the mth row is located by the vector

$$\vec{\mathbf{p}}_{n,m} = \begin{cases} \left(x_a + n\Delta x\right)\hat{\mathbf{x}} + m\Delta y\hat{\mathbf{y}}, & m \text{ even} \\ \left(x_b + n\Delta x\right)\hat{\mathbf{x}} + m\Delta y\hat{\mathbf{y}}, & m \text{ odd} \end{cases} . \tag{5.1}$$

The indices locating the elements are

$$\begin{aligned} n &\in \left\{-N, -N+1, \cdots, -1, 0, 1, \cdots, N-1, N\right\} \\ m &\in \left\{-M, -M+1, \cdots, -1, 0, 1, \cdots, M-1, M\right\} \end{aligned} . \tag{5.2}$$

For the even array, illustrated in Figure 21, an element is located by

$$\vec{\mathbf{p}}_{n,m} = \begin{cases} \left(x_a + \left(n - \tfrac{1}{2}\operatorname{sgn}(n)\right)\Delta x\right)\hat{\mathbf{x}} + \left(m - \tfrac{1}{2}\operatorname{sgn}(m)\right)\Delta y\hat{\mathbf{y}}, & m \text{ even} \\ \left(x_b + \left(n - \tfrac{1}{2}\operatorname{sgn}(n)\right)\Delta x\right)\hat{\mathbf{x}} + \left(m - \tfrac{1}{2}\operatorname{sgn}(m)\right)\Delta y\hat{\mathbf{y}}, & m \text{ odd} \end{cases} , \tag{5.3}$$

where

$$\operatorname{sgn}(x) \equiv \begin{cases} 1, & x > 0 \\ 0, & x = 0 \\ -1, & x < 0 \end{cases} . \tag{5.4}$$

The indices locating each element are

$$n \in \left\{\pm 1, \pm 2, \cdots \pm N\right\} \text{ and } m \in \left\{\pm 1, \pm 2, \cdots \pm M\right\} . \tag{5.5}$$

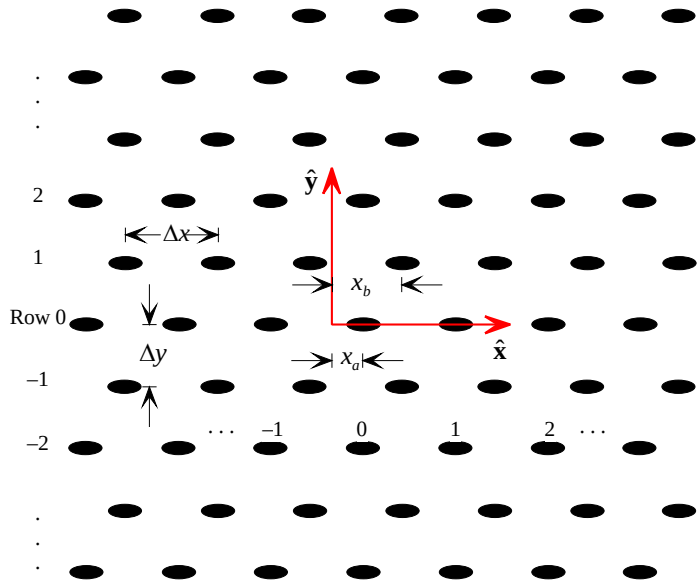

Figure 20 Two-dimensional planar-array geometry when the number of elements in each row is odd, and the number of rows is odd.

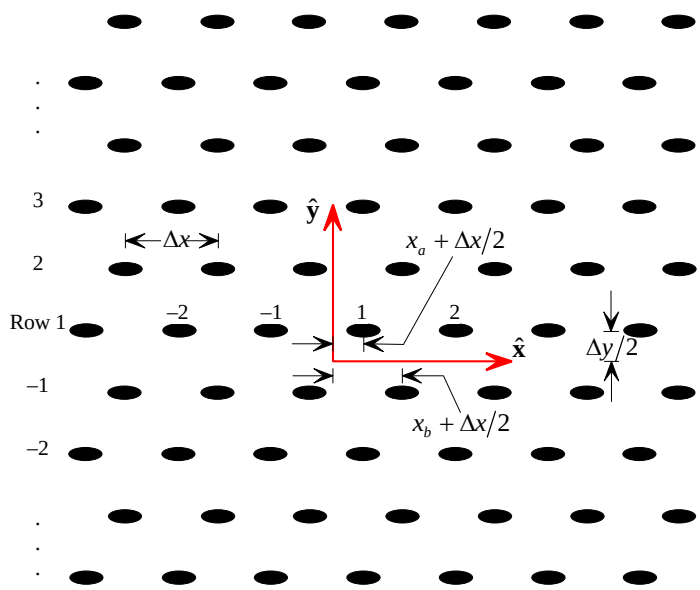

Figure 21 Two-dimensional planar-array geometry when the number of elements in each row is even, and the number of rows is even.

We will consider a field with $e^{j\omega t}$ time dependence. The field point will be located by

$$\vec{\mathbf{r}} = r\begin{pmatrix} \hat{\mathbf{x}}\sin\theta\cos\phi + \\ \hat{\mathbf{y}}\sin\theta\sin\phi + \\ \hat{\mathbf{z}}\cos\theta \end{pmatrix}. \tag{5.6}$$

A far-field vector radiation function is given by superposition of the contributions from each element

$$\vec{\mathbf{d}}_{array}\left(\vec{\mathbf{r}}\right) = \sum_{n,m} A_{n,m} e^{j\left(\psi_{n,m} - \xi_{n,m}\right)} \vec{\mathbf{d}}_{n,m}\left(\hat{\mathbf{r}}_{n,m}\right), \tag{5.7}$$

where $A_{n,m}$ is the excitation amplitude, $\psi_{n,m}(\theta,\phi)$ is the relative phase of an incident plane wave from the direction (θ,ϕ), $\xi_{n,m}$ is the excitation phase, and $\vec{\mathbf{d}}_{n,m}(\hat{\mathbf{r}}_{n,m})$ is the electric-field vector-directivity function for element n,m, and the direction to the field point is

$$\hat{\mathbf{r}}_{n,m} \equiv \frac{\vec{\mathbf{r}} - \vec{\mathbf{p}}_{n,m}}{\left|\vec{\mathbf{r}} - \vec{\mathbf{p}}_{n,m}\right|}. \tag{5.8}$$

A radiation pattern for a particular polarization is obtained from $\hat{\mathbf{e}} \cdot \vec{\mathbf{d}}_{array}(\vec{\mathbf{r}})$, where $\hat{\mathbf{e}}$ is the unit vector in the direction of the particular polarization. For elliptical or circular polarization, $\hat{\mathbf{e}}$ is complex. The directivity of the array for that polarization is obtained from the normalized radiation function as described in Appendix II. The normalized radiation function, or array factor, has a peak amplitude of one, and is the form in which array-pattern information is presented here.

With reference to the center of the array, the propagation phase at the nth element in the mth row at frequency *f* will is

$$\psi_{n,m} = -2\pi \frac{f}{c}\left(\left|\vec{\mathbf{r}} - \vec{\mathbf{p}}_{n,m}\right| - \left|\vec{\mathbf{r}} - \vec{\mathbf{p}}_0\right|\right), \tag{5.9}$$

where $\vec{\mathbf{p}}_0$ is the center of the array. In an odd array, the $(0,0)$ element is located at the array center, which is

$$\vec{\mathbf{p}}_0 = \vec{\mathbf{p}}_{0,0} = x_a \hat{\mathbf{x}}. \tag{5.10}$$

For an even array, there is no $(0,0)$ element, and the array center is

$$\vec{\mathbf{p}}_0 = 0. \tag{5.11}$$

For the odd array, the propagation phase is

$$\psi_{n,m} = \begin{cases} 2\pi \dfrac{f}{c}\left[n\Delta x \sin\theta\cos\phi + m\Delta y \sin\theta\sin\phi\right], \ m \text{ even} \\ 2\pi \dfrac{f}{c}\left[\left(x_b - x_a + n\Delta x\right)\sin\theta\cos\phi + m\Delta y \sin\theta\sin\phi\right], \ m \text{ odd} \end{cases}. \tag{5.12}$$

From (5.10) and (5.12),

$$\psi_{n,m} = \begin{cases} n\kappa_x + m\kappa_y, \ m \text{ even} \\ \left(\dfrac{x_b - x_a}{\Delta x} + n\right)\kappa_x + m\kappa_y, \ m \text{ odd} \end{cases}. \tag{5.13}$$

In the above equations

$$\kappa_x \equiv k_0 \Delta x \sin\theta\cos\phi, \tag{5.14}$$

$$\kappa_y \equiv k_0 \Delta y \sin\theta\sin\phi, \tag{5.15}$$

$$\Delta x = \Delta x_{odd} = \frac{L_x}{2N}, \tag{5.16}$$

$$\Delta y = \Delta y_{odd} = \frac{L_y}{2M}, \tag{5.17}$$

and

$$k_0 = 2\pi \frac{f}{c}. \tag{5.18}$$

For the even array, the propagation phase is

$$\psi_{n,m} = \begin{cases} 2\pi \dfrac{f}{c}\left[\sin\theta\cos\phi\left(\dfrac{x_a}{\Delta x} + n - \tfrac{1}{2}\operatorname{sgn}(n)\right)\Delta x + \sin\theta\sin\phi\left(m - \tfrac{1}{2}\operatorname{sgn}(m)\right)\Delta y\right], \ m \text{ even} \\ 2\pi \dfrac{f}{c}\left[\sin\theta\cos\phi\left(\dfrac{x_b}{\Delta x} + n - \tfrac{1}{2}\operatorname{sgn}(n)\right)\Delta x + \sin\theta\sin\phi\left(m - \tfrac{1}{2}\operatorname{sgn}(m)\right)\Delta y\right], \ m \text{ odd} \end{cases}, \tag{5.19}$$

where

$$\Delta x = \Delta x_{even} = \frac{L_x}{2N-1}, \tag{5.20}$$

$$\Delta y = \Delta y_{even} = \frac{L_y}{2M-1}. \tag{5.21}$$

Defining incremental excitation phases, ξ_x and ξ_y, the excitation phase for the *n*, *m* element in the odd array is

$$\xi_{n,m} \equiv \begin{cases} n\xi_x + m\xi_y, \ m \text{ even} \\ \left(\dfrac{x_b - x_a}{\Delta x} + n\right)\xi_x + m\xi_y, \ m \text{ odd} \end{cases}. \tag{5.22}$$

In the even array, the excitation phase for the *n*, *m* element is

$$\xi_{n,m} \equiv \begin{cases} \left(\dfrac{x_a}{\Delta x} + n - \tfrac{1}{2}\operatorname{sgn}(n)\right)\xi_x + \left(m - \tfrac{1}{2}\operatorname{sgn}(m)\right)\xi_y, \ m \text{ even} \\ \left(\dfrac{x_b}{\Delta x} + n - \tfrac{1}{2}\operatorname{sgn}(n)\right)\xi_x + \left(m - \tfrac{1}{2}\operatorname{sgn}(m)\right)\xi_y, \ m \text{ odd} \end{cases}. \tag{5.23}$$

The incremental steering phases are

$$\begin{aligned} \xi_x &= k_0 \Delta x \sin\theta_\xi \cos\phi_\xi \\ \xi_y &= k_0 \Delta y \sin\theta_\xi \sin\phi_\xi \end{aligned}. \tag{5.24}$$

Now the main lobe of the array factor will be steered to the spherical angles give by

$$\theta_\xi = \sin^{-1}\sqrt{\left(\frac{\xi_x}{k_0\Delta x}\right)^2 + \left(\frac{\xi_y}{k_0\Delta y}\right)^2}, \tag{5.25}$$

and

$$\phi_\xi = \tan^{-1}\left(\frac{\xi_y}{\xi_x}\frac{\Delta x}{\Delta y}\right), \tag{5.26}$$

or

$$\phi_\xi = \cos^{-1}\left(\frac{\xi_x}{\sqrt{\xi_x^2 + \frac{\Delta x^2}{\Delta y^2}\xi_y^2}}\right) = \sin^{-1}\left(\frac{\xi_y}{\sqrt{\frac{\Delta y^2}{\Delta x^2}\xi_x^2 + \xi_y^2}}\right). \tag{5.27}$$

5.1 Far-field radiation pattern and the array factor

In order to simplify the computation of the far-field radiation pattern of the array, it is assumed that the radiation pattern of each element is identical so that it can be factored from the summation. This is an approximation, which is very good for the interior elements of a large array, but becomes less precise for the elements near the edge. Nevertheless, it is useful, even for small arrays, in that it allows an expression for an array factor, S_{array}, to be obtained. Thus, when $\vec{\mathbf{d}}_{n,m}\left(\hat{\mathbf{r}}_{n,m}\right) \cong \vec{\mathbf{d}}_{n',m'}\left(\hat{\mathbf{r}}_{n',m'}\right) = \vec{\mathbf{d}}\left(\hat{\mathbf{r}}\right)$ for all elements in the array (this condition requires $\left|\vec{\mathbf{r}}\right|$ much greater than array dimensions so that $\hat{\mathbf{r}}_{n,m} \cong \hat{\mathbf{r}}_{n',m'} = \hat{\mathbf{r}}$, in addition to an array composed of a large number of elements), then

$$\vec{\mathbf{d}}_{array}\left(\vec{\mathbf{r}}\right) \cong \vec{\mathbf{d}}\left(\hat{\mathbf{r}}\right)\sum_{n,m} A_{n,m} e^{j\left(\psi_{n,m} - \xi_{n,m}\right)} = \vec{\mathbf{d}}\left(\hat{\mathbf{r}}\right) S_{array}\left(\hat{\mathbf{r}},[\xi]\right), \tag{5.28}$$

where the array factor is defined

$$S_{array}\left(\hat{\mathbf{r}},[\xi]\right) \equiv \sum_{n,m} A_{n,m} e^{j\left(\psi_{n,m} - \xi_{n,m}\right)}, \tag{5.29}$$

and $\left[\xi\right]$ is the matrix of excitation phases. The excitation phases are functions of the signal instantaneous frequency and the direction, $\hat{\mathbf{r}}$, to which the beam is steered. With no loss of generality in the array factor (5.29), the assumption is made that the excitation amplitudes are real, that $A_{n,m} \geq 0$, that all excitation phase components are described by $\left[\xi\right]$, and that the excitation amplitudes are normalized so that

$$\sum_{n,m} A_{n,m} = 1. \tag{5.30}$$

Thus, the array factor is also normalized so

$$\max\left[S_{array}\left(\hat{\mathbf{r}},[\xi]\right)\right] = 1. \tag{5.31}$$

5.1.1 Directivity of the array factor

The peak directivity of an array of isotropic radiators is

$$D_{array} = 4\pi / \Omega_{array}, \tag{5.32}$$

where Ω_{array} is the beam solid angle, which is obtained by integrating the square of the normalized array factor over all solid angles [6],

$$\Omega_{array} = \int_0^{2\pi}\int_0^{\pi}\left|S_{array}\left(\theta,\phi\right)\right|^2 \sin\theta d\theta d\phi. \tag{5.33}$$

However, it is probably more realistic to assume a semi-isotropic radiator, i.e. a radiator that radiates uniformly only in one half space. Thus, for the planar arrays considered here, the beam solid angle is redefined

$$\Omega_{array} = \int_0^{2\pi}\int_0^{\pi/2}\left|S_{array}\left(\theta,\phi\right)\right|^2 \sin\theta d\theta d\phi, \tag{5.34}$$

where the integration over θ stops at $\pi/2$ rather than π. Using this definition, the array directivity pattern is

$$D\left(\hat{\mathbf{r}},[\xi]\right) \equiv \frac{4\pi}{\Omega_{array}}\left|S_{array}\left(\hat{\mathbf{r}},[\xi]\right)\right|^2 . \tag{5.35}$$

For the odd array (see Appendix II)

$$\Omega_{odd\ array} = 2\pi \sum_{n=-N}^{N}\sum_{n'=-N}^{N}\sum_{m=-M}^{M}\sum_{m'=-M}^{M} A_{n,m}A^*_{n',m'}\cos\left(\xi_{n,m}-\xi_{n',m'}\right)\mathrm{sinc}\left(2\pi\frac{f}{c}\sqrt{\left(\beta_{x,n}-\beta_{x,n'}\right)^2+\left(\beta_{y,m}-\beta_{y,m'}\right)^2}\right) \tag{5.36}$$

and for the even array

$$\Omega_{even\ array} = 2\pi \sum_{\substack{n=-N\\ n\neq 0}}^{N}\sum_{\substack{n'=-N\\ n'\neq 0}}^{N}\sum_{\substack{m=-M\\ m\neq 0}}^{M}\sum_{\substack{m'=-M\\ m'\neq 0}}^{M} A_{n,m}A^*_{n',m'}\cos\left(\xi_{n,m}-\xi_{n',m'}\right)\mathrm{sinc}\left(2\pi\frac{f}{c}\sqrt{\left(\beta_{x,n}-\beta_{x,n'}\right)^2+\left(\beta_{y,m}-\beta_{y,m'}\right)^2}\right) \tag{5.37}$$

where

$$\mathrm{sinc}\left(x\right) \equiv \begin{cases} \dfrac{\sin\left(x\right)}{x} \text{ for } x \neq 0 \\ 1 \text{ for } x = 0 \end{cases}, \tag{5.38}$$

and x is in radians. For the odd array,

$$\beta_{x,n} = \begin{cases} n\Delta x,\ m \text{ even} \\ \left(x_b - x_a + n\Delta x\right),\ m \text{ odd} \end{cases}, \tag{5.39}$$

and

$$\beta_{y,m} = m\Delta y . \tag{5.40}$$

For the even array

$$\beta_{x,n} = \begin{cases} x_a + \left(n - \tfrac{1}{2}\mathrm{sgn}\left(n\right)\right)\Delta x,\ m \text{ even} \\ \left(x_b + \left(n - \tfrac{1}{2}\mathrm{sgn}\left(n\right)\right)\Delta x\right),\ m \text{ odd} \end{cases}, \tag{5.41}$$

and

$$\beta_{y,m} = \left(m - \tfrac{1}{2}\mathrm{sgn}\left(m\right)\right)\Delta y . \tag{5.42}$$

For (5.36) and (5.37) to be valid, the coefficients, $A_{n,m}$, must be normalized according to (5.30). Also, $\xi_{n,m}$ are the appropriate excitation (or steering) phases given by (5.22) for the odd array and (5.23) for the even array. The array directivity will be a function of the position to which it is scanned.

For the special case of a symmetric array with a rectangular lattice ($x_a = x_b$, $A_{n,m} = A_{\pm n,\pm m}$), then

$$\Omega_{Array} = 2\pi \sum_{n=-N}^{N}\sum_{n'=-N}^{N}\sum_{m=-M}^{M}\sum_{m'=-M}^{M} A_{n,m}A^*_{n',m'}\cos\left(\left(n-n'\right)\xi_x+\left(m-m'\right)\xi_y\right)\mathrm{sinc}\left(2\pi\frac{f}{c}\sqrt{\left(n-n'\right)^2\Delta x^2+\left(m-m'\right)^2\Delta y^2}\right), \tag{5.43}$$

for the odd array, and

$$\Omega_{array} = 8\pi \sum_{n=1}^{N}\sum_{n'=1}^{N}\sum_{m=1}^{M}\sum_{m'=1}^{M} A_{n,m}A_{n',m'} \begin{pmatrix} \cos\left((n-n')\xi_x\right)\cos\left((m-m')\xi_y\right)\mathrm{sinc}\left(2\pi\frac{f}{c}\sqrt{(n-n')^2\Delta x^2+(m-m')^2\Delta y^2}\right) \\ +\cos\left((n-n')\xi_x\right)\cos\left((m+m'-1)\xi_y\right)\mathrm{sinc}\left(2\pi\frac{f}{c}\sqrt{(n-n')^2\Delta x^2+(m+m'-1)^2\Delta y^2}\right) \\ +\cos\left((n+n'-1)\xi_x\right)\cos\left((m-m')\xi_y\right)\mathrm{sinc}\left(2\pi\frac{f}{c}\sqrt{(n+n'-1)^2\Delta x^2+(m-m')^2\Delta y^2}\right) \\ +\cos\left((n+n'-1)\xi_x\right)\cos\left((m+m'-1)\xi_y\right)\mathrm{sinc}\left(2\pi\frac{f}{c}\sqrt{(n+n'-1)^2\Delta x^2+(m+m'-1)^2\Delta y^2}\right) \end{pmatrix} \tag{5.44}$$

for the even array. In (5.44) ξ_x and ξ_y are the incremental steering phases given by (5.24).

5.2 Effect of element weight errors on array factor

When errors exist in the element weights, whether from quantization or other sources, the array factor, of course, will deviate from the ideal array factor. The realized array factor will be

$$S_{realized}\left(\hat{\mathbf{r}},[\xi]\right) \equiv \sum_{n,m}\left(A_{n,m} - \Delta A_{n,m}\right)e^{j\left(\psi_{n,m}-\xi_{n,m}\right)}, \tag{5.45}$$

where $A_{n,m}$ is the ideal element weight and $\Delta A_{n,m}$ is the error. In general, the error term, $\Delta A_{n,m}$, can be complex. However, only amplitude errors are considered here, since phase errors are considered separately in the analysis of the quantization of the steering phase. The realized array factor can be considered as the difference of two array factors, the ideal array factor (5.29), and the error-array factor

$$S_{error}\left(\hat{\mathbf{r}},[\xi]\right) \equiv \sum_{n,m}\Delta A_{n,m}e^{j\left(\psi_{n,m}-\xi_{n,m}\right)}. \tag{5.46}$$

However, it is convenient and follows tradition to describe amplitudes and amplitude errors as ratios in decibels. For example, the quantization error in a digital attenuator is described in (4.4) in decibels with respect to the desired attenuation value. Thus, by writing the array factor as

$$S_{realized}\left(\hat{\mathbf{r}},[\xi]\right) \equiv \sum_{n,m}A_{n,m}\eta_{n,m}e^{j\left(\psi_{n,m}-\xi_{n,m}\right)}, \tag{5.47}$$

the error factor

$$\eta_{n,m} = \left(1 - \frac{\Delta A_{n,m}}{A_{n,m}}\right) \tag{5.48}$$

can be written as a ratio, described in decibels

$$\eta_{n,m}(\mathrm{dB}) = 20\log\left(1 - \frac{\Delta A_{n,m}}{A_{n,m}}\right). \tag{5.49}$$

If the T/R modules have a random variation in gain (decibels) that is larger than the least significant bit, the resulting attenuator errors (dB) will be approximately uniformly distributed over

$$-\frac{a_{range}}{2\left(2^b-1\right)} \le \eta_{dB} \le \frac{a_{range}}{2\left(2^b-1\right)} \tag{5.50}$$

with zero mean (section 2.2 Distribution of random phase errors). In this case, the mean of the error factor is

$$\bar{\eta} = \frac{1}{2\alpha}\int_{-\alpha}^{\alpha} 10^{\eta_{dB}/20}\,d\eta_{dB}, \tag{5.51}$$

where

$$\alpha = \frac{a_{range}}{2\left(2^b - 1\right)}. \tag{5.52}$$

Note that a_{range} is given in decibels, and so α is given in decibels. Thus, the mean error factor (a ratio, not in decibels) is given by

$$\bar{\eta} = 10\frac{10^{-\alpha/20}\left(10^{\alpha/10} - 1\right)}{\alpha \ln(10)}, \tag{5.53}$$

which will be near unity for small errors. For small error limits

$$\bar{\eta} = 1 + \frac{\ln^2(10)\alpha^2}{2,400} + \frac{\ln^4(10)\alpha^4}{19,200,000} + \mathrm{O}\left(\alpha^6\right). \tag{5.54}$$

The variance of the weight error is

$$\sigma_\eta^2 = \frac{1}{2\alpha}\int_{-\alpha}^{\alpha}\left(10^{\eta_{dB}/20} - \bar{\eta}\right)^2 d\eta_{dB} = \frac{1}{2\alpha}\int_{-\alpha}^{\alpha} 10^{\eta_{dB}/10} d\eta_{dB} - \bar{\eta}^2, \tag{5.55}$$

so

$$\sigma_\eta^2 = 5\frac{10^{-\alpha/10}}{\alpha\ln(10)}\left[\left(10^{\alpha/5} - 1\right) - 20\frac{\left(10^{\alpha/10} - 1\right)^2}{\alpha\ln(10)}\right]. \tag{5.56}$$

For small errors

$$\sigma_\eta^2 = \frac{\ln^2(10)}{1200}\alpha^2\left(1 + \frac{\ln^2(10)}{1500}\alpha^2\right) + \mathrm{O}\left(\alpha^6\right). \tag{5.57}$$

It is appropriate to define an expected directivity for the array, assuming that the elements are isotropic,

$$\begin{aligned}\bar{D}\left(\hat{\mathbf{r}},[\xi]\right) &\equiv \frac{4\pi}{\sum_{n,m}\left|A_{n,m}\right|^2} E\left[\left|S_{realized}\left(\hat{\mathbf{r}},[\xi]\right)\right|^2\right] \\ &= \frac{4\pi}{\sum_{n,m}\left|A_{n,m}\right|^2} E\left[\sum_{n,m}\sum_{n',m'}\left(A_{n,m}\eta_{n,m}\right)\left(A_{n',m'}\eta_{n',m'}\right)e^{j\left(\psi_{n,m} - \psi_{n',m'} - \xi_{n,m} + \xi_{n',m'}\right)}\right],\end{aligned} \tag{5.58}$$

where $E[\ ]$ is the expectation operator

$$E\left[f(\zeta)\right] = \int_{-\infty}^{\infty} f(\zeta)\, p(\zeta)\, d\zeta, \tag{5.59}$$

with $p(\zeta)$ the probability density function for ζ. The probability density function has the property that

$$\int_{-\infty}^{\infty} p(\zeta)\, d\zeta = 1. \tag{5.60}$$

In (5.58), the expectation operator is comprised of integrations over all of the random variables, $\eta_{n,m}$, which are assumed to be identically distributed and independent random variables. In respect to the array

properties, the expectation represents an average of the property over an ensemble of arrays, each having its own set of fixed errors.

The expected directivity is

$$\bar{D}\left(\hat{\mathbf{r}},[\xi]\right)=\bar{\eta}^2 D\left(\hat{\mathbf{r}},[\xi]\right)+4\pi\sigma_\eta^2 . \tag{5.61}$$

Thus, the average (or expected) directivity pattern has a directivity that differs from the ideal directivity by a factor of $\bar{\eta}^2$, and an error-sidelobe term that is independent of position. The error-sidelobe ratio is

$$SLL_{error}=\frac{4\pi\sigma_\eta^2}{\bar{\eta}^2 G\left(\hat{\mathbf{r}},[\xi]\right)}=\frac{\sigma_\eta^2}{\bar{\eta}^2}\frac{\sum_{n,m}\left|A_{n,m}\right|^2}{\left|\sum_{n,m}A_{n,m}\right|^2} . \tag{5.62}$$

When the array is uniformly illuminated with $A_{n.m}=1$ for all n,m, then the error-sidelobe ratio is

$$SLL_{error}=\frac{\sigma_\eta^2}{\bar{\eta}^2}\frac{1}{N_{total}M_{total}} \text{ for uniform illumination ,} \tag{5.63}$$

where

$$\left\{N_{total},M_{total}\right\}=\begin{cases}\left\{2N+1,\,2M+1\right\} & \text{for odd array}\\ \left\{2N,\,2M\right\} & \text{for even array}\end{cases} . \tag{5.64}$$

Obviously, from an examination of (5.62) and (5.63), it is clear that larger arrays are more tolerant of amplitude errors.

6. Uniformly illuminated array

If the array is uniformly illuminated so that $A_{n,m}=1$ for all n,m, then the array factor will be very similar for both the odd and even arrays. This situation results because all elements contribute equally, so having an even or odd number is not very significant.

6.1 Odd array

For the odd array, the array factor can be written

$$S_{array}\left(\hat{\mathbf{r}},\xi_x,\xi_y\right)=\frac{\sin\left(\left(2N+1\right)\frac{\left(\kappa_x-\xi_x\right)}{2}\right)}{\sin\left(\frac{\left(\kappa_x-\xi_x\right)}{2}\right)}\frac{\sin\left(\left(2M+1\right)\frac{\left(\kappa_y-\xi_y\right)}{2}\right)}{\sin\left(\frac{\left(\kappa_y-\xi_y\right)}{2}\right)} . \tag{6.1}$$

Zeros in the array factor occur when

$$\left(2N+1\right)\frac{\left(\kappa_x-\xi_x\right)}{2}=p\pi,\ p=\pm1,\pm2,\pm3,\cdots , \tag{6.2}$$

and

$$(2M+1)\frac{(\kappa_y-\xi_y)}{2}=q\pi,\ q=\pm1,\pm2,\pm3,\cdots. \tag{6.3}$$

From (6.2) and (6.3), we obtain the location of the zeros,

$$\theta=\sin^{-1}\left(\frac{1}{k_0}\sqrt{\frac{1}{\Delta x^2}\left(\xi_x+\frac{2p\pi}{(2N+1)}\right)^2+\frac{1}{\Delta y^2}\left(\xi_y+\frac{2q\pi}{(2M+1)}\right)^2}\right),\begin{cases}p=\pm1,\pm2,\pm3,\cdots\\ q=\pm1,\pm2,\pm3,\cdots\end{cases}, \tag{6.4}$$

and

$$\phi=\tan^{-1}\left(\frac{\Delta x}{\Delta y}\frac{\left(\xi_y+\frac{2q\pi}{(2M+1)}\right)}{\left(\xi_x+\frac{2p\pi}{(2N+1)}\right)}\right),\begin{cases}p=\pm1,\pm2,\pm3,\cdots\\ q=\pm1,\pm2,\pm3,\cdots\end{cases}. \tag{6.5}$$

When the beam of the uniformly illuminated odd array is pointed to broadside, the 3–dB beamwidth, $\Delta\theta_{3dB}$, in the plane defined by $\hat{\mathbf{z}}$ and $\hat{\mathbf{x}}\cos\phi+\hat{\mathbf{y}}\sin\phi$ can be estimated with accuracy better than 2% when $N,M>2$ by

$$\begin{aligned}\Delta\theta_{3dB}(\phi)=2\theta_{3dB}(\phi)&\cong 2\sin^{-1}\left(\frac{0.2215\lambda}{\sqrt{N(N+1)\Delta x^2\cos^2(\phi)+M(M+1)\Delta y^2\sin^2\phi}}\right)\\ &\cong\frac{0.443\lambda}{\sqrt{N(N+1)\Delta x^2\cos^2(\phi)+M(M+1)\Delta y^2\sin^2\phi}}\end{aligned} \tag{6.6}$$

When the beam is steered to a position $\{\theta_0,\phi_0\}$, the 3–dB beamwidth in the plane defined by $\hat{\mathbf{z}}$ and $\hat{\mathbf{x}}\cos\phi_0+\hat{\mathbf{y}}\sin\phi_0$ is approximated by

$$\begin{aligned}\Delta\theta_{3dB}(\phi_0)=2\theta_{3dB}(\phi_0)\cong&\sin^{-1}\left(\sin(\theta_0)+\frac{0.2215\lambda}{\sqrt{N(N+1)\Delta x^2\cos^2(\phi_0)+M(M+1)\Delta y^2\sin^2\phi_0}}\right)\\ &-\sin^{-1}\left(\sin(\theta_0)-\frac{0.2215\lambda}{\sqrt{N(N+1)\Delta x^2\cos^2(\phi_0)+M(M+1)\Delta y^2\sin^2\phi_0}}\right)\end{aligned}. \tag{6.7}$$

This approximation is obtained by expanding the array factor (6.1) in a power series in $s=\sin(\theta)-\sin(\theta_0)$.

Another approach to approximating the 3–dB beamwidth gives

$$\Delta\theta_{3dB}(\phi_0)=2\theta_{3dB}(\phi_0)\cong\frac{0.443\lambda}{\cos(\theta_0)\sqrt{N(N+1)\Delta x^2\cos^2(\phi_0)+M(M+1)\Delta y^2\sin^2\phi_0}}. \tag{6.8}$$

This expression gives essentially the same result as (6.7), but explicit in this approximation is the $1/\cos(\theta_0)$ factor, which makes clear that the projected area of the array has a major roll in determining the beamwidth. This approximation is obtained by expanding the array factor in $\delta\theta$ after the substitution $\sin(\theta)=\sin(\theta_0+\delta\theta)$ into (6.1). The approximations(6.7) and (6.8) also assume

$$\xi_x = k_0 \Delta x \sin(\theta_0)\cos(\phi_0)$$
$$\xi_y = k_0 \Delta y \sin(\theta_0)\sin(\phi_0)\,.$$
$$\phi = \phi_0$$

Thus, the expression for the 3–dB beamwidth applies only in the plane defined by $\hat{\mathbf{z}}$ and $\hat{\mathbf{x}}\cos\phi_0 + \hat{\mathbf{y}}\sin\phi_0$. See Appendix III for a method of defining the beamwidth when the beam is steered away from the normal to the array.

The 3–dB beamwidth broadens slightly as θ_0 increases from broadside, at $\theta_0 = 0°$, and has broadened significantly by the time the beam is scanned to $\theta_0 \to 45°$ to $60°$. In fact, when the element spacing is $\lambda/2$, the beamwidth has been broadened by about a factor of two at $\theta_0 = 60°$, and is about 5 or 6 times broader near $\theta_0 = 80°$ than at broadside. The broadening is more pronounced for closely spaced elements, but when the spacing exceeds the wavelength, λ, the grating-lobe problem occurs. As the beam is scanned to end-fire position, $\theta_0 = 90°$, a portion of the beam is in invisible space, so serious mismatch can occur. It makes sense to limit the scan angle, if consistency of beamwidth is important.

6.2 Even array

For the even array, the array factor can be written

$$S_{array}\left(\hat{\mathbf{r}},\xi_x,\xi_y\right) = \frac{\sin\left(N\left(\kappa_x - \xi_x\right)\right)}{\sin\left(\dfrac{\left(\kappa_x - \xi_x\right)}{2}\right)}\frac{\sin\left(M\left(\kappa_y - \xi_y\right)\right)}{\sin\left(\dfrac{\left(\kappa_y - \xi_y\right)}{2}\right)}\,. \tag{6.9}$$

This array factor has zeros when

$$N\left(\kappa_x - \xi_x\right) = p\pi,\ p = \pm1,\pm2,\pm3,\cdots, \tag{6.10}$$

and

$$M\left(\kappa_y - \xi_y\right) = q\pi,\ q = \pm1,\pm2,\pm3,\cdots. \tag{6.11}$$

From (6.10) and (6.11), we obtain the location of the zeros

$$\theta = \sin^{-1}\left(\frac{1}{k_0}\sqrt{\frac{1}{\Delta x^2}\left(\xi_x + \frac{p\pi}{N}\right)^2 + \frac{1}{\Delta y^2}\left(\xi_y + \frac{q\pi}{M}\right)^2}\right), \begin{cases} p = \pm1,\pm2,\pm3,\cdots \\ q = \pm1,\pm2,\pm3,\cdots \end{cases}, \tag{6.12}$$

and

$$\phi = \tan^{-1}\left(\frac{\Delta x}{\Delta y}\frac{\left(\xi_y + \dfrac{q\pi}{(M)}\right)}{\left(\xi_x + \dfrac{p\pi}{N}\right)}\right), \begin{cases} p = \pm1,\pm2,\pm3,\cdots \\ q = \pm1,\pm2,\pm3,\cdots \end{cases}. \tag{6.13}$$

When the beam of the uniformly illuminated even array is pointed to broadside, the 3–dB beamwidth in the plane defined by $\hat{\mathbf{z}}$ and $\hat{\mathbf{x}}\cos\phi + \hat{\mathbf{y}}\sin\phi$ can be estimated with accuracy better than 2% when $N, M > 2$ by

$$\Delta\theta_{3dB}(\phi) = 2\theta_{3dB}(\phi) \cong 2\sin^{-1}\left(\frac{0.2215\lambda}{\sqrt{\left(N^2-\frac{1}{4}\right)\Delta x^2\cos^2(\phi)+\left(M^2-\frac{1}{4}\right)\Delta y^2\sin^2\phi}}\right).$$
$$\cong \frac{0.443\lambda}{\sqrt{\left(N^2-\frac{1}{4}\right)\Delta x^2\cos^2(\phi)+\left(M^2-\frac{1}{4}\right)\Delta y^2\sin^2\phi}} \tag{6.14}$$

When the beam is steered to a position $\{\theta_0, \phi_0\}$, the 3–dB beamwidth in the plane defined by $\hat{\mathbf{z}}$ and $\hat{\mathbf{x}}\cos\phi_0 + \hat{\mathbf{y}}\sin\phi_0$ is approximated by

$$\Delta\theta_{3dB}(\phi_0) = 2\theta_{3dB}(\phi_0) \cong \sin^{-1}\left(\sin(\theta_0)+\frac{0.2215\lambda}{\sqrt{\left(N^2-\frac{1}{4}\right)\Delta x^2\cos^2(\phi)+\left(M^2-\frac{1}{4}\right)\Delta y^2\sin^2\phi}}\right)$$
$$-\sin^{-1}\left(\sin(\theta_0)-\frac{0.2215\lambda}{\sqrt{\left(N^2-\frac{1}{4}\right)\Delta x^2\cos^2(\phi)+\left(M^2-\frac{1}{4}\right)\Delta y^2\sin^2\phi}}\right). \tag{6.15}$$

This approximation is obtained by expanding the array factor (6.9) in a power series in $s = \sin(\theta) - \sin(\theta_0)$.

Another approximation for the 3–dB beamwidth is

$$\Delta\theta_{3dB}(\phi_0) = 2\theta_{3dB}(\phi_0) \cong \frac{0.443}{\cos(\theta_0)\sqrt{\left(N^2-\frac{1}{4}\right)\Delta x^2\cos^2(\phi)+\left(M^2-\frac{1}{4}\right)\Delta y^2\sin^2\phi}}, \tag{6.16}$$

which is essentially the same result as (6.15), but explicitly contains the $1/\cos(\theta_0)$ factor. This shows that the projected area of the array has a major roll in determining the beamwidth. This approximation is obtained by expanding the array factor in $\delta\theta$ after the substitution $\sin(\theta) = \sin(\theta_0 + \delta\theta)$ into (6.9). The expression for the 3–dB beamwidth applies only in the plane defined by $\hat{\mathbf{z}}$ and $\hat{\mathbf{x}}\cos\phi_0 + \hat{\mathbf{y}}\sin\phi_0$.

Like the beamwidth of the odd array, the 3–dB beamwidth broadens slightly as θ_0 increases from broadside, at $\theta_0 = 0°$, and has broadened significantly by the time the beam is scanned to $\theta_0 \to 45°$ to $60°$.

6.3 Comparison of the even and odd uniform arrays

Normalized array factors in the plane $\phi = 0$ for both odd and even arrays are plotted in Figure 22 for $N = 10$ and $\lambda/2$ element spacing. The main difference is in the width of the sidelobes, causing the locations of the nulls and peaks to be shifted at large angles from the main lobe. In this example, at $\theta = 90°$, the even array shows a null, while the odd array shows a peak. However, this effect is dependent on the element spacing, and will be different if the spacing is changed from $\lambda/2$.

The least difference between the odd and even array patterns occurs when the arrays have the same length. Figure 23 illustrates the similarity between the odd and even array patterns when the array length

is the same, while the element spacing is slightly different. For each array, $N = 10$, and the element spacing is $\lambda/2$ for the odd array. For the even array, the element spacing is slightly larger, $\dfrac{\lambda}{2 - 1/N}$. The array factors are nearly identical, with the major differences in the far sidelobe region $60° \le \theta \le 90°$. Clearly, as N is increased, the element spacing becomes closer to the same, and the array patterns will differ even less.

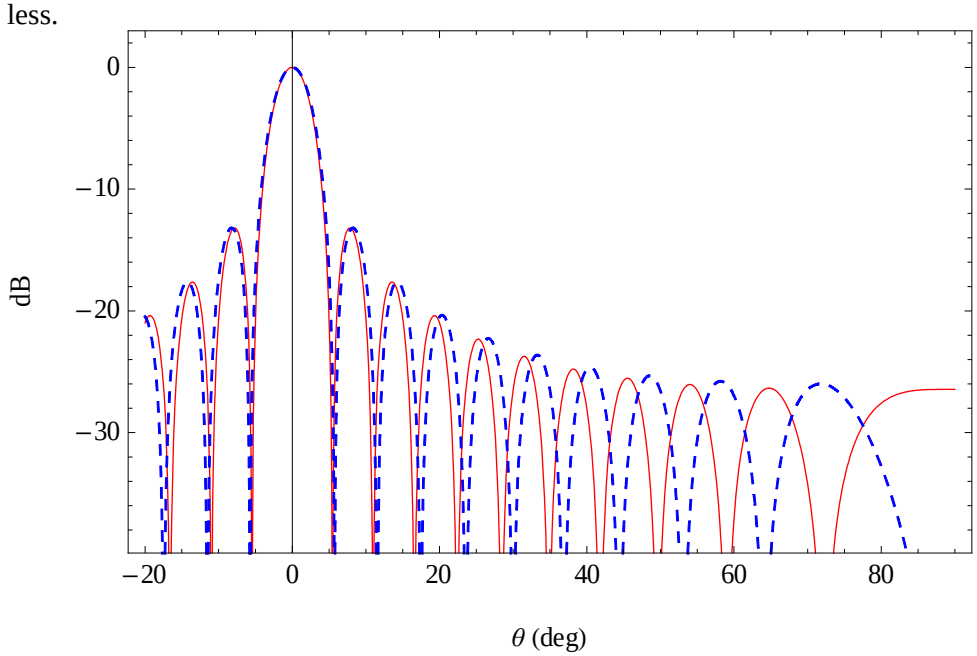

Figure 22 Normalized array factor in the $\phi = 0$ plane for odd array (solid curve) and even array (dashed curve) for $N = 10$ (21 elements and 20 elements respectively), with constant element spacing.

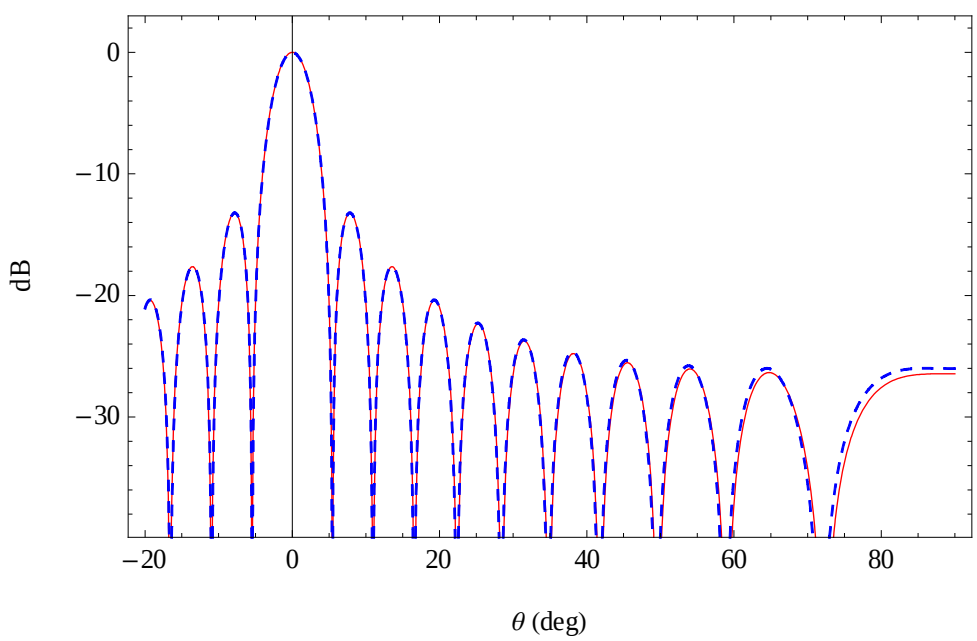

Figure 23 Normalized array factor in the $\phi = 0$ plane for odd array (solid curve) and even array (dashed curve) for $N = 10$ (21 elements and 20 elements respectively), with constant array size.

This Page Intentionally Blank

7. The Taylor array

In order to reduce the sidelobes in an array, it is necessary to taper the illumination from the center to the edges of the array. The Taylor illumination will be treated here. Before considering the quantization error with the discrete Taylor array, some background about the continuous line Taylor distribution will be given. In 1955, Taylor described the illumination for a continuous line source, which is now referred to as the Taylor illumination [1, 7]. Because the Taylor illumination provides a near-optimum beamwidth for a given sidelobe level, it is an appropriate choice for the illumination taper of an array. For simplicity, only the rectangular-grid array, $x_a = x_b = 0$, and the array factor without mutual impedance interactions, are considered in this section.

7.1 Continuous line source

The line source is defined with a length $L = 2a$, and its illumination is an even function about its center. The continuous Taylor illumination model is [1]

$$W(\xi) = 1 + 2\sum_{m=1}^{\bar{n}-1} F_m \cos(\pi m \xi), \tag{7.1}$$

where $\xi = x/a$ is the normalized coordinate along the line source with $x = 0$ at the center, and

$$F_m = \frac{(-1)^{m+1}}{2\prod_{\substack{n=1\\n\neq m}}^{\bar{n}-1}\left(1-\frac{m^2}{n^2}\right)} \prod_{n=1}^{\bar{n}-1}\left[1-\frac{m^2}{\sigma_p^2\left[A^2+\left(n-\frac{1}{2}\right)^2\right]}\right],\ 1 \le m \le \bar{n}-1, \tag{7.2}$$

where the parameter σ_p^2 is given by

$$\sigma_p^2 = \frac{\bar{n}^2}{A^2 + \left(\bar{n}-\frac{1}{2}\right)^2}. \tag{7.3}$$

The peak sidelobe level in decibels is approximately

$$SLL_{dB} \cong -20\log\left(\cosh(\pi A)\right), \tag{7.4}$$

or

$$A \cong \frac{1}{\pi}\cosh^{-1}\left(10^{\frac{-SLL_{dB}}{20}}\right) = \frac{1}{\pi}\ln\left(10^{\frac{-SLL_{dB}}{20}} + \sqrt{10^{\frac{-SLL_{dB}}{10}} - 1}\right). \tag{7.5}$$

The approximation in (7.4) and (7.5) improves as $\bar{n} \to \infty$.

The array factor for the line source is designated $F(u)$, where

$$u = \frac{2a}{\lambda}\sin\theta, \tag{7.6}$$

and θ is measured from the normal to the line source. It is convenient to describe array factors with the variable u because the array factor is independent of array size and beam position in this variable. The normalized $(F(0)=1)$ far-field array factor, $F(u)$, is obtained by applying the Fourier transform to (7.1), and is given by

$$F(u)=\sum_{m=-(\bar{n}-1)}^{\bar{n}-1} F_m \frac{\sin \pi(u+m)}{\pi(u+m)}=\frac{\sin \pi u}{\pi u}+\sum_{m=1}^{\bar{n}-1} F_m\left[\frac{\sin \pi(u+m)}{\pi(u+m)}+\frac{\sin \pi(u-m)}{\pi(u-m)}\right] \tag{7.7}$$

where $F_{-m}=F_m$ is given by (7.2), and $F_0=1$. The Taylor array factor is illustrated in Figure 24 for the case $\bar{n}=10$, and $SLL=-60$ dB.

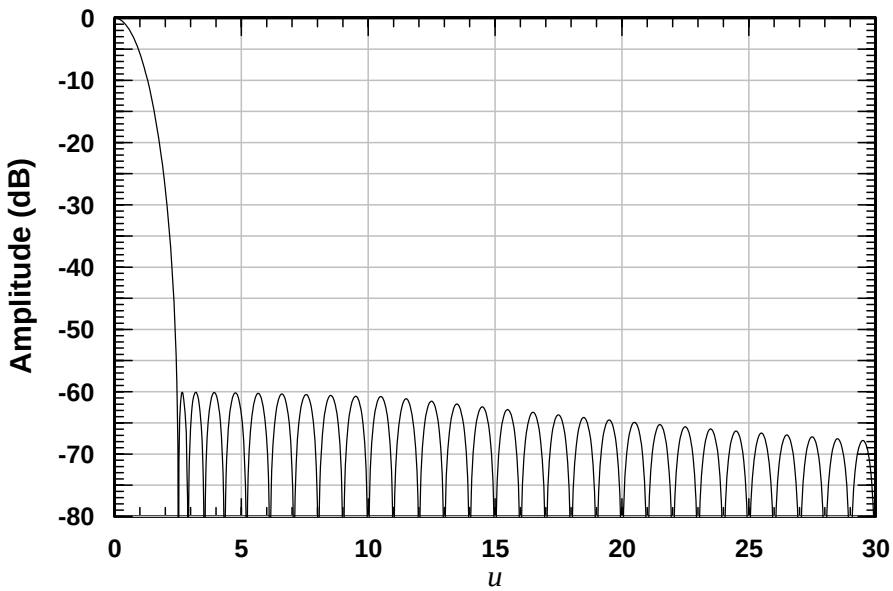

Figure 24 Array factor for a Taylor-weighted continuous linear distribution with $\bar{n}=10$, *and* $SLL=-60$ dB.

The normalized array factor can also be written [1]

$$F(u)=\frac{\sin \pi u}{\pi u} \frac{\prod_{n=1}^{\bar{n}-1}\left[1-\frac{u^2}{\sigma_p^2\left(A^2+\left(n-\frac{1}{2}\right)^2\right)}\right]}{\prod_{n=1}^{\bar{n}-1}\left(1-\frac{u^2}{n^2}\right)}, \tag{7.8}$$

which is not quite as convenient computationally as (7.7) because of the zeros in the denominator at $u=n$, where $1 \le |n| \le \bar{n}-1$. However, $\sin \pi u$ also has a zero at each of these values of *u*, which cancels the equivalent zero in the denominator. What Taylor has actually done, in fact, is to cancel the first $\bar{n}-1$ zeros of $\frac{\sin \pi u}{\pi u}$, and replace them with zeros located at $|u_n|=\sigma_p\sqrt{\left(A^2+\left(n-\frac{1}{2}\right)^2\right)}$. Thus, the first $\bar{n}-1$ pairs of zeros of the Taylor array factor (7.7), (7.8) occur at

$$u_n=\pm\bar{n}\sqrt{\frac{A^2+\left(n-\frac{1}{2}\right)^2}{A^2+\left(\bar{n}-\frac{1}{2}\right)^2}},\ 1 \le n \le \bar{n}-1, \tag{7.9}$$

or

$$\theta_n = \pm\sin^{-1}\left(\frac{\lambda}{2a}\bar{n}\sqrt{\frac{A^2+\left(n-\frac{1}{2}\right)^2}{A^2+\left(\bar{n}-\frac{1}{2}\right)^2}}\right),\ 1 \le n \le \bar{n}-1. \tag{7.10}$$

This process of relocating the first few zeros of the function has the effect of lowering the near sidelobes. Figure 25 illustrates the difference between the array factor due to uniform illumination, $\frac{\sin \pi u}{\pi u}$, and that from the Taylor illumination with $\bar{n} = 5$ and sidelobe level $SLL = -40$ dB. Clearly, the first four zeros of $\frac{\sin \pi u}{\pi u}$ have been moved to new locations, further away from the center of the main lobe. The fifth and higher zeros remain unmoved. Because the zeros have been moved away from the center of the main lobe, of necessity, the mainlobe has become broader. Energy has been transferred from the sidelobe region into the main lobe. Thus, all of the sidelobes have been reduced in amplitude.

The sidelobes far from the main lobe are also of interest. When $u >> \bar{n}-1$, (7.8) shows that

$$F(u) \cong \frac{\sin \pi u}{\pi u}\prod_{n=1}^{\bar{n}-1}\left[\frac{n^2}{\sigma_p^2\left(A^2+\left(n-\frac{1}{2}\right)^2\right)}\right] \text{ for } u >> \bar{n}-1. \tag{7.11}$$

Thus the sidelobes far from the main lobe behave as those from a uniformly illuminated array, but attenuated by a factor

$$\textit{sidelobe attenuation factor} = \prod_{n=1}^{\bar{n}-1}\left[\frac{n^2}{\sigma_p^2\left(A^2+\left(n-\frac{1}{2}\right)^2\right)}\right].$$

Far from the main lobe, the peaks of the sidelobes follow an envelope given by

$$f_{SL}(u) = \frac{1}{\pi u}\prod_{n=1}^{\bar{n}-1}\left[\frac{n^2}{\sigma_p^2\left(A^2+\left(n-\frac{1}{2}\right)^2\right)}\right]. \tag{7.12}$$

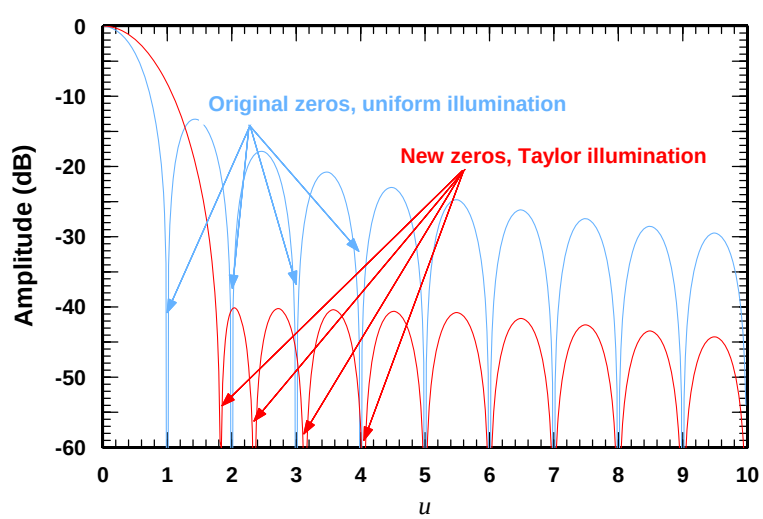

Figure 25 Comparison of array factor for a uniform linear source (dashed) with the array factor for a Taylor-weighted continuous linear distribution with $\bar{n} = 5$, and $SLL = -40$ dB (solid).

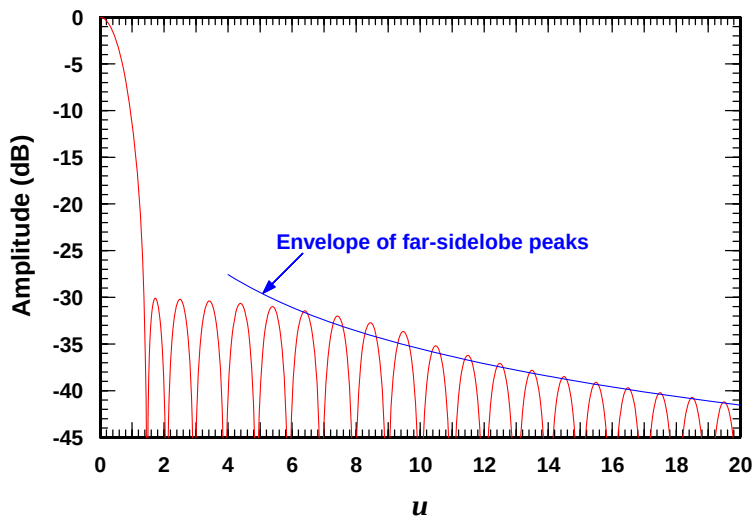

Figure 26 Taylor array factor for $\bar{n} = 10$ *and* $SLL_{dB} = -30$*, showing the far-sidelobe peak envelope given by (7.12).*

7.1.1 Connection between Taylor and Tchebyscheff illumination

The Taylor illumination produces an array factor that is related to the Tchebyscheff polynomials. A Tchebyscheff-shaped array factor is considered optimum in the sense of *minimizing the mainlobe width for a given sidelobe level*, and the normalized version is given by

$$F_{Tchebyscheff}(u, A) = \begin{cases} \dfrac{\cosh\left(\pi\sqrt{A^2 - u^2}\right)}{\cosh(\pi A)}, & |u| \le |A| \\ \dfrac{\cos\left(\pi\sqrt{u^2 - A^2}\right)}{\cosh(\pi A)}, & |u| > |A| \end{cases} . \tag{7.13}$$

Taylor designed his weighting so that the resulting normalized array factor approaches the normalized ideal Tchebyscheff array factor in the region near the main lobe. That is

$$F(u) \approx F_{Tchebyscheff}(u, A), \ |u| < \bar{n} . \tag{7.14}$$

The similarity is illustrated in Figure 27 for -40 dB sidelobes with $\bar{n} = 5$. While the similarity is obvious for $u < \bar{n}$, the agreement is not perfect. The Taylor array approaches the Tchebyscheff array more closely as $\bar{n}$ get larger. While the first few zeros are fairly close to the same for the two array factors, the locations of the zeros disagree more as *u* gets larger. The main difference between the patterns, however, is that the sidelobe level for the Tchebyscheff array remains constant as *u* increases, but the sidelobes begin to fall away after the first few for the Taylor array. The differences between the two arrays are much less significant when $\bar{n} = 35$, as illustrated in Figure 28. However, even with this large value for $\bar{n}$, the Taylor and Tchebyscheff array factors do not agree some distance away from the main lobe, although the agreement of the main lobe and first sidelobes is quite good.

Suppose the width of the main lobe between the first zeros is specified to be $2\theta_0$. Then, from (7.9), we have

$$A = \sqrt{\frac{\frac{4a^2}{\lambda^2}\sin^2\theta_0\left(\bar{n}-\frac{1}{2}\right)^2 - \frac{\bar{n}^2}{4}}{\bar{n}^2 - \frac{4a^2}{\lambda^2}\sin^2\theta_0}}\,, \tag{7.15}$$

and the peak sidelobe level in decibels is approximately

$$SLL_{dB} \cong 20\log\left(\cosh\left(\pi\sqrt{\frac{\frac{4a^2}{\lambda^2}\sin^2\theta_0\left(\bar{n}-\frac{1}{2}\right)^2 - \frac{\bar{n}^2}{4}}{\bar{n}^2 - \frac{4a^2}{\lambda^2}\sin^2\theta_0}}\right)\right). \tag{7.16}$$

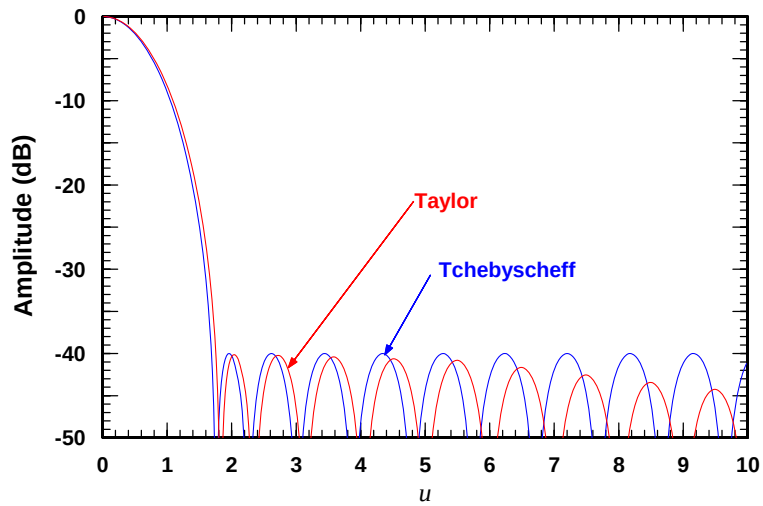

Figure 27 Comparison of Tchebyscheff array factor (blue) and Taylor ($\bar{n} = 5$) array factor (red) for -40 dB *sidelobes.*

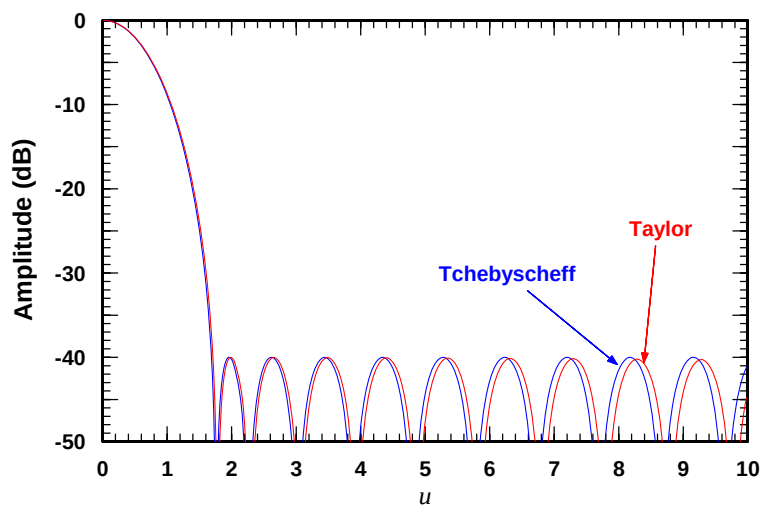

Figure 28 Comparison of Tchebyscheff array factor (blue) and Taylor ($\bar{n} = 35$) array factor (red) for -40 dB *sidelobes.*

When the values for the antenna beamwidth, θ_{3dB}, is specified, the half width of the array, *a*, is determined. To solve for *a*, given *A*, $\bar{n}$ and θ_{3dB}, we will use a Taylor-series expansion

$$F(u+\Delta u) = F(u) + \frac{\partial F}{\partial u}\Delta u + \cdots, \tag{7.17}$$

and iterate

$$u_{3\,dB,i+1} \approx u_{3\,dB,i} - \frac{F\left(u_{3\,dB,i}\right) - \frac{1}{\sqrt{2}}}{\left.\frac{\partial F}{\partial u}\right|_{u=u_{3\,dB,i}}}, \tag{7.18}$$

where

$$\frac{\partial F(u)}{\partial u} = \sum_{m=-(\bar{n}-1)}^{\bar{n}-1} F_m \frac{\pi(u+m)\cos\pi(u+m) - \sin\pi(u+m)}{\pi(u+m)^2}. \tag{7.19}$$

After the iteration has converged, the array half width is

$$a = \frac{\lambda u_{3\,dB}}{2\sin\theta_{3\,dB}}. \tag{7.20}$$

This method of iteration can be unstable if a suitable starting value is not chosen. A useful starting value is $u_{3dB,0} = 0.55$, which was used to start the iterations for the values plotted in Figure 29.

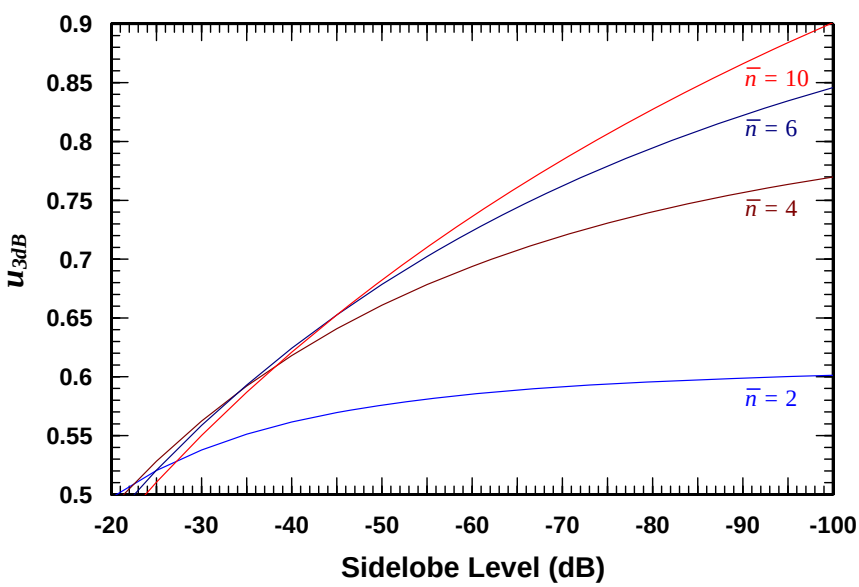

Figure 29 Values of u_{3dB} as a function of sidelobe level.

Sometimes it is useful to compute the 3-dB beamwidth from the array parameters, $a, \bar{n}, SLL$. By expanding (7.7) in a series in θ, and keeping all terms to 4th order, the angle, θ_{3dB}, at which the main lobe is down 3 dB from the peak can be found

$$\theta_{3dB} = \sqrt{\frac{\alpha_2\left(a,\bar{n},SLL\right) - \sqrt{\alpha_2^2\left(a,\bar{n},SLL\right) - 2\left(2-\sqrt{2}\right)\alpha_4\left(a,\bar{n},SLL\right)}}{2\alpha_4\left(a,\bar{n},SLL\right)}}\,, \tag{7.21}$$

where

$$\alpha_2\left(a,\bar{n},SLL\right) = \frac{2}{3}\pi^2 a^2 + 8a^2 \sum_{k=1}^{\bar{n}-1} \left(-1\right)^k \frac{1}{k^2} F_k\left(\bar{n},SLL\right), \tag{7.22}$$

and

$$\begin{aligned}\alpha_4\left(a,\bar{n},SLL\right) = {} & 2\pi^2 a^2 \left(\frac{1}{9} + \frac{1}{15}\pi^2 a^2\right) \\ & + \frac{8}{3} a^2 \sum_{k=1}^{\bar{n}-1} \left(-1\right)^k \frac{1}{k^2} F_k\left(\bar{n},SLL\right)\left(1 + 2\pi^2 a^2 \left(1 - \frac{6}{\pi^2 k^2}\right)\right)\end{aligned}. \tag{7.23}$$

The behavior of the width of the main lobe at –3 dB from the peak can be understood by examining the plots in Figure 30, Figure 31, and Figure 32. The angle from the normal, θ_{3dB}, is plotted as functions of linear-array half-length, *a*, design sidelobe level, *SLL*, or Taylor order, $\bar{n}$, respectively. The example array has $a = 10\lambda$, $\bar{n} = 10$, and $SLL = -40$ dB.

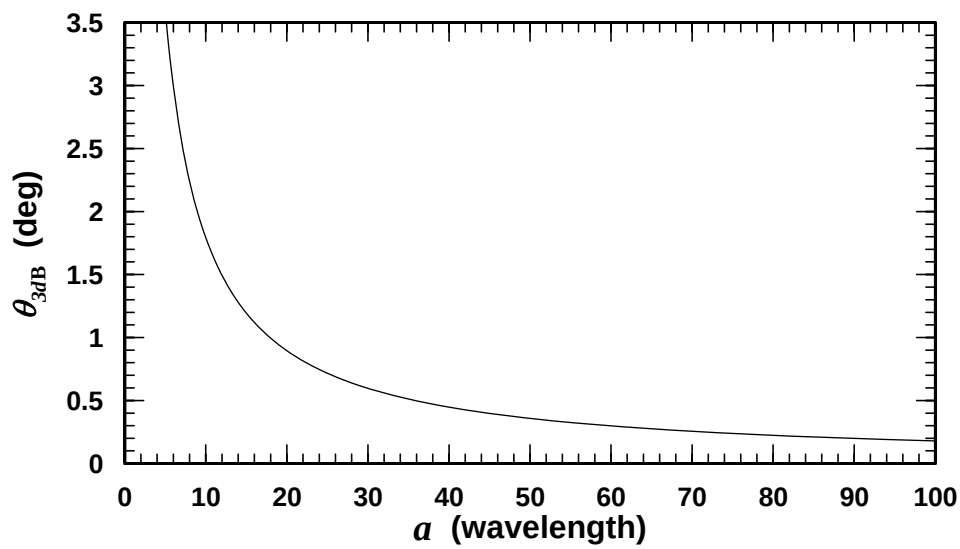

Figure 30 θ_{3dB} *as a function of half-length, a, for* $\bar{n} = 10$ *and* $SLL_{dB} = -40$.

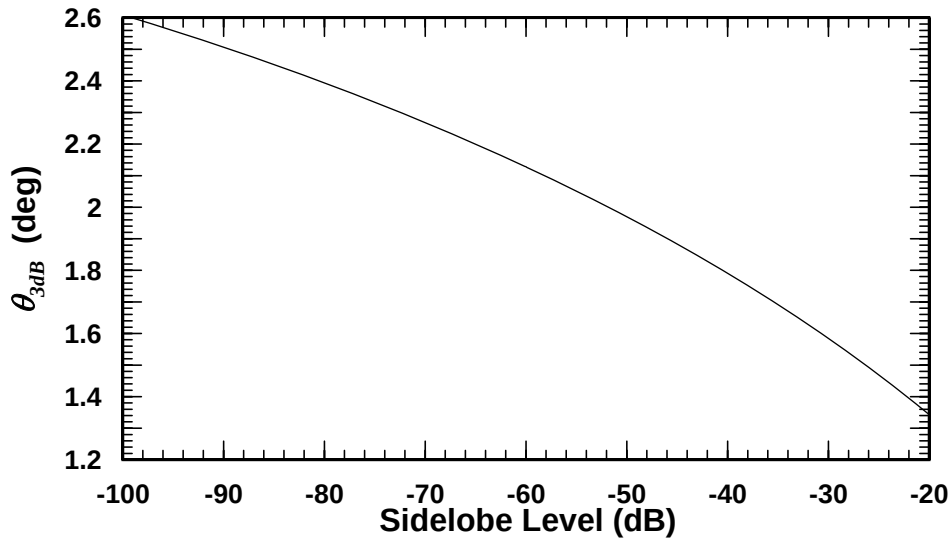

Figure 31 θ_{3dB} *as a function of sidelobe level with half-length* $a = 10\lambda$ *, and* $\bar{n} = 10$.

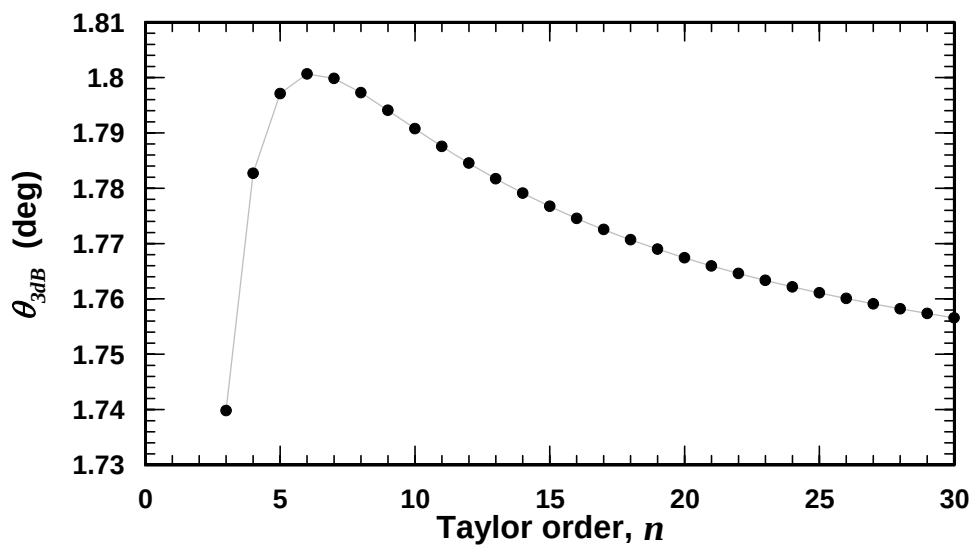

Figure 32 θ_{3dB} *as a function of order,* $\bar{n}$ *, for* $SLL_{dB} = -40$ *and* $a = 10$ wavelengths .

When the order $\bar{n}$ is large, the weighting function does not decrease monotonically as the distance increases away from the array center. Instead, the weighting increases at the edges of the array, as illustrated in Figure 33. However, it is not generally desirable to increase the illumination at the edge of an array, so to avoid this situation, the order, $\bar{n}$, should be constrained.

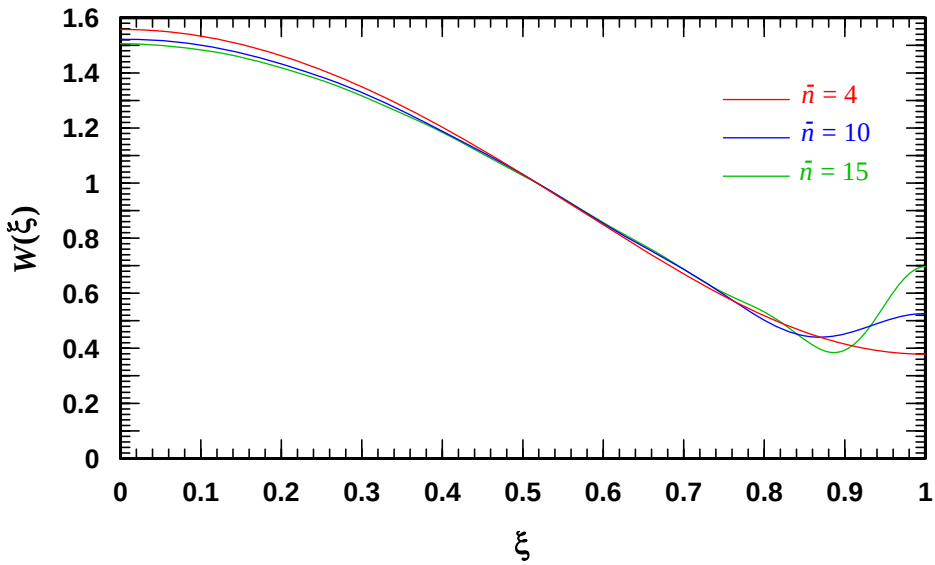

Figure 33 Taylor illumination function, $W(\xi)$*, for* $SLL_{dB} = -30$*, and three different values of* $\bar{n}$*.*

At the edge, the illumination function is

$$W(1) = 1 + 2\sum_{m=1}^{\bar{n}-1} (-1)^m F_m \,. \tag{7.24}$$

The derivative of the illumination function is, from (7.1)

$$\frac{\partial}{\partial \xi} W(\xi) = -2\pi \sum_{m=1}^{\bar{n}-1} m F_m \sin(\pi m \xi), \tag{7.25}$$

leading to n interesting feature of the Taylor illumination that

$$\left.\frac{\partial}{\partial \xi} W(\xi)\right|_{\xi=1} = 0, \tag{7.26}$$

for any $\bar{n}$. Considered as a function of $\bar{n}$, $W(1)$ is a discontinuous function because of the summation. Because the upper limit of the summation index depends on $\bar{n}$, method of handling the upper limit for non-integer $\bar{n}$ is not uniquely determined. For example, the upper index of the sum in (7.1) and the products in (7.2) could be determined by either by taking the integer part of $\bar{n}$, or by rounding $\bar{n}$ to the nearest integer. Rounding to the nearest integer has the desirable effect of moving the discontinuities away from the integer values, which, of course, are the locations where the illumination function is valid. The illumination function is plotted in Figure 34 as a function of real $\bar{n}$ for three different sidelobe levels. The discontinuities are most pronounced for the smaller values of $\bar{n}$.

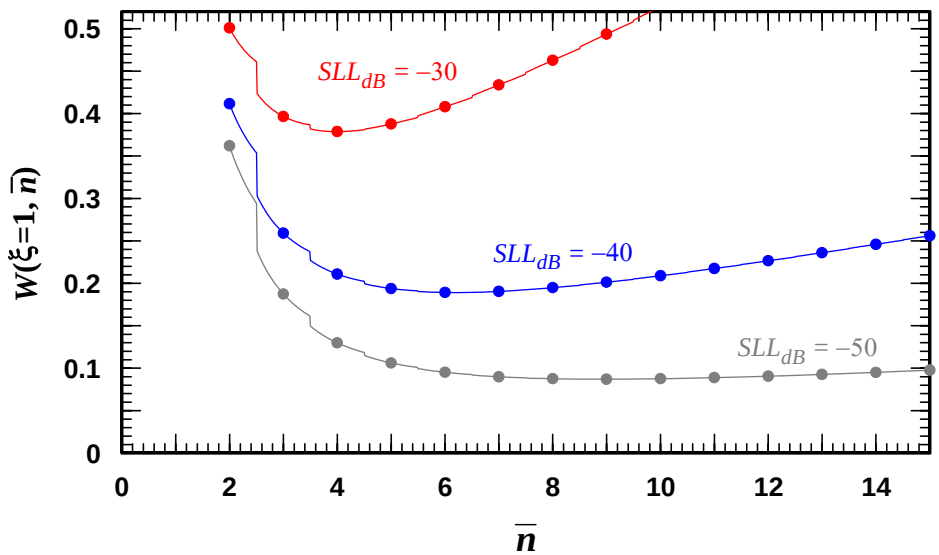

Figure 34 Illumination function, $W(\xi)$, viewed as a function of continuous $\bar{n}$ at $\xi = 1$.

With the understanding that the derivative does not exist at the half-integer values for $\bar{n}$

$$\frac{\partial}{\partial \bar{n}} W(1) = 2\sum_{m=1}^{\bar{n}-1} (-1)^m \frac{\partial}{\partial \bar{n}} F_m \,. \tag{7.27}$$

From (7.2)

$$\frac{\partial}{\partial \bar{n}} F_m = \frac{(-1)^m m^2 \sigma_p}{\prod_{\substack{n=1 \\ n\neq m}}^{\bar{n}-1} \left(1 - \frac{m^2}{n^2}\right)} \frac{\partial}{\partial \bar{n}} \sigma_p \sum_{k=1}^{\bar{n}-1} \prod_{n=1, n\neq k}^{\bar{n}-1} \left[\frac{\sigma_p^2 \left[A^2 + \left(n - \frac{1}{2}\right)^2 \right] - m^2}{\sigma_p^2 \left[A^2 + \left(n - \frac{1}{2}\right)^2 \right]^2} \right], \tag{7.28}$$

where

$$\frac{\partial}{\partial \bar{n}} \sigma_p = \frac{4A^2 - 2\bar{n} + 1}{4\left[A^2 + \left(\bar{n} - \frac{1}{2}\right)^2 \right]^{3/2}} \,. \tag{7.29}$$

The illumination at the edge begins to increase at the value of $\bar{n}$ where

$$\frac{\partial}{\partial \bar{n}} W(1) = 0 \,. \tag{7.30}$$

Thus, the condition for monotonically decreasing weights is satisfied when

$$\bar{n} = \text{floor}\left(\frac{1}{2} + 2A^2 \right), \tag{7.31}$$

where $\text{floor}(x)$ is the greatest integer $\leq x$. This represents an upper limit on the value of the Taylor order, $\bar{n}$.

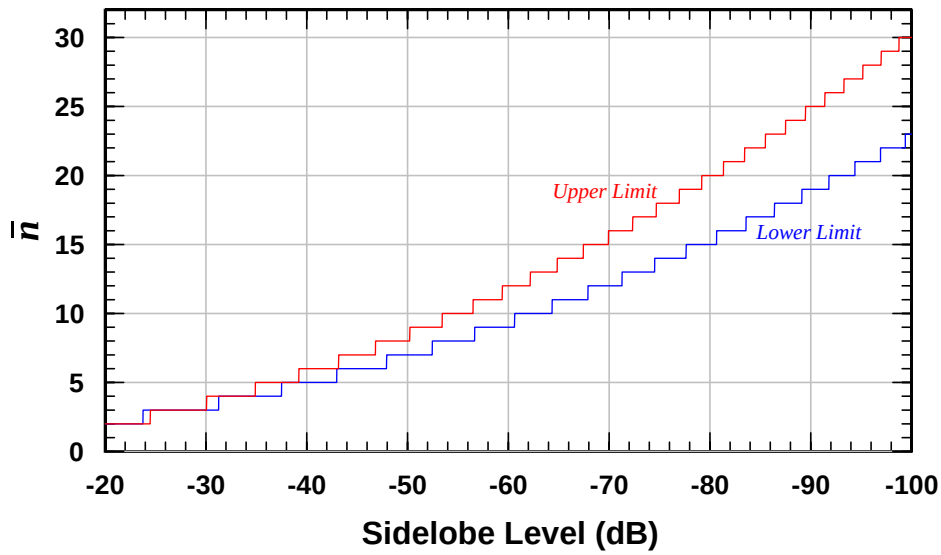

Figure 35 Recommended range for $\bar{n}$ as a function of sidelobe level.

The minimum value of $\bar{n}$ is determined by requiring that the peak of the $\bar{n}^{\text{th}}$ sidelobe be at least as low as the specified sidelobe level. This condition is satisfied when

$$\bar{n} = \text{rnd}\left(\left(\frac{SLL_{dB}}{22.8}\right)^2 - \frac{SLL_{dB}}{36.3} + 0.759\right), \tag{7.32}$$

where $\text{rnd}(x)$ is the integer nearest x. Using this set of criteria, the desired range for $\bar{n}$ is plotted in Figure 35.

7.2 Rectangular arrays with Taylor illumination

7.2.1 Odd array

The element weights for the odd two-dimensional (rectangular) Taylor array of order $\bar{n}$ are adapted from the continuous line illumination [1], giving weights

$$\begin{aligned} A_{n,m} &= \sum_{p=-(\bar{n}_{row}-1)}^{\bar{n}_{row}-1} F_p(\alpha_x,\sigma_x)\exp\left(j\frac{\pi}{N}np\right) \sum_{q=-(\bar{n}_{column}-1)}^{\bar{n}_{column}-1} F_q(\alpha_y,\sigma_y)\exp\left(j\frac{\pi}{N}mq\right) \\ &= \left[1+2\sum_{p=1}^{\bar{n}_{row}-1} F_p(\alpha_x,\sigma_x)\cos\left(\frac{\pi}{N}np\right)\right]\left[1+2\sum_{q=1}^{\bar{n}_{column}-1} F_q(\alpha_y,\sigma_y)\cos\left(\frac{\pi}{N}mq\right)\right], \end{aligned} \tag{7.33}$$

where the coefficients are

$$F_0 = 1, \tag{7.34}$$

$$F_{-k} = F_k, \tag{7.35}$$

and

$$F_k = (-1)^{k+1} \frac{\prod_{n=1}^{\bar{n}-1} \left[1 - \frac{k^2}{\sigma^2 \left[\alpha^2 + \left(n - \frac{1}{2} \right)^2 \right]} \right]}{2 \prod_{\substack{n=1 \\ n \neq k}}^{\bar{n}-1} \left(1 - \frac{k^2}{n^2} \right)}, \; 1 \le k \le \bar{n} - 1, \tag{7.36}$$

where the parameter α is related to the peak sidelobe level, SLL_{dB}, in decibels, ($SLL_{dB} < 0$)

$$\alpha = \frac{\cosh^{-1}\left(10^{\frac{-SLL_{dB}}{20}} \right)}{\pi}, \tag{7.37}$$

and the parameter σ is

$$\sigma = \sqrt{\frac{\bar{n}^2}{\alpha^2 + \left(\bar{n} - \frac{1}{2} \right)^2}} \, . \tag{7.38}$$

The element spacing is Δx along the $\hat{\mathbf{x}}$ direction and Δy along the $\hat{\mathbf{y}}$ direction. Thus, the dimensions of the array are

$$L_x = 2a_x = 2N\Delta x \, , \tag{7.39}$$

and

$$L_y = 2a_y = 2M\Delta y \, . \tag{7.40}$$

The array factor is

$$S_{array}\left(\hat{\mathbf{r}}, [\xi] \right) \equiv \sum_{n=-N}^{N} \sum_{m=-M}^{M} A_{n,m} e^{j\left(\psi_{n,m} - \xi_{n,m} \right)} \, , \tag{7.41}$$

which can be summed in a more convenient form for the ideal weights,

$$S_{array}\left(\hat{\mathbf{r}}, \xi_x, \xi_y \right) = S_{\substack{Taylor \\ odd}}\left(\kappa_x - \xi_x, \alpha_x, \sigma_x, \bar{n}_x, N \right) S_{\substack{Taylor \\ odd}}\left(\kappa_y - \xi_y, \alpha_y, \sigma_y, \bar{n}_y, M \right) \tag{7.42}$$

where

$$S_{\substack{Taylor \\ odd}}\left(\kappa, \alpha, \sigma, \bar{n}, \eta \right) = \sum_{p=-(\bar{n}-1)}^{\bar{n}-1} F_p\left(\alpha, \sigma \right) \frac{\sin\left((2\eta + 1) \frac{1}{2} \left(\kappa + \frac{\pi}{\eta} p \right) \right)}{\sin\left(\frac{1}{2} \left(\kappa + \frac{\pi}{\eta} p \right) \right)}, \tag{7.43}$$

where the total number of elements in the row (column) is $2\eta + 1$. The peak value of $S_{\substack{Taylor \\ odd}}$ occurs at $\kappa = 0$ and is

$$S_{\substack{Taylor \\ odd}}\left(0, \alpha, \sigma, \bar{n}, \eta \right) = \sum_{p=-(\bar{n}-1)}^{\bar{n}-1} F_p\left(\alpha, \sigma \right) \frac{\sin\left(\frac{\left(\eta + \frac{1}{2} \right) p}{\eta} \pi \right)}{\sin\left(\frac{p}{\eta} \frac{\pi}{2} \right)} \, . \tag{7.44}$$

When there are no random amplitude errors present, the error array associated with the quantization is

$$S_{error,odd}\left(\hat{\mathbf{r}},[\xi]\right) \equiv \sum_{n=-N}^{N}\sum_{m=-M}^{M}\left[A_{n,m} - a_b\left(A_{n,m}\right)\right]e^{j\left(\psi_{n,m}-\xi_{n,m}\right)} \ . \tag{7.45}$$

When the gain of each T/R module varies randomly about a nominal value, the array factor can be described by

$$S_{error,odd}\left(\hat{\mathbf{r}},[\xi]\right) \equiv \sum_{n=-N}^{N}\sum_{m=-M}^{M} A_{n,m}\eta_{n,m}e^{j\left(\psi_{n,m}-\xi_{n,m}\right)} \ , \tag{7.46}$$

where the random variable $\eta_{n,m}$ is

$$\eta_{n,m} = 10^{\eta_{dB}/20} \ , \tag{7.47}$$

and η_{dB} is distributed over the range given by (5.50) ($\pm$least significant bit). When the random gain of the T/R module is Gaussian about the nominal value, and the standard deviation is half of the least significant bit or more, the error η_{dB} is essentially uniformly distributed (see analysis of error for phase shifter).

7.2.2 Even array

The element weights for the even two-dimensional (rectangular) Taylor array of order $\bar{n}$ are adapted from the continuous line illumination [1], giving weights

$$\begin{aligned} A_{n,m} = &\left[1 + 2\sum_{p=1}^{\bar{n}_{row}-1} F_p\left(\alpha_x,\sigma_x\right)\cos\left(\frac{\pi}{N-\frac{1}{2}}\left(|n|-\tfrac{1}{2}\right)p\right)\right]\cdot \\ &\left[1 + 2\sum_{q=1}^{\bar{n}_{column}-1} F_q\left(\alpha_y,\sigma_y\right)\cos\left(\frac{\pi}{M-\frac{1}{2}}\left(|m|-\tfrac{1}{2}\right)q\right)\right], \end{aligned} \tag{7.48}$$

where the coefficients $F_k\left(\alpha,\sigma\right)$ are given by (7.36) with (7.34) and (7.35), as with the odd array. The array factor is

$$S_{array}\left(\hat{\mathbf{r}},[\xi]\right) \equiv \sum_{n=1}^{N}\sum_{m=1}^{M}\begin{bmatrix} A_{n,m}e^{j\left(\psi_{n,m}-\xi_{n,m}\right)} + A_{-n,m}e^{j\left(\psi_{-n,m}-\xi_{-n,m}\right)} \\ +A_{n,-m}e^{j\left(\psi_{n,-m}-\xi_{n,-m}\right)} + A_{-n,-m}e^{j\left(\psi_{-n,-m}-\xi_{-n,-m}\right)} \end{bmatrix}, \tag{7.49}$$

which is summed for the ideal weights,

$$S_{array}\left(\hat{\mathbf{r}},\xi_x,\xi_y\right) = S_{\substack{Taylor\\even}}\left(\kappa_x-\xi_x,\alpha_x,\sigma_x,\bar{n}_x,N\right)S_{\substack{Taylor\\even}}\left(\kappa_y-\xi_y,\alpha_y,\sigma_y,\bar{n}_y,M\right) \tag{7.50}$$

where

$$S_{\substack{Taylor\\even}}\left(\kappa,\alpha,\sigma,\bar{n},\eta\right) = \sum_{p=-(\bar{n}-1)}^{\bar{n}-1} F_p\left(\alpha,\sigma\right)\frac{\sin\left(\eta\left(\kappa+\dfrac{\pi}{\eta-\frac{1}{2}}p\right)\right)}{\sin\left(\dfrac{1}{2}\left(\kappa+\dfrac{\pi}{\eta-\frac{1}{2}}p\right)\right)}, \tag{7.51}$$

where the total number of elements in the row (column) is 2η. The peak value of $S_{\substack{Taylor\\even}}$ occurs at $\kappa = 0$ and is

$$S_{\substack{Taylor\\even}}\left(0,\alpha,\sigma,\bar{n},\eta\right)=\sum_{p=-\left(\bar{n}-1\right)}^{\bar{n}-1}F_p\left(\alpha,\sigma\right)\frac{\sin\left(\left(\dfrac{\eta\,p}{\eta-\frac{1}{2}}\pi\right)\right)}{\sin\left(\dfrac{p}{\eta-\frac{1}{2}}\dfrac{\pi}{2}\right)}. \tag{7.52}$$

The error array is

$$S_{error,even}\left(\hat{\mathbf{r}},[\xi]\right)\equiv\sum_{n=1}^{N}\sum_{m=1}^{M}\begin{bmatrix}\Delta A_{n,m}e^{j\left(\psi_{n,m}-\xi_{n,m}\right)}+\Delta A_{-n,m}e^{j\left(\psi_{-n,m}-\xi_{-n,m}\right)}\\+\Delta A_{n,-m}e^{j\left(\psi_{n,-m}-\xi_{n,-m}\right)}+\Delta A_{-n,-m}e^{j\left(\psi_{-n,-m}-\xi_{-n,-m}\right)}\end{bmatrix}, \tag{7.53}$$

where

$$\Delta A_{n,m}=A_{n,m}-a_b\left(A_{n,m}\right). \tag{7.54}$$

When random errors are present in the T/R module gain, the element weight error, $\Delta A_{n,m}$, will be a random variable

$$\Delta A_{n,m}=A_{n,m}\left(1-\eta_{n,m}\right) \tag{7.55}$$

so the error array factor is

$$S_{error,even}\left(\hat{\mathbf{r}},[\xi]\right)\equiv\sum_{n=1}^{N}\sum_{m=1}^{M}\begin{bmatrix}A_{n,m}\left(1-\eta_{n,m}\right)e^{j\left(\psi_{n,m}-\xi_{n,m}\right)}+A_{-n,m}\left(1-\eta_{-n,m}\right)e^{j\left(\psi_{-n,m}-\xi_{-n,m}\right)}\\+A_{n,-m}\left(1-\eta_{n,-m}\right)e^{j\left(\psi_{n,-m}-\xi_{n,-m}\right)}+A_{-n,-m}\left(1-\eta_{-n,-m}\right)e^{j\left(\psi_{-n,-m}-\xi_{-n,-m}\right)}\end{bmatrix}. \tag{7.56}$$

As with the odd array, $\eta_{n,m}$ is a random variable given by (7.47).

7.2.3 Consequences of discrete illumination function

The illumination function for an array of discrete elements can be considered a sampled version of a continuous illumination function. The Fourier transform of a sampled function is similar to the Fourier transform of the continuous function, but it is periodic, with the period related to the sampling density (see, for example, Bracewell [8]). Since the array factor is related to the illumination function through a Fourier transform, it too will be periodic. Doerry [9] has pointed out that the periodicity property can affect the sidelobes through the phenomenon of aliasing. The effect is this: if the aliased main lobe is too close the primary lobe, its sidelobes will interfere with the sidelobes near the true main lobe. The interference can be both constructive and destructive. This aliasing phenomenon is mathematically similar to the grating lobe phenomenon, which is also due directly to the periodicity of the array factor. In an antenna array, this problem can be controlled by choosing the proper element spacing and number of elements.

Two Taylor array factors are compared in Figure 36. Both arrays are $23\lambda/2$ long, but the blue curve is for a continuous line distribution, while the red curve is for an array with 24 individual elements, with $\lambda/2$ spacing. The main lobes of the two arrays match very well, but the sidelobes differ. The difference is due to the aliasing effect in the discrete Taylor distribution. The array factor of the continuous distribution is not aliased. In this case, the third sidelobe exceeds the design level by about 0.3 dB, which is quite acceptable. However, the sidelobes do not fall away as fast as those from the continuous distribution do.

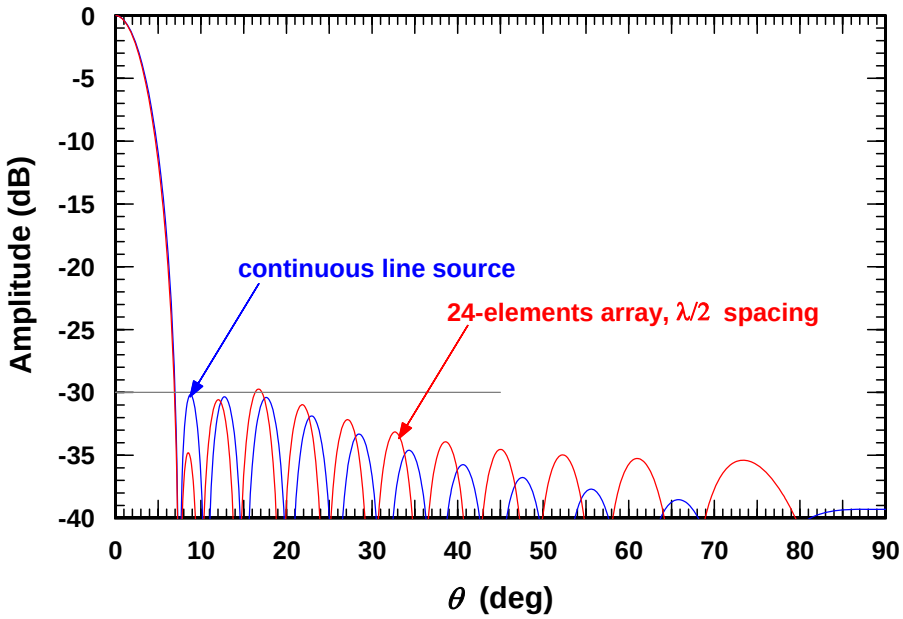

Figure 36 Two equal size Taylor array factors with $\bar{n} = 3$ *and* $SLL_{dB} = -30$. *The blue curve is a continuous line source (no aliasing), and the red curve is a discrete-element array, with mild aliasing.*

Decreasing the number of elements, while keeping the array size unchanged, makes the aliasing problem worse. This fact is illustrated in Figure 37, where the blue curve is for an array with just 12 elements. The third sidelobe is about 2 dB higher than the design value. The element spacing for this example is 1.045 wavelengths, and in this example, a grating lobe appears at about $\theta = 73°$.

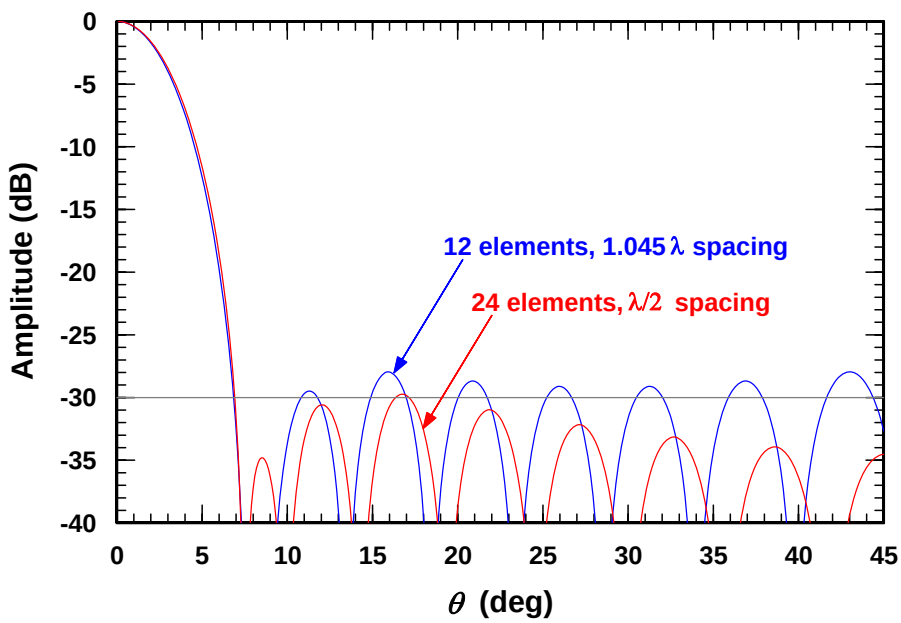

Figure 37 Two equal size, discrete, Taylor array factors with $\bar{n} = 3$ *and* $SLL_{dB} = -30$, *illustrating the increased sidelobe level due to aliasing.*

Since the average sidelobe level is larger when aliasing is present, the location of the first null is moved slightly toward the center of the main lobe, and the width of the main lobe is reduced slightly. The energy added to the sidelobes by the aliasing phenomenon is taken from the main lobe.

When the number of elements in an array is large, the distinction between the even and odd arrays is not significant. In this case, the relation between the argument *u*, used in the description of the continuous line distribution, and κ, used in the description of the discrete arrays, is given by

$$\kappa \cong \frac{\pi}{N} u \,, \tag{7.57}$$

where $2N$ or $2N+1$ is the number of elements in the even or odd array, respectively. The main lobe of the next period of the array factor occurs at $\kappa = 2\pi$, or $u \cong 2N$. The period sidelobe at $u_{SL} = n$ will coincide with the $\bar{n}^{th}$ sidelobe of the first period, where

$$u_{SL} = 2N - \bar{n} \,. \tag{7.58}$$

To ensure that aliasing raises the peak sidelobe level by no more than ε_{alias} dB, the $n = u_{SL}$ sidelobe should be

$$\xi_{alias,dB} = 20\log\left(10^{\varepsilon_{dB}/20} - 1\right) \tag{7.59}$$

decibels below the design sidelobe level. Substituting (7.58) into (7.12), the requirement is

$$f_{SL}\left(u_{SL}\right) \le 10^{\left(SLL_{dB} - \xi_{alias,dB}\right)/20} \,, \tag{7.60}$$

or

$$N \ge \bar{n} + \frac{1}{\pi(10^{\varepsilon_{dB}/20} - 1)} \cosh\left(\pi \mathrm{A}\right) \prod_{n=1}^{\bar{n}-1} \left[\frac{n^2}{\sigma_p^2 \left(A^2 + \left(n - \frac{1}{2}\right)^2 \right)} \right] \,, \tag{7.61}$$

with σ_p^2 and *A* given by (7.3) and (7.5), respectively. Based on informal (but similar) considerations, Doerry [9] suggests

$$\frac{\left|SLL_{dB}\right|}{9} \le \bar{n} \le \frac{N_{total}}{5} \,, \tag{7.62}$$

which is simpler but less stringent than (7.61), and implies an absolute lower limit for *N*

$$2N > 5\,\mathrm{ceil}\left(\frac{\left|SLL_{dB}\right|}{9} \right), \tag{7.63}$$

where $\mathrm{ceil}(x)$ means the smallest integer larger than or equal *x*. It should be noted that (7.62) is actually a suggestion for picking $\bar{n}$, and the considerations in [9] really do not address choosing *N* in terms of the sidelobe performance. However, (7.63) is justified as an absolute lowest limit for choosing *N*, although (7.61) is the recommended lower bound. The lower limit for *N* is plotted in Figure 38 as a function of sidelobe level, SLL_{dB}, for several values of the Taylor order, $\bar{n}$, when $\varepsilon_{alias} = 0.5$ dB and $\varepsilon_{alias} = 3$ dB. In order that the effect of aliasing on the near-in sidelobes be no worse than a factor of $\varepsilon_{alias} = 0.5$ dB, the aliased component must be at least 24.5 dB below the design sidelobes in this region, while for $\varepsilon_{alias} = 3$ dB, aliased component must be only 7.7 dB below the design sidelobe level.

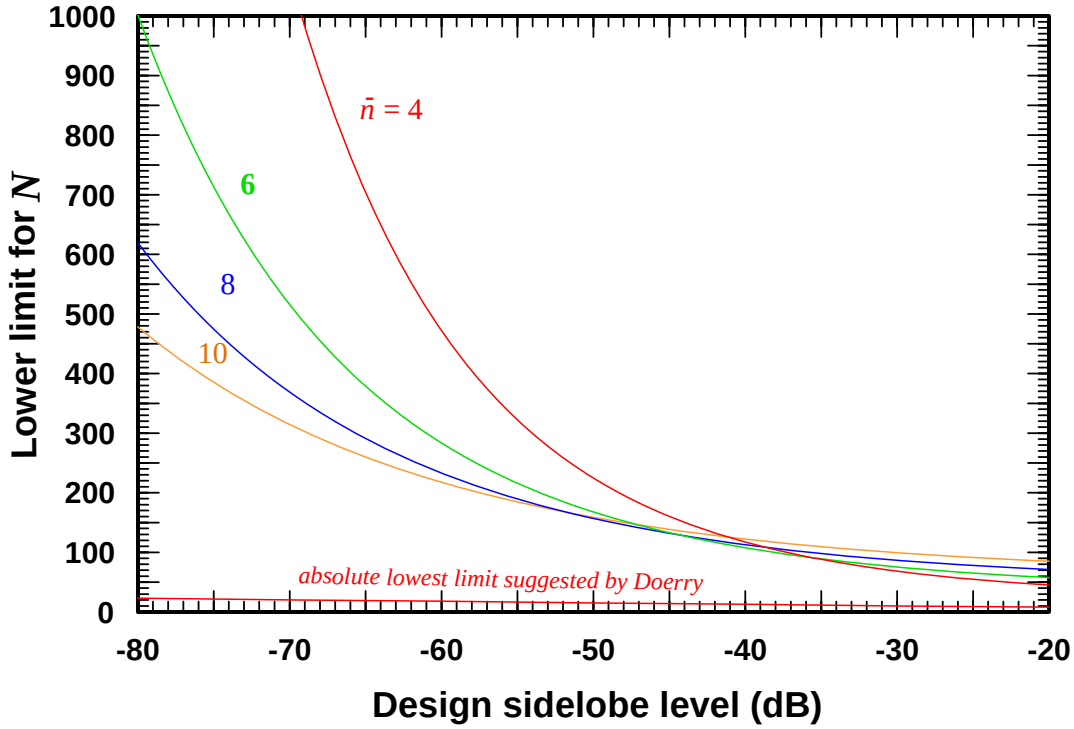

(a)

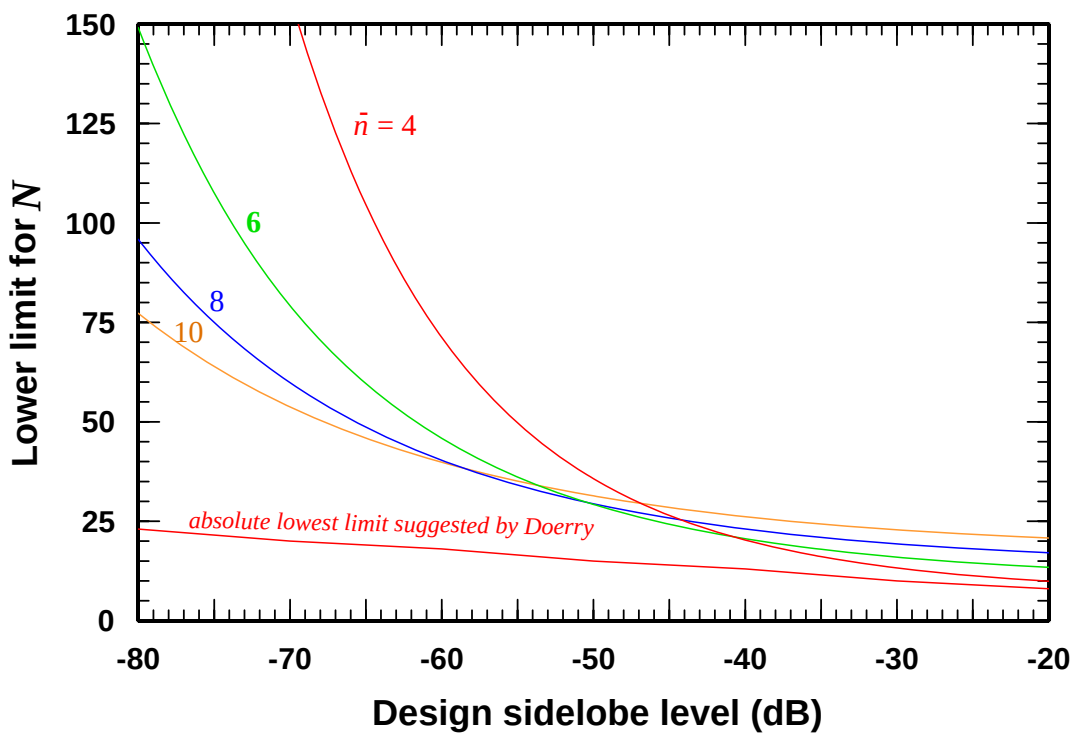

(b)

Figure 38 Minimum value of N for given design sidelobe level and Taylor order, for (a) $\varepsilon_{alias} = 0.5$ dB*, and (b)* $\varepsilon_{alias} = 3$ dB.

This Page Intentionally Blank

7.2.4 Summary of Design Rules for Taylor Array

Specification: θ_{3dB} half beam width

SLL_{dB} sidelobe level $\left(SLL_{dB} < 0\right)$

ε_{dB} sidelobe degradation due to aliasing ($\varepsilon_{dB} > 0$)

Compute:

Taylor parameter:
$$A = \frac{1}{\pi}\cosh^{-1}\left(10^{\frac{-SLL_{dB}}{20}}\right) = \frac{1}{\pi}\ln\left(10^{\frac{-SLL_{dB}}{20}} + \sqrt{10^{\frac{-SLL_{dB}}{10}} - 1}\right)$$

Taylor order:
$$\mathrm{rnd}\left(\left(\frac{SLL_{dB}}{22.8}\right)^2 - \frac{SLL_{dB}}{36.3} + 0.759\right) \le \bar{n} \le \mathrm{floor}\left(\frac{1}{2} + 2A^2\right)$$

Taylor parameter:
$$\sigma_p^2 = \frac{\bar{n}^2}{A^2 + \left(\bar{n} - \frac{1}{2}\right)^2}$$

Taylor coefficients:
$$F_m = \frac{(-1)^{m+1}}{2\prod_{\substack{n=1\\ n\neq m}}^{\bar{n}-1}\left(1 - \frac{m^2}{n^2}\right)}\prod_{n=1}^{\bar{n}-1}\left[1 - \frac{m^2}{\sigma_p^2\left[A^2 + \left(n - \frac{1}{2}\right)^2\right]}\right],\ 1 \le m \le \bar{n} - 1$$

Minimum N to avoid aliasing in sidelobe region:
$$N \ge \bar{n} + \frac{1}{\pi(10^{\varepsilon_{dB}/20} - 1)}\cosh(\pi \mathrm{A})\prod_{n=1}^{\bar{n}-1}\left[\frac{n^2}{\sigma_p^2\left(A^2 + \left(n - \frac{1}{2}\right)^2\right)}\right]$$

Iterate:
$$u_{3dB,0} = 0.55$$
$$u_{3\,dB,i+1} \approx u_{3\,dB,i} - \left(F\left(u_{3\,dB,i}\right) - \frac{1}{\sqrt{2}}\right)\Big/\left.\frac{\partial F}{\partial u}\right|_{u = u_{3\,dB,i}}$$
$$F(u) = \sum_{m=-(\bar{n}-1)}^{\bar{n}-1} F_m \frac{\sin\pi(u+m)}{\pi(u+m)}$$
$$\frac{\partial F(u)}{\partial u} = \sum_{m=-(\bar{n}-1)}^{\bar{n}-1} F_m \frac{\pi(u+m)\cos\pi(u+m) - \sin\pi(u+m)}{\pi(u+m)^2}$$

Compute half width of array:
$$a = \frac{\lambda u_{3\,dB}}{2\sin\theta_{3\,dB}}$$

Odd array $\left(2N + 1 \text{ elements}\right)$: $\quad element\ spacing = \dfrac{a}{N}$

Element weights
$$A_n = 1 + 2\sum_{p=1}^{\bar{n}_{row}-1} F_p(\alpha,\sigma)\cos\left(\frac{\pi}{N}np\right)$$

Even array $2N$ elements: $\quad element\ spacing = \dfrac{2a}{2N-1}$

Element weights
$$A_n = 1 + 2\sum_{p=1}^{\bar{n}_{row}-1} F_p(\alpha,\sigma)\cos\left(\frac{\pi}{N - \frac{1}{2}}\left(|n| - \frac{1}{2}\right)p\right)$$

7.3 Effect of amplitude quantization on the Taylor array

When the array taper is controlled by digital attenuators, error will occur due to the attenuator quantization, and possibly due to the limited range of the attenuator. The required range of the attenuator will be determined by the ratio of the weight at the edge of the array to the weight at the center of the array. For a one-dimensional taper, this ratio is

$$\frac{W(1)}{W(0)} = \frac{1 + 2\sum_{m=1}^{\bar{n}-1} (-1)^m F_m}{1 + 2\sum_{m=1}^{\bar{n}-1} F_m}. \tag{7.64}$$

For a two-dimensional taper, the ratio is

$$\frac{W(1)}{W(0)} = \frac{\left(1 + 2\sum_{m=1}^{\bar{n}_{row}-1} (-1)^m F_{m,\,row}\right)}{\left(1 + 2\sum_{m=1}^{\bar{n}_{row}-1} F_{m,\,row}\right)} \frac{\left(1 + 2\sum_{n=1}^{\bar{n}_{col}-1} (-1)^n F_{n,\,col}\right)}{\left(1 + 2\sum_{n=1}^{\bar{n}_{col}-1} F_{n,\,col}\right)}. \tag{7.65}$$

The minimum recommended Taylor order is obtained from (7.32), while the maximum Taylor order is obtained from (7.31). For $n = \bar{n}_{\min}$ (red curve) and $n = \bar{n}_{\max}$ (blue curve), the required attenuator range is plotted in Figure 39 as a function of sidelobe level. The required attenuator range for the one-dimensional taper, a_{range}, is almost independent of the order of the Taylor illumination, and can be estimated to within $\pm 1/2$ dB by

$$a_{range} = -\left(8 + 0.63 \cdot SLL_{dB} - 0.0014 \cdot SLL_{dB}^2\right) \text{ dB} \tag{7.66}$$

Note that the attenuator range a_{range} is positive, while the sidelobe level is negative. For a two-dimensional taper, the required attenuator range must be larger than for a one-dimensional taper. For a symmetrical taper, the required attenuator range will double, increasing the number of required bits by one.

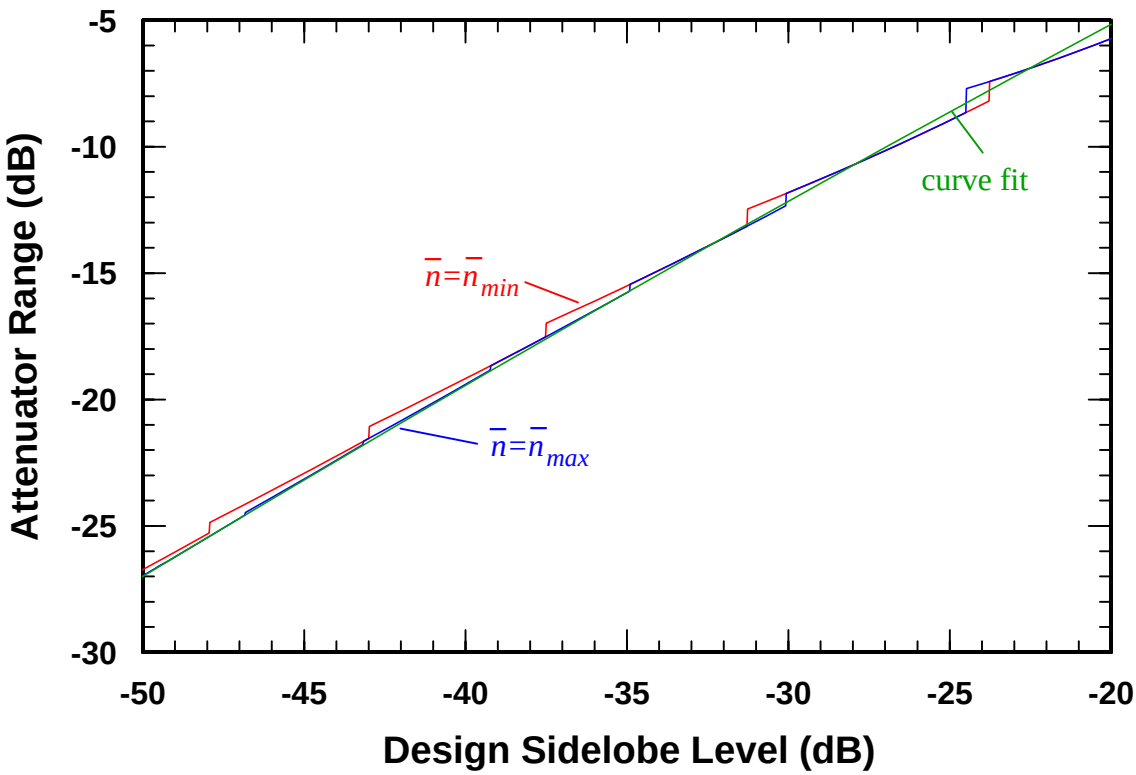

Figure 39 Attenuator range for one-dimensional taper as a function of design sidelobe level.

The quantization of the digital attenuator causes errors in the illumination of the array. The primary effect of this is an increase in the sidelobes of the array factor. The error sidelobe level is given by (5.62), and it depends on the mean and the standard deviation of the error factor, the illumination taper, and the number of elements in the array.

When the T/R modules have a random variation in gain (decibels) that is approximately uniformly distributed with zero mean, the error sidelobe level (5.62), is

$$SLL_{error} = \left[\frac{\alpha \ln(10)\left(10^{\alpha/5} - 1\right)}{20\left(10^{\alpha/10} - 1\right)^2} - 1 \right] \frac{\sum_{n,m} \left| A_{n,m} \right|^2}{\left| \sum_{n,m} A_{n,m} \right|^2}, \tag{7.67}$$

where

$$\alpha = -\frac{\Delta g_{T/R} + a_{range,row} + a_{range,col}}{2\left(2^b - 1\right)}, \tag{7.68}$$

where $\Delta g_{T/R}$ is the addition to the attenuator range required to accommodate the random gain variation between T/R modules, and it is assumed that the required ranges for the row and column tapers are different. Note that the addition to the attenuator range, $\Delta g_{T/R}$, is given in decibels and is negative, as is the design sidelobe level, SLL_{dB}. The error sidelobe level should be γ dB below the design sidelobe

level to ensure that the quantization errors produce no more than a $\pm\delta$ dB effect on the side lobe level, where

$$\gamma = 20 \cdot \log\left(\frac{10^{\delta/10}-1}{10^{\delta/10}+1}\right). \tag{7.69}$$

For no more than ± 0.5 dB effect on the side lobe level, $\gamma = -25$ dB. Thus, for this criterion, the resolution of the attenuator is obtained from

$$\left[\frac{\alpha \ln(10)\left(10^{\alpha/5}-1\right)}{20\left(10^{\alpha/10}-1\right)^2}-1\right]\frac{\sum_{n,m}\left|A_{n,m}\right|^2}{\left|\sum_{n,m}A_{n,m}\right|^2} \le 10^{\frac{SLL_{dB}+\gamma}{10}} \tag{7.70}$$

Expanding (7.70) to third order in α,

$$\alpha \le \frac{20\sqrt{3}}{\ln(10)} 10^{\frac{SLL_{dB}+\gamma}{20}} \frac{\left|\sum_{n,m}A_{n,m}\right|}{\sqrt{\sum_{n,m}\left|A_{n,m}\right|^2}}, \tag{7.71}$$

and from (7.68)

$$b = \text{ceiling}\left[\frac{1}{\ln 2}\ln\left(1-\frac{\Delta g_{T/R}+a_{range,row}+a_{range,col}}{2\alpha}\right)\right]. \tag{7.72}$$

7.3.1 Summary of Design Rules for Digital Attenuator

Specification: Quantization errors produce no more than a $\pm\delta$ dB effect on the side lobe level

Side lobe level: $SLL_{dB,elevation}$, $SLL_{dB,azimuth}$ in decibels $\left(SLL_{dB} < 0\right)$

Unit-to-unit gain variation of T/R modules: $\pm\Delta g_{T/R}$ in decibels

Compute:

Required taper ranges (in decibels):

$$a_{row} = -\left(8 + 0.63 \cdot SLL_{dB,\,azimuth} - 0.0014 \cdot SLL_{dB,\,azimuth}^2\right)$$

$$a_{col} = -\left(8 + 0.63 \cdot SLL_{dB,\,elevation} - 0.0014 \cdot SLL_{dB,\,elevation}^2\right)$$

Required attenuator range: $a_{range} = \left|\Delta g_{T/R}\right| + a_{row} + a_{col}$ in decibels

Note: $a_{range} > 0$

Tolerable error- sidelobe level: $\gamma = 20 \cdot \log\left(\dfrac{10^{\delta/10} - 1}{10^{\delta/10} + 1}\right)$ in decibels

Range of tolerable error: $$\alpha \le \frac{20\sqrt{3}}{\ln(10)} 10^{\frac{\min\left(SLL_{dB,elevation}, SLL_{dB,azimuth}\right) + \gamma}{20}} \frac{\left|\sum_{n,m} A_{n,m}\right|}{\sqrt{\sum_{n,m} \left|A_{n,m}\right|^2}}$$

Number of bits: $$b = \text{ceiling}\left[\frac{1}{\ln 2} \ln\left(1 + \frac{a_{range}}{2\alpha}\right)\right]$$

This Page Intentionally Blank

7.4 Design example

As an example, consider a linear even array with a required beamwidth of $\theta_{3dB} = 3°$, and a design sidelobe level $SLL_{dB} = -40$ dB, with $\varepsilon_{dB} = 0.5$ dB degradation in sidelobe level due to aliasing. Using the design rules for the Taylor array, the following values are computed:

Taylor parameter $A = 1.6865$

Taylor order $\bar{n} = 5$

Taylor parameter $\sigma_p^2 = 1.082519$

Taylor coefficients: $F_0 = 1$

$F_1 = 0.387482$

$F_2 = -0.00956429$

$F_3 = 0.0046963$

$F_4 = -0.00133399$

Minimum N to avoid aliasing: $N = 115$

Half-width of array: $u_{3dB} = 0.623002$

$a = 5.952\lambda$

Even array, $2N$ elements: $\textit{optimum element spacing} = 0.052\lambda$

Since the optimum element spacing is not practical, fewer elements will be used, and the sidelobes will be increased due to the aliasing affect.

Choose: $N = 13$ (26 elements)

$\textit{element spacing} = 0.476\lambda$.

Required attenuator range: $a_{range} = 19.4$ dB

Choose: $a_{range} = 20$ dB to allow for gain variation in T/R modules

For specification that error sidelobe is to produce no more than ± 0.5 dB effect on design sidelobe level:

Range of tolerable error: $|\alpha| \le 0.0264$ dB

Number of bits: $b = 9$

For specification that error sidelobe level is equal to design sidelobe level:

Range of tolerable error: $|\alpha| \le 0.47$ dB

Number of bits: $b = 5$

The design seems straightforward until the element spacing is computed. The minimum number of elements to prevent aliasing in the sidelobe region is too large to allow usable element spacing. In fact, the number of elements must be reduced by almost an order of magnitude in order to allow reasonable element spacing on the order of a half wavelength. This will result in some aliasing in the sidelobe region, and the sidelobe level will exceed the design sidelobe level. The normalized directivity patterns for the array without aliasing ($N = 115$), and with aliasing ($N = 13$) are plotted in Figure 40. In this case, the peak sidelobe level is increased by slightly more than 1 dB. While the reduction in the number of elements seems extreme, the effect of the aliasing is not severe.

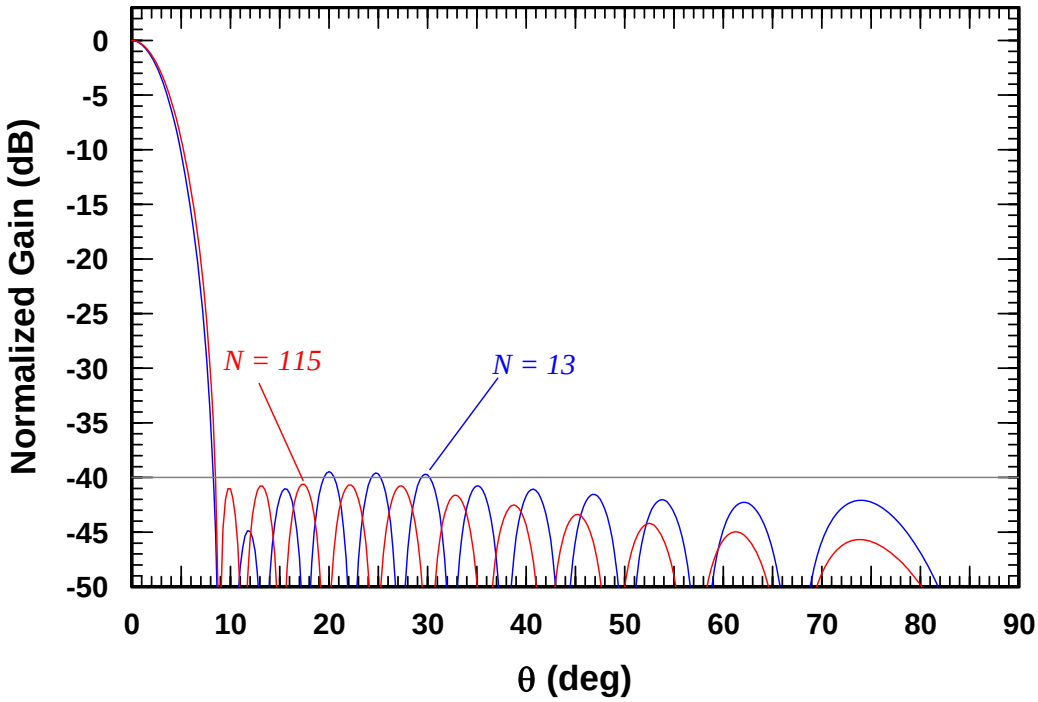

Figure 40 Normalized directivity for design example with optimum number of elements to avoid aliasing and practical number of elements.

In order for the error sidelobe level to have negligible affect on the sidelobe level, the number of bits required in the attenuator is nine. However, relaxing the error sidelobe level to equal the design sidelobe level only requires five bits in the attenuator, but the use of the 5-bit attenuator could result in peak sidelobes 6 dB higher than with the 9-bit attenuator. The normalized directivity pattern is plotted in Figure 40 for both 9-bit and 5-bit attenuators, and the peak sidelobe level with the 5-bit attenuator is about –36 dB.

The computed directivity patterns assume that the gain of each T/R module varies randomly by an amount that is larger than the least-significant bit of the attenuator. This ensures that the error in the amplitude of each element is approximately uniformly distributed between ± half of the least-significant bit.

Figure 42 compares the sidelobe regions when the linear array is implemented with a 9-bit attenuator and with an ideal, continuous attenuator. As can be seen, the differences between the sidelobe levels are essentially negligible.

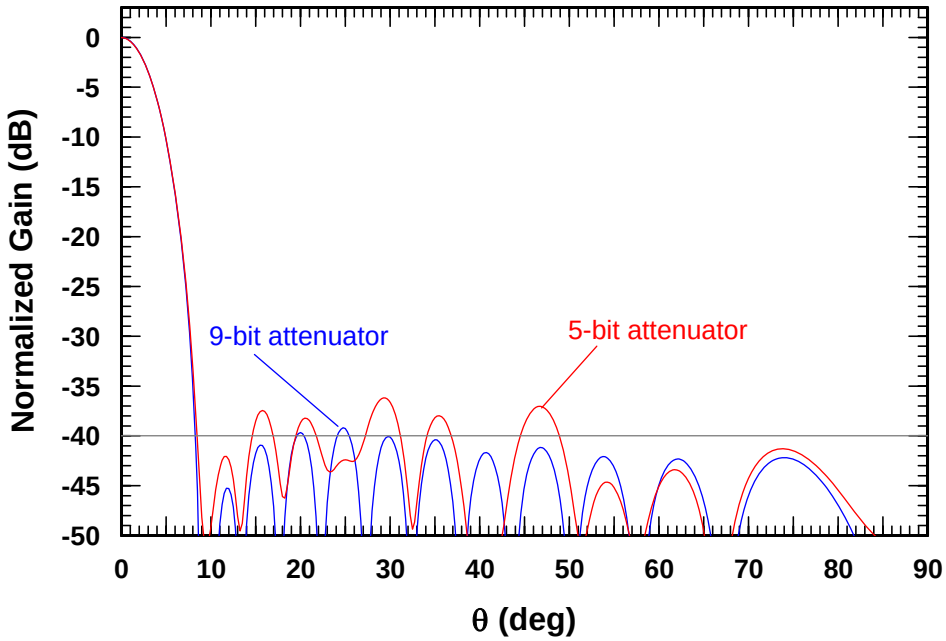

Figure 41 Comparison of normalized directivity for design example with 9-bit attenuator and 5-bit attenuator.

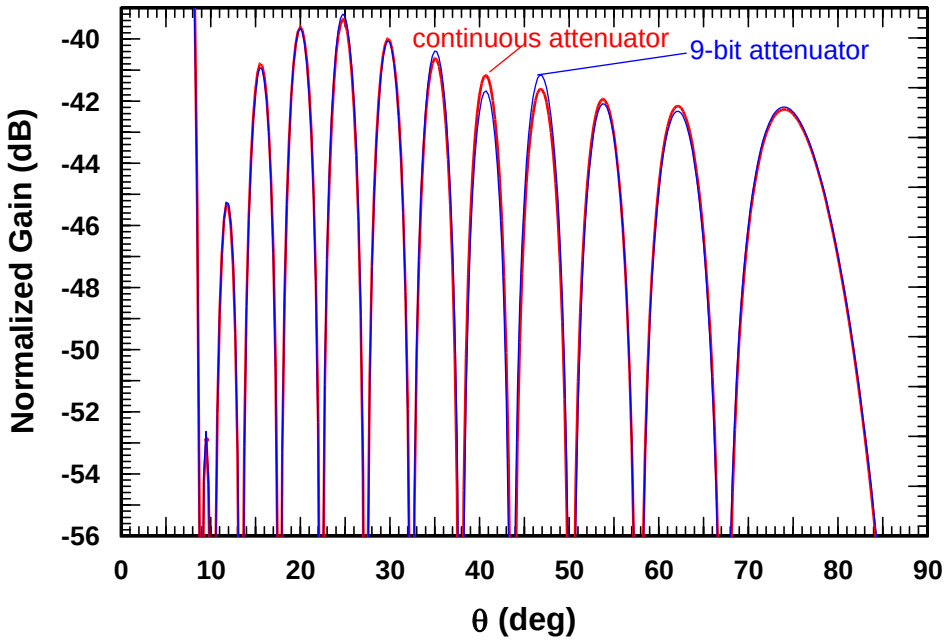

Figure 42 Comparison of sidelobe region for directivity pattern of design example with 9-bit attenuator and continuous (ideal) attenuator.

This Page Intentionally Blank

8. Issue of tapered illumination on transmit

For monostatic radar applications, including synthetic-aperture radar, the product of both the transmit- and receive-antenna patterns is the important antenna consideration. This product is referred to as the two-way antenna pattern. Placing the antenna specification requirements on the two-way antenna pattern, rather than specifying transmit and receive patterns individually, allows for some flexibility, since the transmit and receive patterns are not required to be identical. However, transmitter efficiency is an important consideration, and may dictate some of the design choices.

Tapering the array illumination for the transmitter can reduce the efficiency of the transmitter, and it reduces the peak power available with a given set of T/R modules. Generally, the output transmit stage of a T/R module will be a nonlinear circuit, such as a class C amplifier. Using class C rather than class A amplifiers is a way to reduce dissipated power in the T/R module, while maintaining the highest output power. However, when the array illumination is tapered, it is necessary to reduce (and control) the output power from the T/R modules located away from the center of the array. When the output stage is nonlinear, reducing the drive to the stage with a programmable attenuator is not appropriate. Changing the output power by changing bias conditions is a possible solution, but can lead to mismatch problems, and can be complicated to implement. The simple, but inefficient, approach is simply to place the programmable attenuator between the output stage and the array element.

8.1 Taylor illumination for transmit array

8.1.1 Rectangular array

Consider a linear array with Taylor illumination for both transmit and receive functions. In general, the parameters of the illumination can be different for transmit and receive, so the two-way antenna pattern for a linear array is

$$S_{\substack{2-way\,Taylor\\odd}}\left(\kappa,\alpha_{tx},\sigma_{tx},\bar{n}_{tx},\alpha_{rx},\sigma_{rx},\bar{n}_{rx},\eta\right)=$$

$$\sum_{p=-(\bar{n}_{tx}-1)}^{\bar{n}_{tx}-1} F_p\left(\alpha_{tx},\sigma_{tx}\right)\frac{\sin\left(\left(2\eta+1\right)\frac{1}{2}\left(\kappa+\frac{\pi}{\eta}p\right)\right)}{\sin\left(\frac{1}{2}\left(\kappa+\frac{\pi}{\eta}p\right)\right)}\sum_{q=-(\bar{n}_{rx}-1)}^{\bar{n}_{rx}-1} F_q\left(\alpha_{rx},\sigma_{rx}\right)\frac{\sin\left(\left(2\eta+1\right)\frac{1}{2}\left(\kappa+\frac{\pi}{\eta}q\right)\right)}{\sin\left(\frac{1}{2}\left(\kappa+\frac{\pi}{\eta}q\right)\right)} \tag{8.1}$$

for the odd array, and

$$S_{\substack{2-way\,Taylor\\even}}\left(\kappa,\alpha_{tx},\sigma_{tx},\bar{n}_{tx},\alpha_{rx},\sigma_{rx},\bar{n}_{rx},\eta\right)=$$

$$\sum_{p=-(\bar{n}_{tx}-1)}^{\bar{n}_{tx}-1} F_p\left(\alpha_{tx},\sigma_{tx}\right)\frac{\sin\left(\eta\left(\kappa+\frac{\pi}{\eta-\frac{1}{2}}p\right)\right)}{\sin\left(\frac{1}{2}\left(\kappa+\frac{\pi}{\eta-\frac{1}{2}}p\right)\right)}\sum_{q=-(\bar{n}_{rx}-1)}^{\bar{n}_{rx}-1} F_q\left(\alpha_{rx},\sigma_{rx}\right)\frac{\sin\left(\eta\left(\kappa+\frac{\pi}{\eta-\frac{1}{2}}q\right)\right)}{\sin\left(\frac{1}{2}\left(\kappa+\frac{\pi}{\eta-\frac{1}{2}}q\right)\right)} \tag{8.2}$$

for the even array.

A transmit efficiency, compared to uniform illumination, is defined

$$\mathcal{E}_{tx,odd}=\frac{1}{\left(2N+1\right)W_0^2}\sum_{n=-N}^{N}W_n^2 \tag{8.3}$$

for the odd linear array, and

$$\mathcal{E}_{tx,even} = \frac{1}{NW_1^2}\sum_{n=1}^{N} W_n^2 \tag{8.4}$$

for the even linear array. The weights are given by

$$W_n\left(\alpha_{tx},\sigma_{tx}\right) = 1 + 2\sum_{p=1}^{\bar{n}_{tx}-1} F_p\left(\alpha_{tx},\sigma_{tx}\right)\cos\left(\frac{\pi}{N}np\right) \tag{8.5}$$

for the odd array, and

$$W_n\left(\alpha_{tx},\sigma_{tx}\right) = 1 + 2\sum_{p=1}^{\bar{n}_{tx}-1} F_p\left(\alpha_{tx},\sigma_{tx}\right)\cos\left(\frac{\pi}{N-\frac{1}{2}}\left(|n|-\tfrac{1}{2}\right)p\right) \tag{8.6}$$

for the even array. The efficiency for the linear array is a weak function of the number of elements in the array, but a strong function of the design sidelobe level. Figure 43 plots the efficiency as a function of design sidelobe level, for the minimum value of $\bar{n}$ given by (7.32)

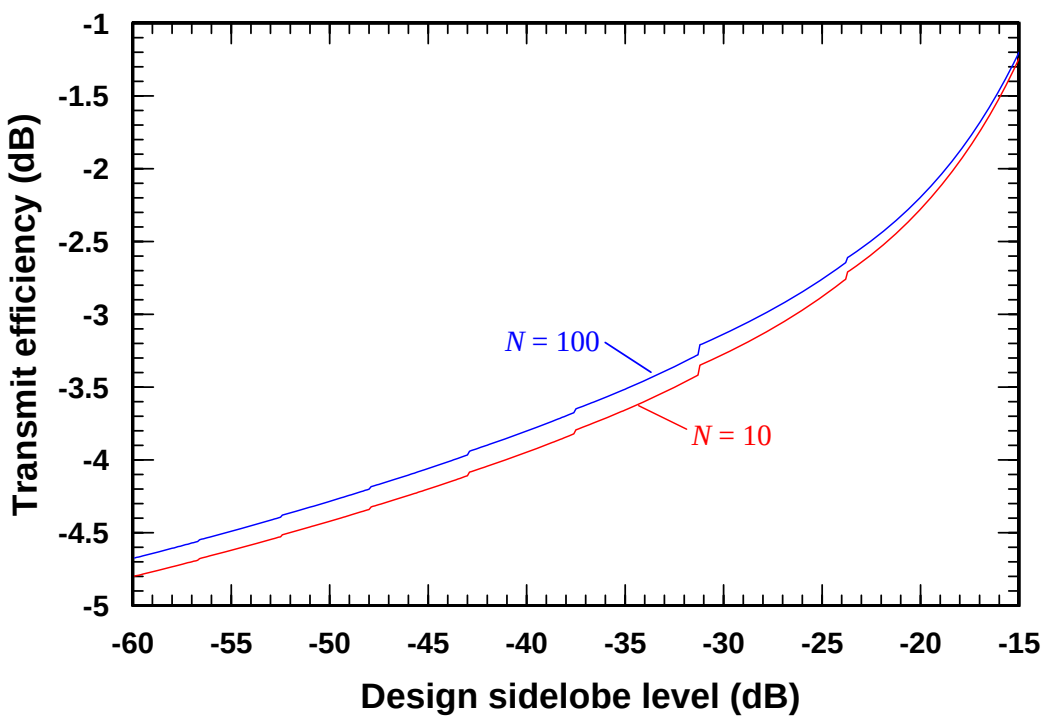

Figure 43 Transmitter efficiency for the linear Taylor-weighted array.

For the two-dimensional array, the transmit efficiency, compared to uniform illumination, is defined

$$\mathcal{E}_{tx,odd} = \frac{1}{\left(2N_{row}+1\right)\left(2N_{col}+1\right)W_{0,row}^2 W_{0,col}^2}\sum_{n=-N_{row}}^{N_{row}}\sum_{m=-N_{col}}^{N_{col}} W_{n,row}^2 W_{m,col}^2 , \tag{8.7}$$

for the odd array, and

$$\mathcal{E}_{tx,even} = \frac{1}{N_{row}N_{col}W_{1,row}^2 W_{1,col}^2}\sum_{n=1}^{N_{row}}\sum_{m=1}^{N_{col}} W_{n,row}^2 W_{m,col}^2 . \tag{8.8}$$

for the even array. As expected, the transmit efficiency for the two-dimensional array, plotted in Figure 44, is somewhat lower than for the linear (one-dimensional) array.

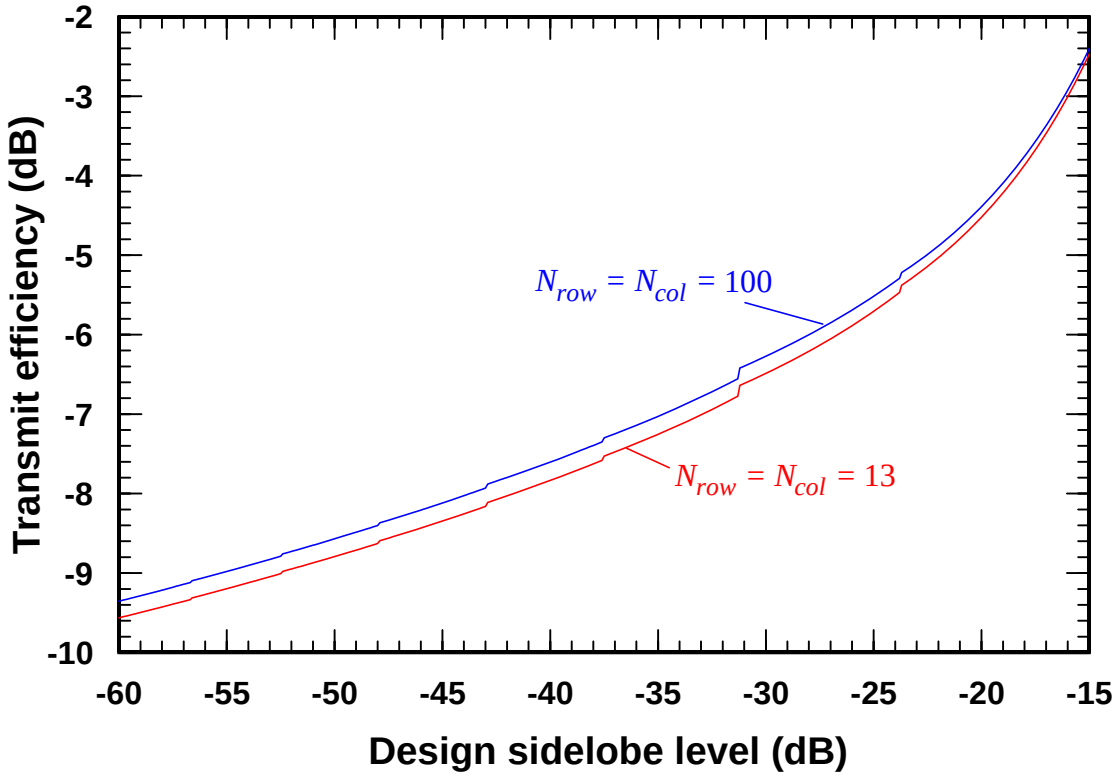

Figure 44 Transmitter efficiency for the two-dimensional Taylor-weighted array.

Consider an even array with $N = 13$, similar to the design example above, with $\lambda/2$ element spacing. For a two-way sidelobe requirement of -40 dB, a Taylor illumination with -20 dB sidelobes and $\bar{n} = 2$ can be used for both transmit and receive arrays. The transmit efficiency for a linear array, from (8.4) is -2.3 dB, while for the two-dimensional array, the efficiency (8.8) is -4.5 dB. The normalized two-way antenna pattern is plotted in Figure 45 and Figure 46, where the peak two-way sidelobe level is –42 dB. The pattern exhibits the characteristic of a rectangular aperture, with the peak sidelobes along the principal axes of the array. Except for the lowered efficiency, due to the transmit taper, the two-way pattern is quite respectable. In the two-dimensional plot of Figure 46,

$$u = \frac{2a}{\lambda} \sin\theta \cos\phi$$

and

$$v = \frac{2a}{\lambda} \sin\theta \sin\phi .$$

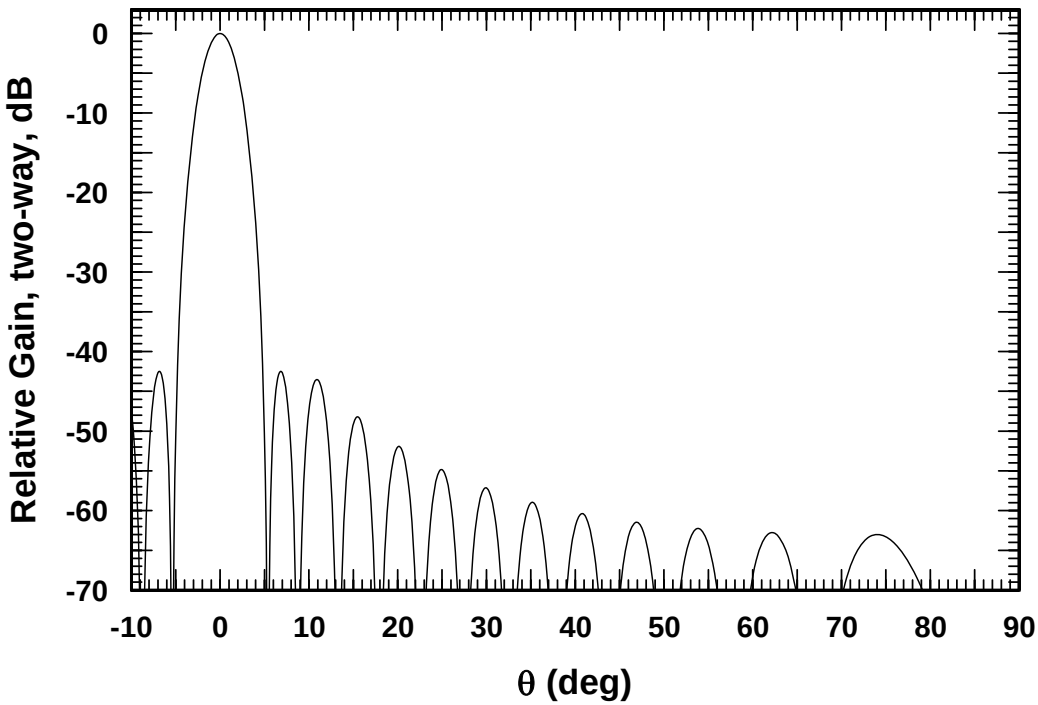

Figure 45 Two-way antenna pattern with Taylor illumination with -20 dB *one-way design sidelobes and* $\bar{n} = 2$.

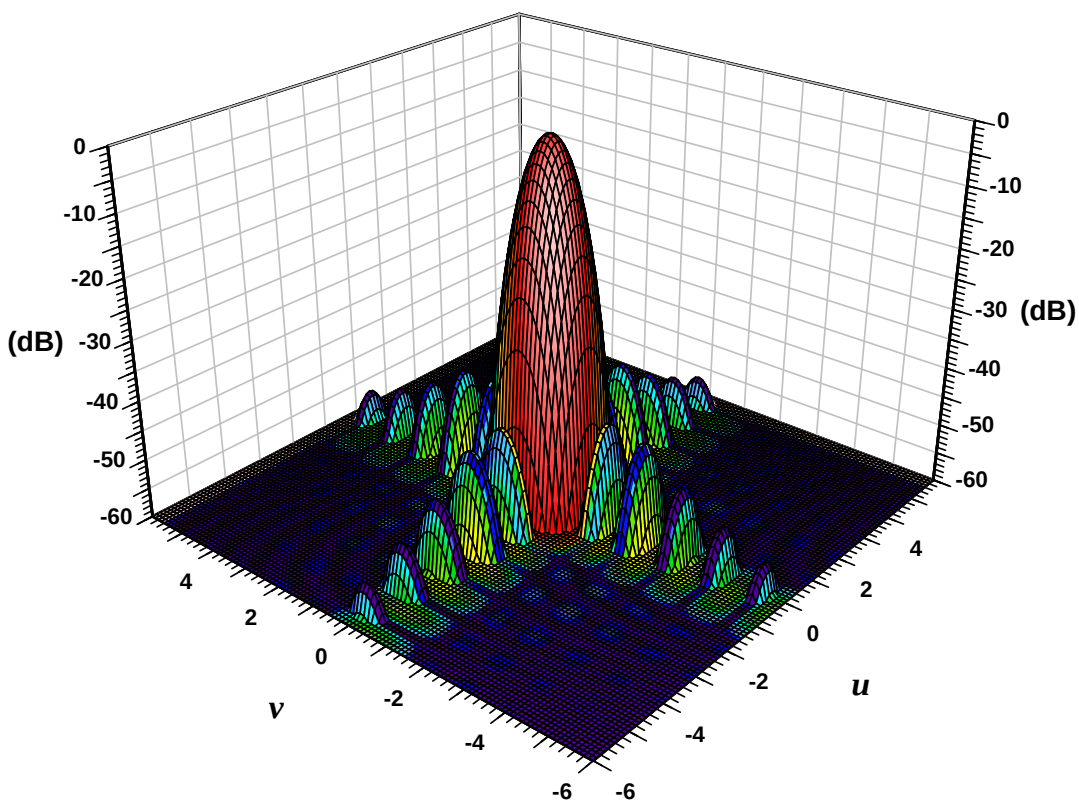

Figure 46 Normalized two-way array factor for a two-dimensional even array with a Taylor illumination, $SLL = -20$ dB , $\bar{n} = 2$ *, for both transmit and receive.*

The two-way sidelobe level can be adjusted by giving transmit and receive arrays the same or different weighting, as illustrated in Figure 47, where several choices are plotted. Of course, if the transmit and receive sidelobe levels are too different, a significantly larger first sidelobe will appear. As seen in Figure 47, this occurs for the case of an $\bar{n} = 2$, -20 dB Taylor transmit array with an $\bar{n} = 5$, -40 dB receive array. The transmit array has its first sidelobe inside the mainlobe of the receive array, making the first sidelobe of the two-way pattern larger. However, the next few sidelobes are much lower, so this may be an appropriate combination for some applications.

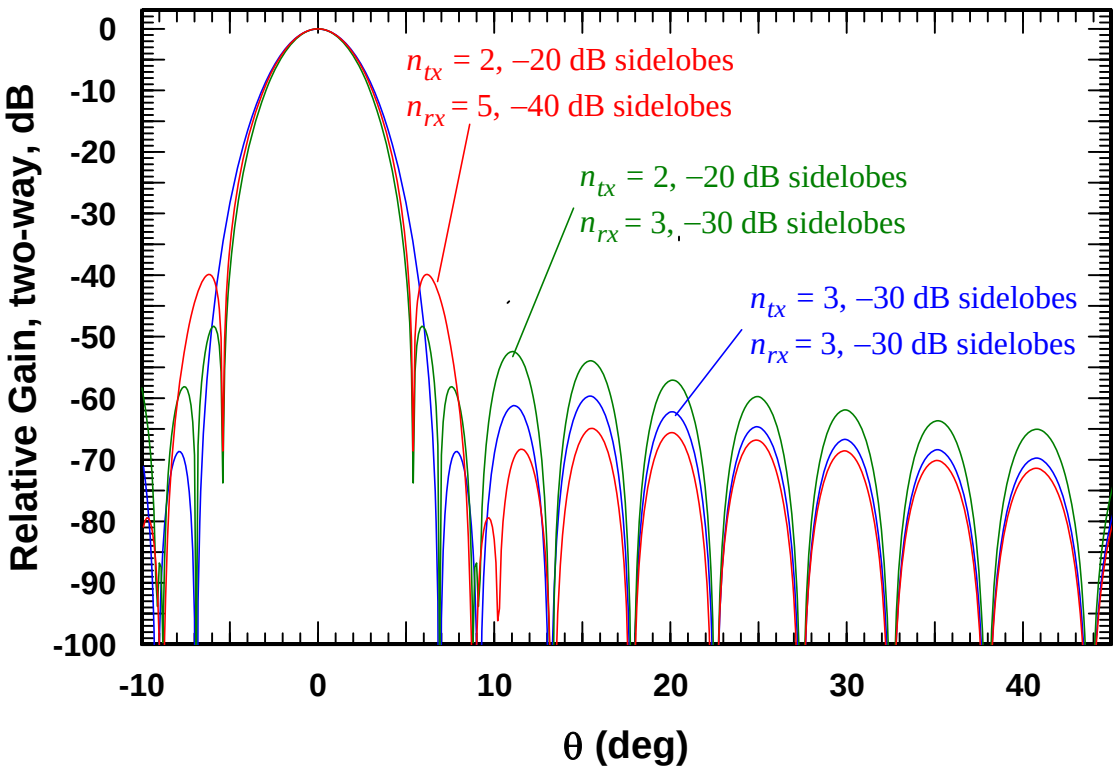

Figure 47 Two-way antenna patterns with Taylor illumination with several sets of design parameters.

8.1.2 Truncated array

In a two-dimensional rectangular array, the weight at each element is the product of two weights, one each from a one-dimensional taper. When an element is near the edge of the array, and a significant distance from the principal axes of the array, then its weight can very small. In particular, the elements in the corners will have the smallest weights. In fact, the weight can be so small that the element may have minimal effect on the array factor, and can be eliminated. Thus, when a two-dimensional array has amplitude taper in both dimensions, it may be desirable to remove elements in the corner regions to reduce cost. This will lso reduce the required range for the attenuator, and could reduce the number of required bits by one. However, truncating the array by eliminating many elements with small weights, while having little or no effect on the main lobe, may cause significant changes in the sidelobe region. Two truncation approaches are considered:
truncation to a specified amplitude, and
truncation to a circular aperture.

Figure 48 shows the element weights for an $N_{row} = N_{col} = 50$ odd array, with $\bar{n} = 5$, $SLL = -45$ dB Taylor illumination (note that the value chosen for $\bar{n}$ is just smaller than the minimum recommended value). The element weights $W_{0,\pm 50}$, $W_{\pm 50,0}$, on the edge of the principal axes, have an amplitude equal -11.6 dB. The center weight $W_{0,0}$ has an amplitude equal 10.7 dB. When the weights are truncated at -12 dB, eliminating the unneeded elements yields a nearly circular array rather than the rectangular array obtained when using all of the elements. Figure 49 shows the element weights after truncation of the array. In this case, only 7677 elements are used, rather than the original 10201 elements. Thus, the array is reduced to about 75% of its original size. When the array cost is dominated by T/R module cost, then eliminating the unnecessary elements reduces the cost significantly.

However, the reduced cost comes at the expense of the sidelobe level. The array factor for the truncated, near-circular array with a rectangular grid is plotted in Figure 50. These sidelobes have peaks at about -37 dB, about 8 dB worse than the design level of -45 dB. In this case, truncation of the aperture caused deterioration of the sidelobe level.

The sidelobe level of the Taylor array can be reduced somewhat by keeping more elements. If the truncation limit is changed to -15 dB (corresponding to a 27 dB dynamic range), the illuminated aperture appears as in Figure 51. In this case, the array contains about 84% of the number of elements in the full rectangular array. The array factor is plotted in Figure 52, where the sidelobe level has been reduced by about 2.5 dB. Table 1 compares the percent element reduction and peak sidelobe levels for three truncation levels.

Table 1 Performance of 2-D Taylor array with design sidelobes of $SLL = -45$ dB *and order* $\bar{n} = 5$.

Truncation level (dB)	% of full array	Peak sidelobe level (dB)
12	75%	–36.8
15	84%	–39.3
18	89%	–40.6

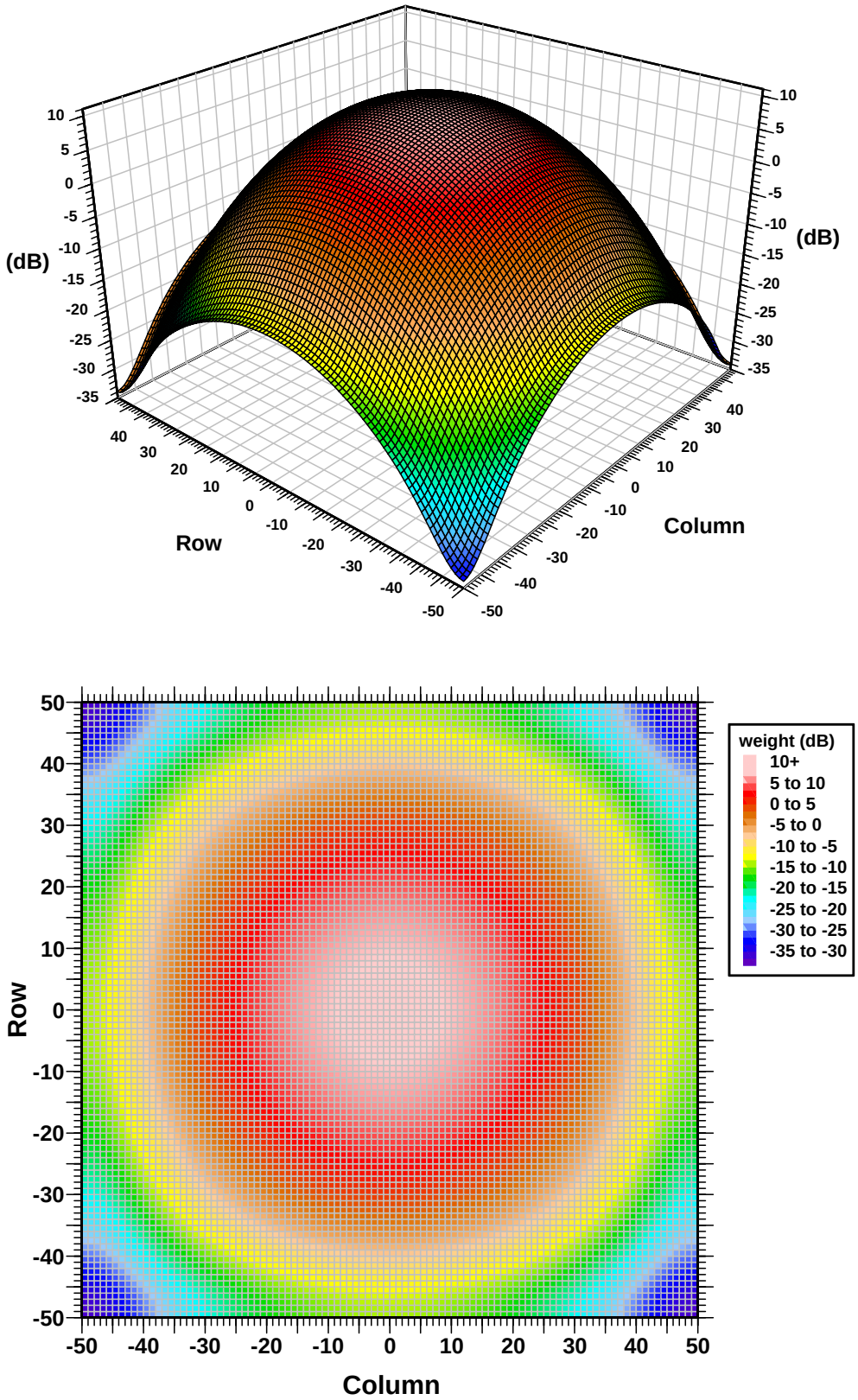

Figure 48 Weights for a two-dimensional odd array with a Taylor illumination, $SLL = -45\ \text{dB}$, $\bar{n} = 5$ *without truncation.*

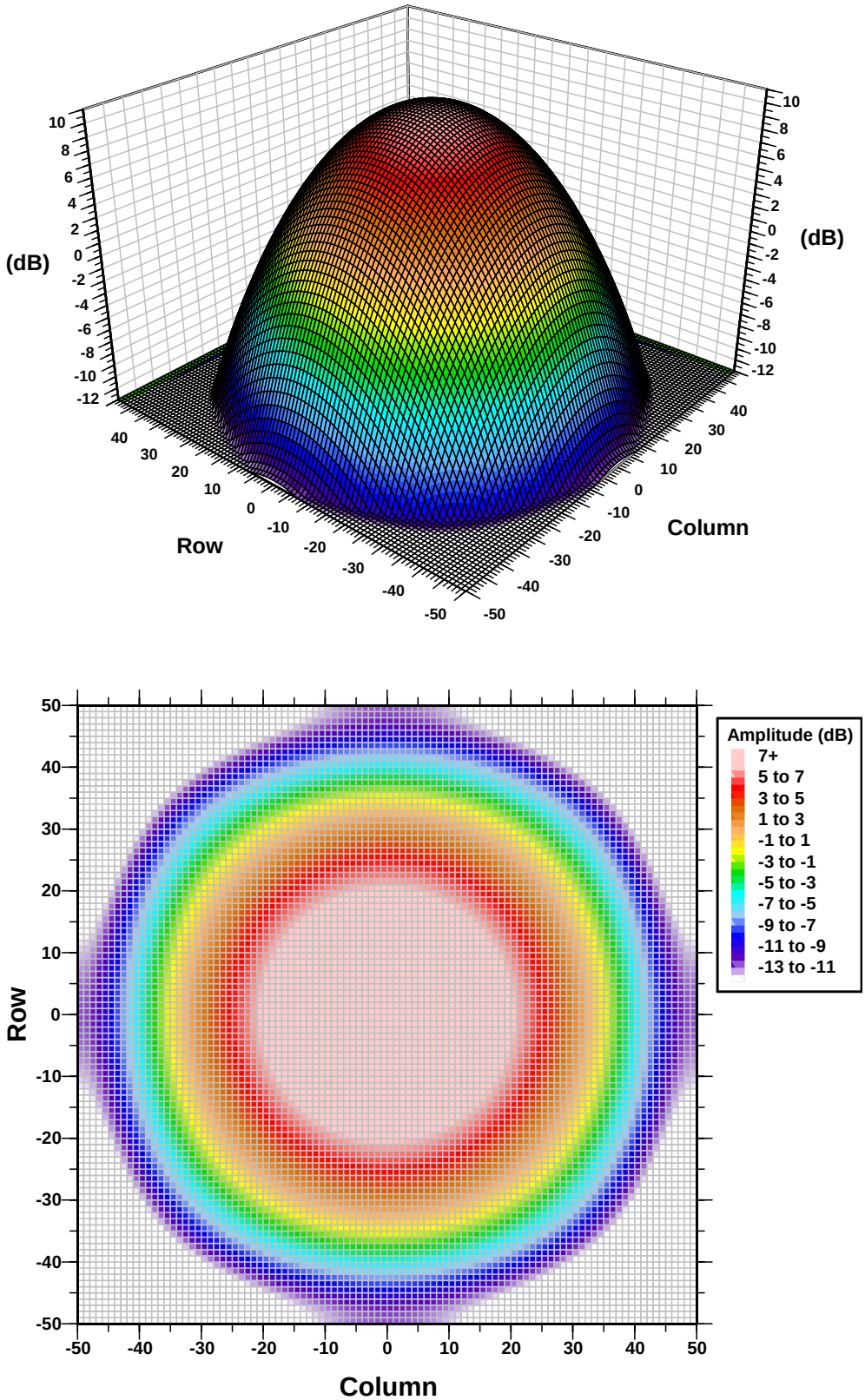

Figure 49 Weights for a two-dimensional odd array with a Taylor illumination, $SLL = -45\ \text{dB}$, $\bar{n} = 5$, *and truncated to* $-12\ \text{dB}$.

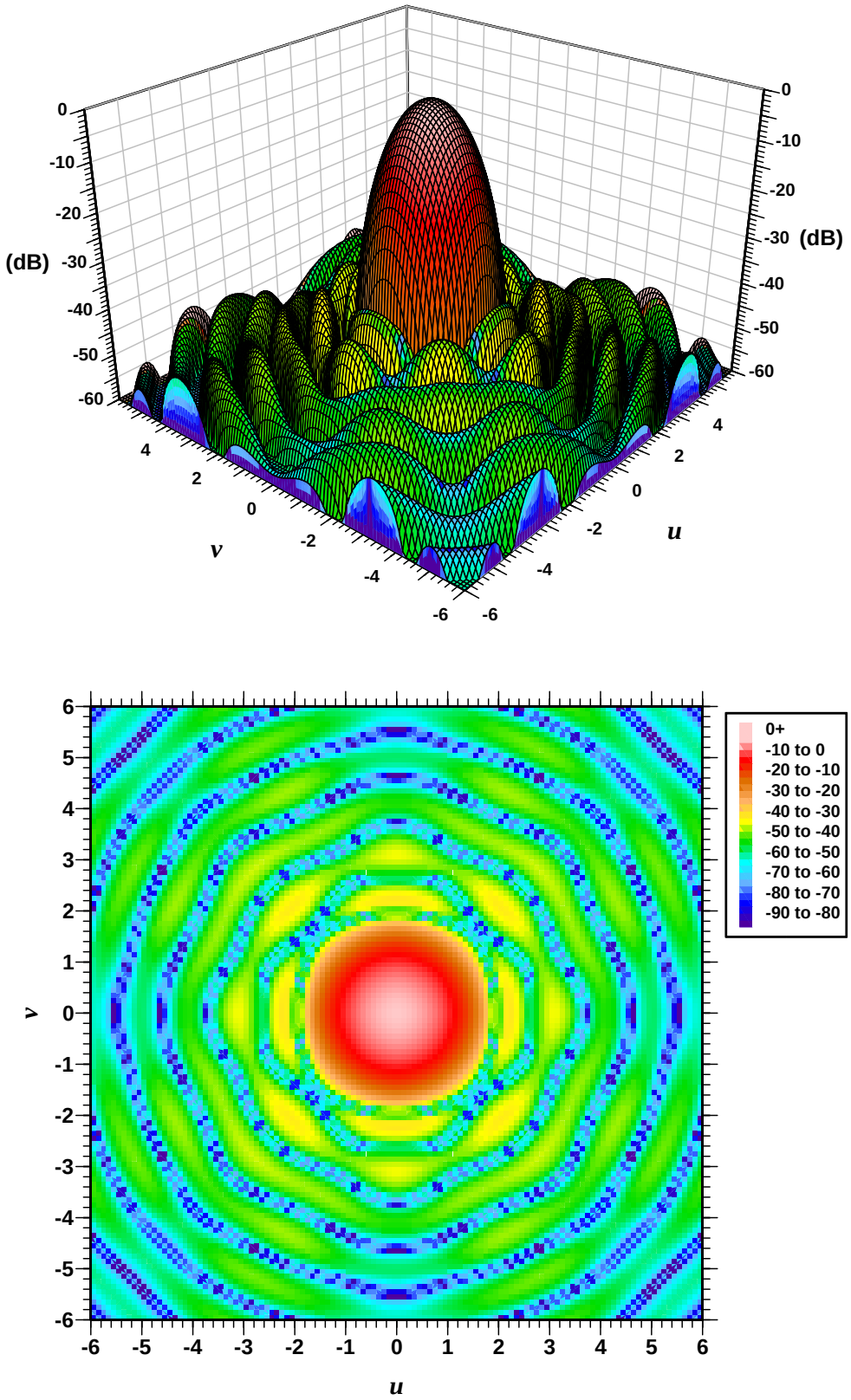

Figure 50 Normalized array factor for a two-dimensional odd array with a Taylor illumination, $SLL = -45\ \text{dB}$, $\bar{n} = 5$, *and truncated to* $-12\ \text{dB}$, *with a nearly circular aperture.*

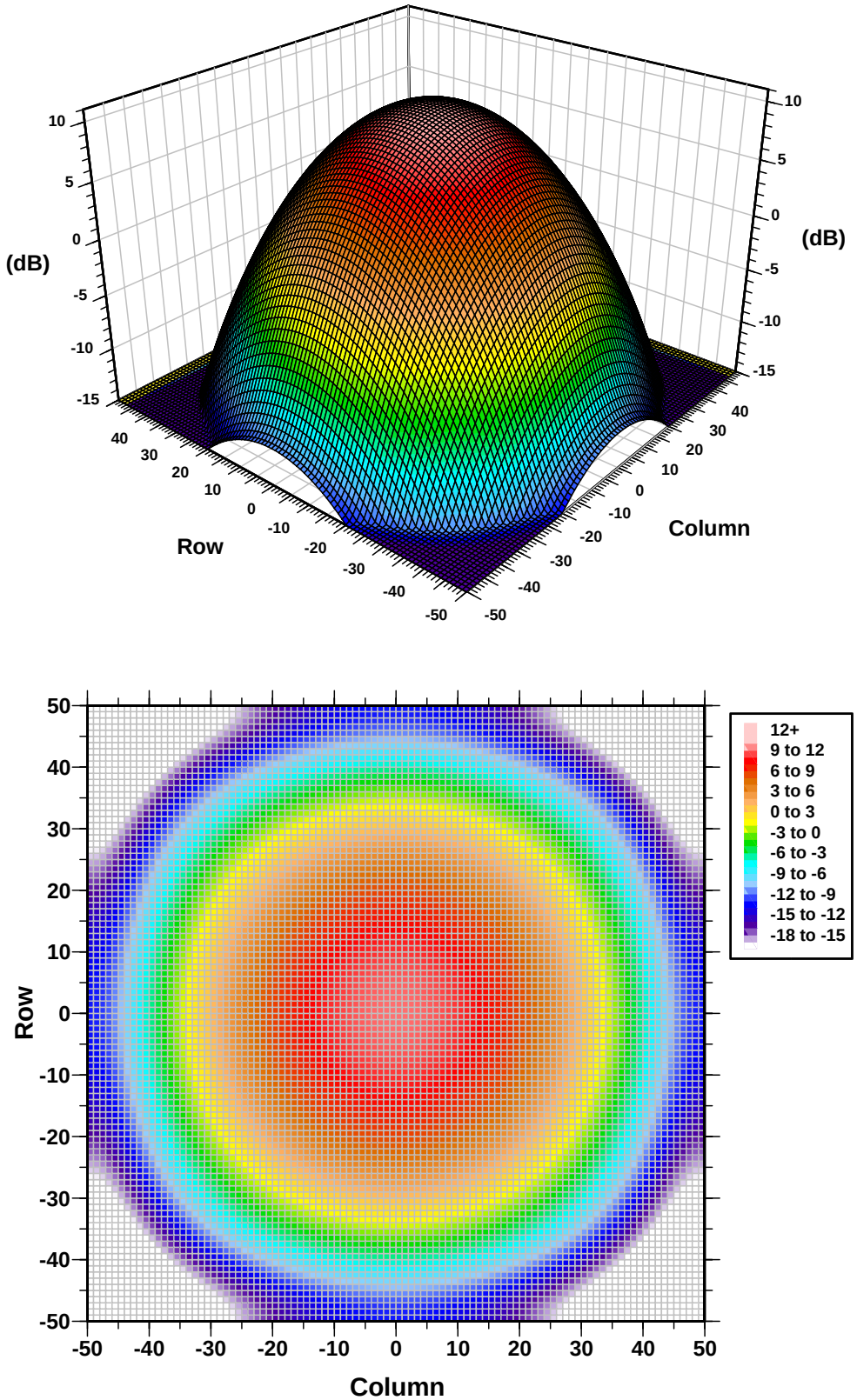

Figure 51 Weights for a two-dimensional odd array with a Taylor illumination, $SLL = -45\ \text{dB}$, $\bar{n} = 5$, *truncated to* $-15\ \text{dB}$.

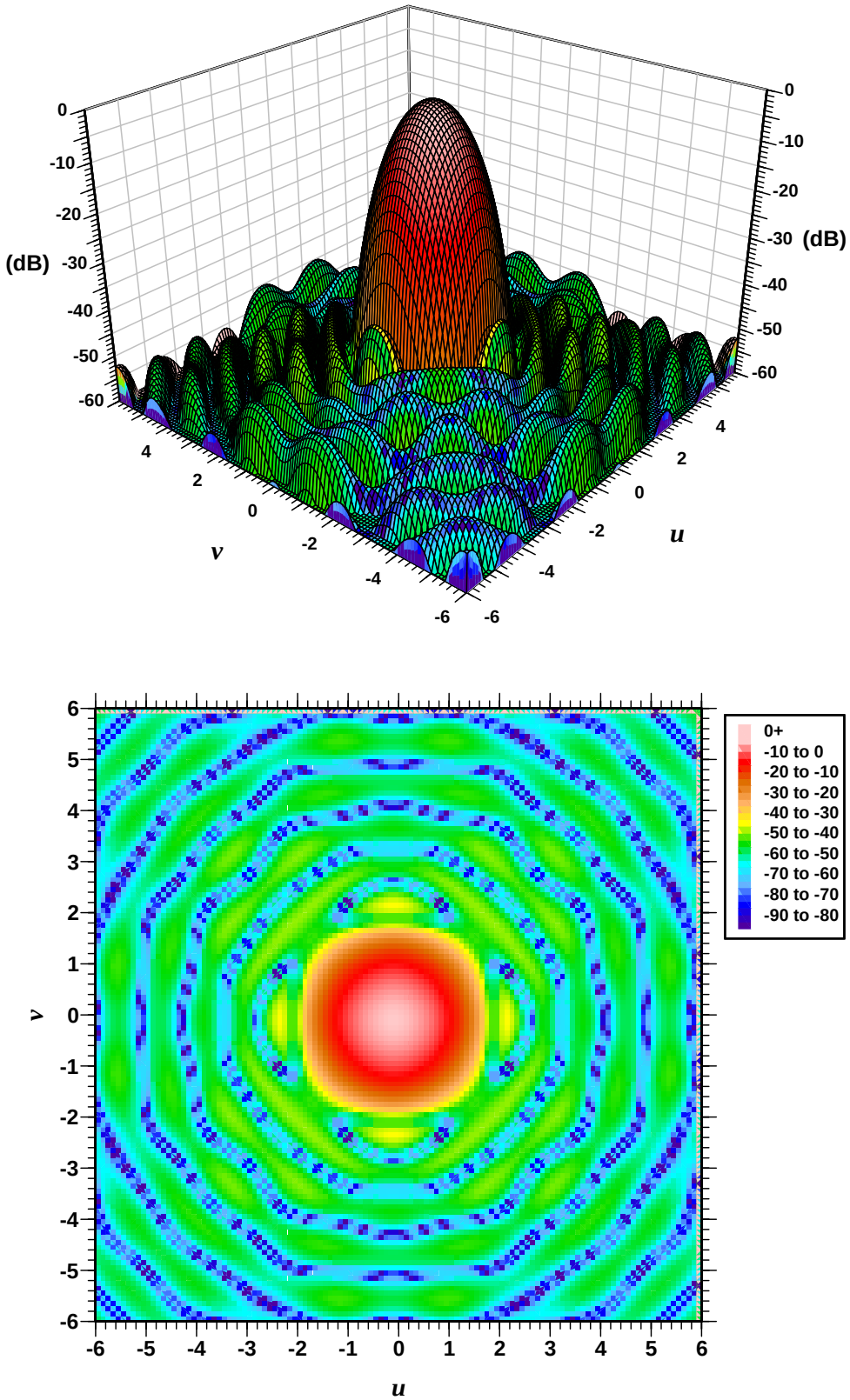

Figure 52 Normalized array factor for a two-dimensional odd array with a Taylor illumination, $SLL = -45$ dB, $\bar{n} = 5$, and truncated to -15 dB.

This Page Intentionally Blank

8.2 Uniform illumination of transmit array

In order to avoid the difficulties and inefficiencies of tapering the transmit array, it is useful to consider the uniformly illuminated array. This has the advantage that the attenuator is to be used only for tapering the receive array, and thus is not required to handle the higher power levels in the transmitter portion of the T/R module. Eliminating the attenuator from the transmit side of the T/R module eliminates the possibility of trimming the output power of each module, so tolerances on the output power specification may need to be made tighter.

8.2.1 Rectangular aperture array

The array factor for the uniformly illuminated rectangular aperture array can be written

$$S_{array}\left(\hat{\mathbf{r}},\xi_x,\xi_y\right)=S_{uniform}\left(\hat{\mathbf{r}},\xi_x,N\right)S_{uniform}\left(\hat{\mathbf{r}},\xi_y,M\right) \tag{8.9}$$

where, for the odd array,

$$S_{\substack{uniform\\odd}}\left(\hat{\mathbf{r}},\xi,\eta\right)=\frac{\sin\left(\left(2\eta+1\right)\frac{\left(\kappa-\xi\right)}{2}\right)}{\sin\left(\frac{\left(\kappa-\xi\right)}{2}\right)}, \tag{8.10}$$

and for the even array

$$S_{\substack{uniform\\even}}\left(\hat{\mathbf{r}},\xi,\eta\right)=\frac{\sin\left(\eta\left(\kappa-\xi\right)\right)}{\sin\left(\frac{\left(\kappa-\xi\right)}{2}\right)}. \tag{8.11}$$

The two-way array factor for a uniformly illuminated transmit array and a Taylor receive array is

$$\begin{aligned}S_{two-way}\left(\hat{\mathbf{r}},\xi_x,\xi_y\right)=&S_{Taylor}\left(\kappa_x-\xi_x,\alpha_x,\sigma_x,\bar{n}_x,N\right)S_{Taylor}\left(\kappa_y-\xi_y,\alpha_y,\sigma_y,\bar{n}_y,M\right)\cdot\\&S_{uniform}\left(\kappa_x-\xi_x,N_{tx}\right)S_{uniform}\left(\kappa_y-\xi_y,M_{ts}\right)\end{aligned} \tag{8.12}$$

where S_{Taylor} is given by (7.43) for the odd array and (7.51) for the even array. Since the uniformly illuminated transmit array will have a narrower main lobe than the Taylor receive array, it is possible that the first transmit sidelobe will fall within the mainlobe of the receive pattern.

For example, consider the even linear array with $N=13$ and $SLL_{dB}=-40\text{ dB}$ in the design example above. The uniformly illuminated transmit and the Taylor receive directivity patterns (normalized to receive mainlobe peak) are illustrated in Figure 53, and the normalized two-way directivity is plotted in Figure 54. The first null of the transmit pattern is well within the region of the mainlobe of the receive pattern. The point of intersection of the mainlobe of the receive pattern with the first sidelobe of the transmit pattern occurs at about –13.9 dB. The first sidelobe of the two-way pattern is -27.7 dB below the peak, while the remaining peak sidelobe is -61 dB down. Thus, the first sidelobe of the two-way pattern is significantly higher than the remaining sidelobes.

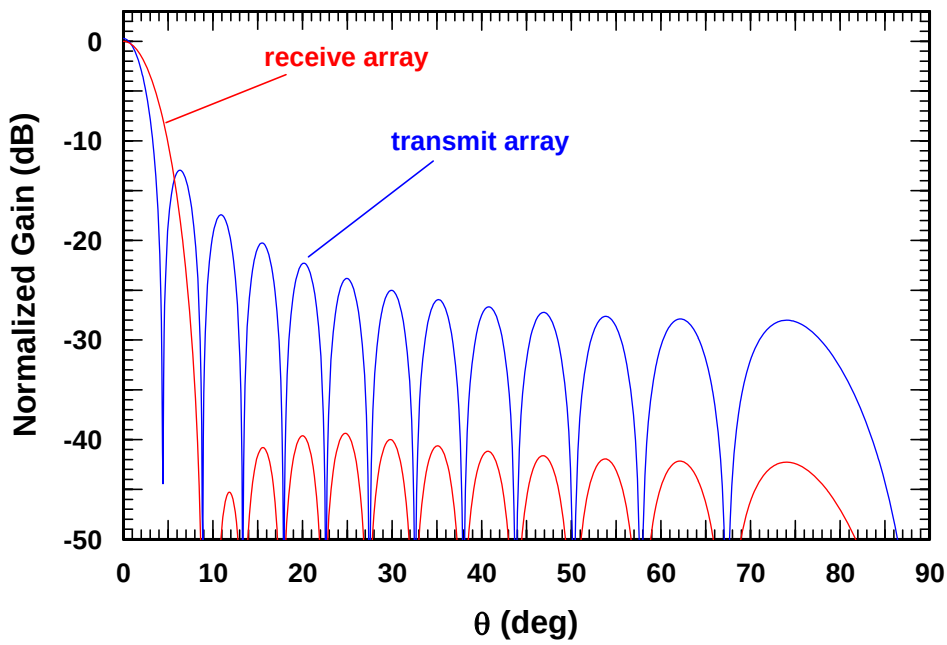

Figure 53 Directivity of uniformly illuminated transmit array (blue) and Taylor receive array (red), normalized to peak of receiver array.

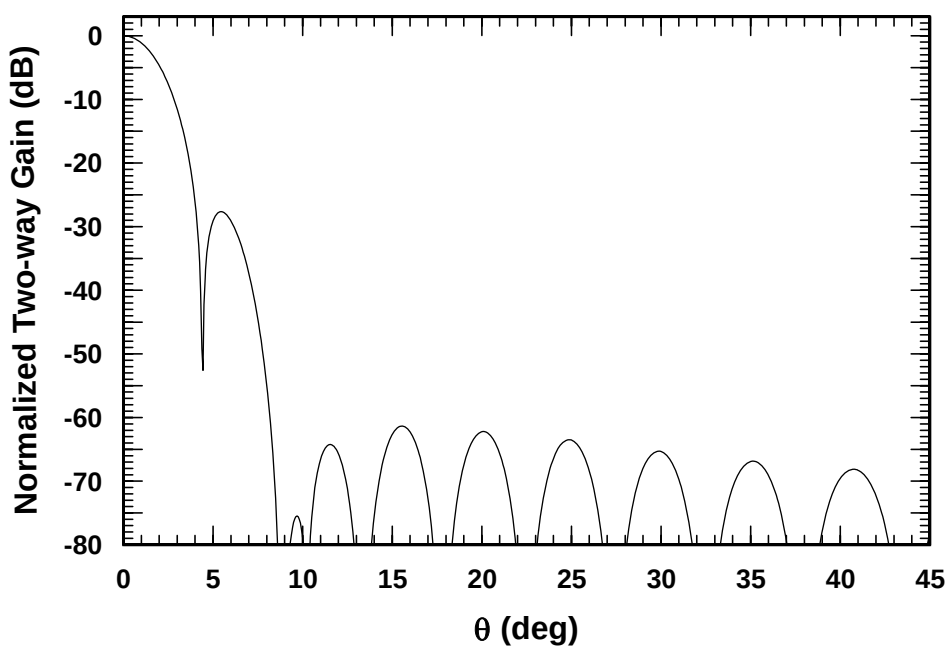

Figure 54 Normalized two-way directivity for uniform transmit array with Taylor receive array.

In order to move the first transmit sidelobe outside the mainlobe of the receiver pattern, one approach is to place the first null of both patterns as close to each other as possible. This can be accomplished by reducing the size of the transmit array. The first null of the transmit pattern occurs at

$$\theta_{\substack{uniform \\ 1^{st}\ null}} = \begin{cases} \sin^{-1}\left(\dfrac{\lambda}{2\Delta s\left(N_{tx}+\frac{1}{2}\right)}\right), \text{odd array} \\ \sin^{-1}\left(\dfrac{\lambda}{2\Delta s N_{tx}}\right), \text{even array} \end{cases} \tag{8.13}$$

and for the Taylor receive pattern at

$$\theta_{\substack{Taylor \\ 1^{st}\ null}} = \begin{cases} \sin^{-1}\left(\dfrac{\lambda}{2N\Delta s}\bar{n}\sqrt{\dfrac{\alpha^2+\frac{1}{4}}{\alpha^2+\left(\bar{n}-\frac{1}{2}\right)^2}}\right), \text{odd array} \\ \sin^{-1}\left(\dfrac{\lambda}{(2N-1)\Delta s}\bar{n}\sqrt{\dfrac{\alpha^2+\frac{1}{4}}{\alpha^2+\left(\bar{n}-\frac{1}{2}\right)^2}}\right), \text{even array} \end{cases} \tag{8.14}$$

where α is given by (7.37), and Δs is the element spacing. The requirement is

$$\begin{aligned} \frac{N}{\left(N_{tx}+\frac{1}{2}\right)} &= \bar{n}\sqrt{\frac{\alpha^2+\frac{1}{4}}{\alpha^2+\left(\bar{n}-\frac{1}{2}\right)^2}} \text{ for odd array} \\ \frac{N-\frac{1}{2}}{N_{tx}} &= \bar{n}\sqrt{\frac{\alpha^2+\frac{1}{4}}{\alpha^2+\left(\bar{n}-\frac{1}{2}\right)^2}} \text{ for even array} \end{aligned}, \tag{8.15}$$

so

$$N_{tx} = \text{ceiling}\left(\frac{N}{\bar{n}\sqrt{\dfrac{\alpha^2+\frac{1}{4}}{\alpha^2+\left(\bar{n}-\frac{1}{2}\right)^2}}} - \frac{1}{2}\right) \text{ for odd array}, \tag{8.16}$$

and

$$N_{tx} = \text{ceiling}\left(\frac{N-\frac{1}{2}}{\bar{n}\sqrt{\dfrac{\alpha^2+\frac{1}{4}}{\alpha^2+\left(\bar{n}-\frac{1}{2}\right)^2}}}\right) \text{ for even array}. \tag{8.17}$$

For the parameters of the design example, (8.17) gives $N_{tx} = 7$. Figure 55 plots the two-way directivity pattern when the transmit array of the design example is reduced. The peak sidelobe is about –57 dB below the mainlobe, while the first sidelobe has been reduced significantly. However, the mainlobe of the two-way pattern has been broadened, and the two-way directivity is reduced.

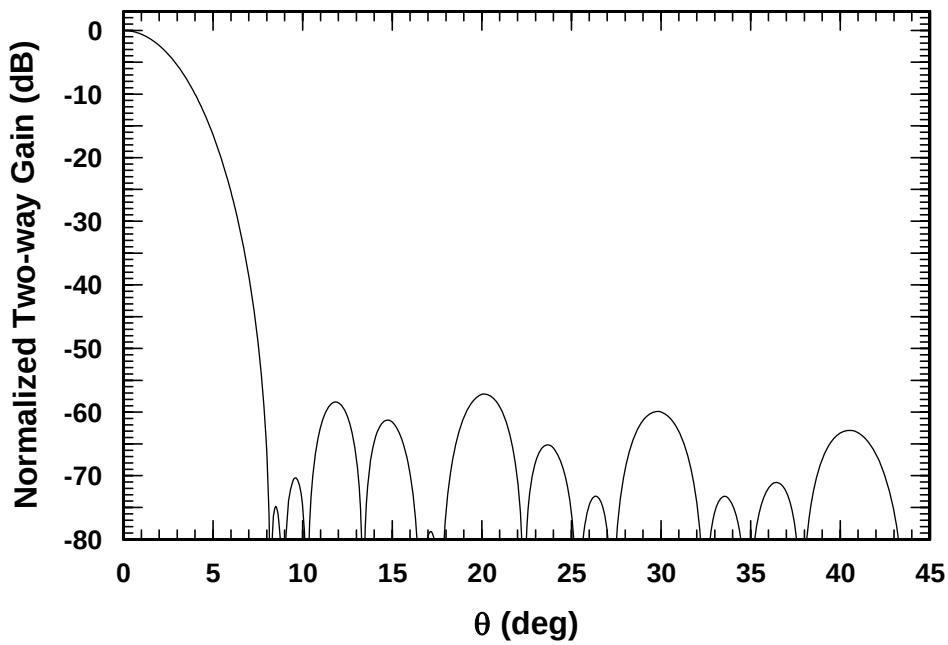

Figure 55 Normalized two-way directivity for uniform transmit array with $N_{tx} = 7$ *combined with Taylor receive array with* $N_{rx} = 13$.

8.2.1.1 Split-uniform illumination of transmit array (linear phase adjustment)

The entire array can be used for transmitting with uniform illumination and still maintain a low first sidelobe in the two-way pattern. This can be achieved by utilizing phase shifters to steer the transmit array slightly differently from the receive array. In this case, the transmit array is divided into two halves, with each half steered slightly away from the direction of the main lobe of the receive array. The amount of steering is chosen to place the first sidelobe of the transmit array in the first null of the receive array. This approach allows the parameters of the Taylor receive array to be chosen independently.

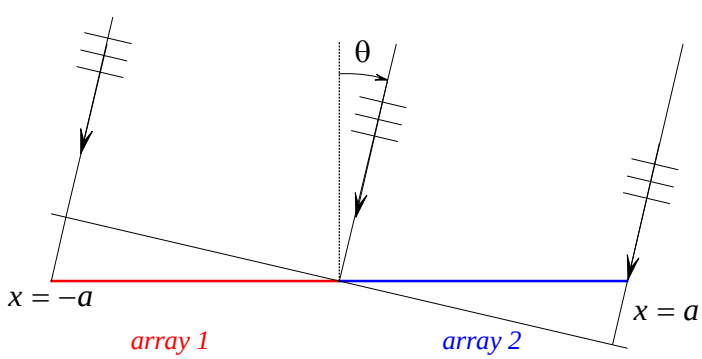

Figure 56 Two linear, uniformly illuminated arrays.

Consider two linear arrays as illustrated in Figure 56. Array 1 will be steered slightly to the left, while array 2 will be steered slightly to the right. The normalized array factor for the combination is

$$S_{tx} = \frac{1}{2a}\int_{-a}^{0} e^{-j\pi 2\frac{x}{\lambda}(\sin\theta+\sin\delta)}dx + \frac{1}{2a}\int_{0}^{a} e^{-j\pi 2\frac{x}{\lambda}(\sin\theta-\sin\delta)}dx$$

$$= e^{-j\pi\frac{a}{\lambda}\sin\delta}\left[e^{j\pi\frac{a}{\lambda}\sin\theta}\frac{\sin\left(\pi\frac{a}{\lambda}(\sin\theta-\sin\delta)\right)}{2\pi\frac{a}{\lambda}(\sin\theta-\sin\delta)} + e^{-j\pi\frac{a}{\lambda}\sin\theta}\frac{\sin\left(\pi\frac{a}{\lambda}(\sin\theta+\sin\delta)\right)}{2\pi\frac{a}{\lambda}(\sin\theta+\sin\delta)}\right] \tag{8.18}$$

or

$$S_{tx} = e^{-j\pi\frac{v}{2}}\left[e^{j\pi\frac{u}{2}}\frac{\sin\left(\pi\frac{u-v}{2}\right)}{\pi(u-v)} + e^{-j\pi\frac{u}{2}}\frac{\sin\left(\pi\frac{u+v}{2}\right)}{\pi(u+v)}\right] \tag{8.19}$$

where

$$u = \frac{2a}{\lambda}\sin\theta, \tag{8.20}$$

and

$$v = \frac{2a}{\lambda}\sin\delta, \tag{8.21}$$

The normalization is chosen so that $S_{tx} = 1$ when $u = v = 0$. The two-way pattern for a linear continuous array, using the split-uniform illumination for the transmitter and a Taylor illumination from (7.43) and (7.51) for receiver is

$$S_{two-way} = e^{-j\pi\frac{v}{2}}\left[e^{j\pi\frac{u}{2}}\frac{\sin\left(\pi\frac{u-v}{2}\right)}{\pi(u-v)} + e^{-j\pi\frac{u}{2}}\frac{\sin\left(\pi\frac{u+v}{2}\right)}{\pi(u+v)}\right]\sum_{m=-(\bar{n}-1)}^{\bar{n}-1} F_m \frac{\sin\pi(u+m)}{\pi(u+m)}$$

$$= e^{-j\pi\frac{v}{2}}\left[e^{j\pi\frac{u}{2}}\frac{\sin\left(\pi\frac{u-v}{2}\right)}{\pi(u-v)} + e^{-j\pi\frac{u}{2}}\frac{\sin\left(\pi\frac{u+v}{2}\right)}{\pi(u+v)}\right]\frac{\sin\pi u}{\pi u}\frac{\prod_{n=1}^{\bar{n}-1}\left[1-\frac{u^2}{\sigma_p^2\left(A^2+\left(n-\frac{1}{2}\right)^2\right)}\right]}{\prod_{n=1}^{\bar{n}-1}\left(1-\frac{u^2}{n^2}\right)}. \tag{8.22}$$

By adjusting δ, a two-way pattern with low sidelobes and minimal ripple in the mainlobe can be achieved. For example, consider the case with $a = 13\lambda$, $\bar{n} = 5$, $SLL = -40$ dB. Choosing $\delta = 3.46°$ produces less than 1 dB ripple in the main lobe, with a main lobe width of $2\theta_{3dB} = 4.75°$. When a reduced-size uniform transmit array with $a = 7\lambda$ is used with the same receive array, the main lobe width is $2\theta_{3dB} = 2.2°$. The two-way patterns for these two configurations are plotted in Figure 57. The directivity of the two-way pattern is -6.5 dB lower using the split-uniform array for transmitting. As indicated in Figure 58, the relative phase varies rather rapidly in the region of the main lobe. In addition, the split-uniform array does not concentrate the transmitter power efficiently over the main lobe of the receive array, as illustrated in Figure 59. For these reasons, the split-uniform transmit array is not recommended.

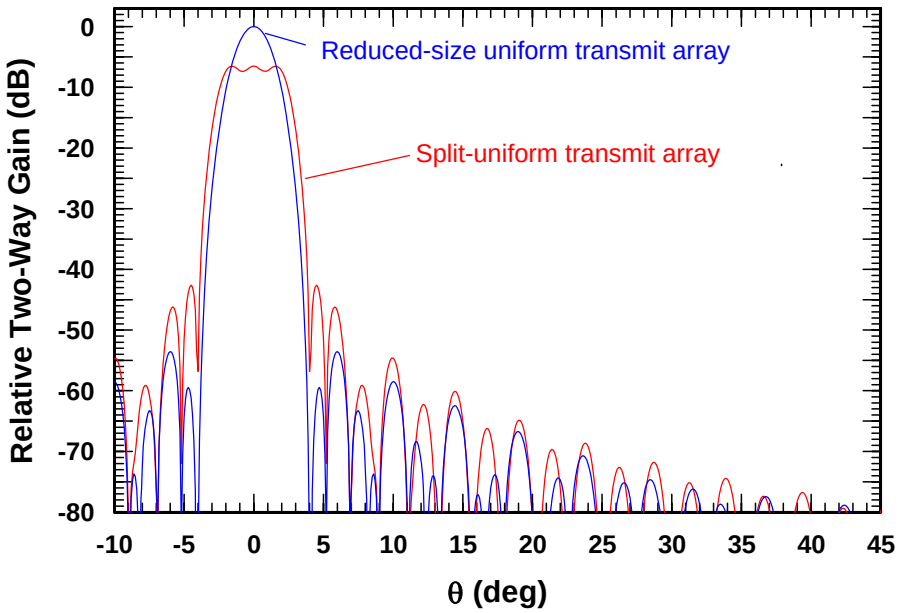

Figure 57 Comparison of two-way patterns using the split-uniform transmit array and the reduced-size transmit array.

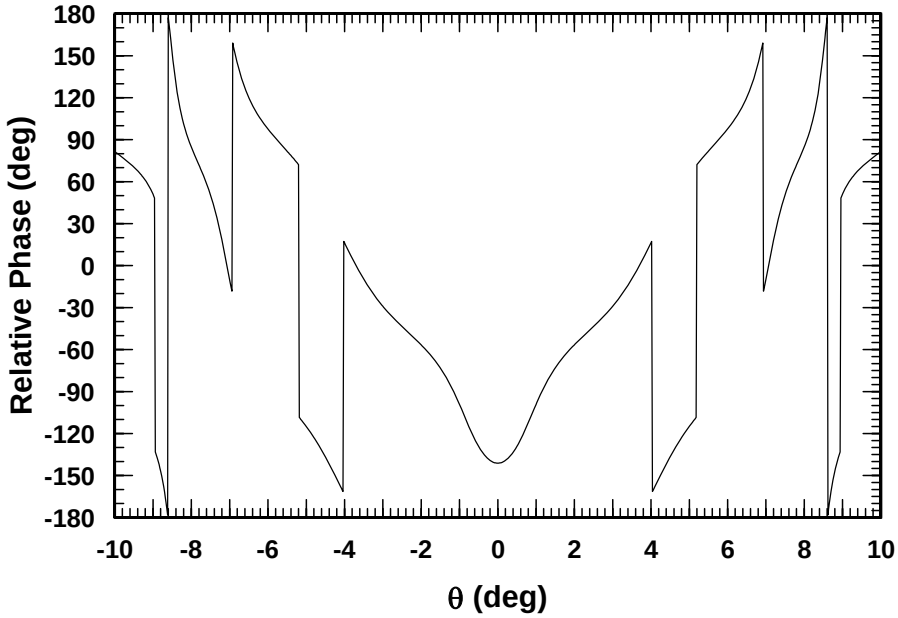

Figure 58 Relative phase for two-way pattern using the split-uniform transmit array.

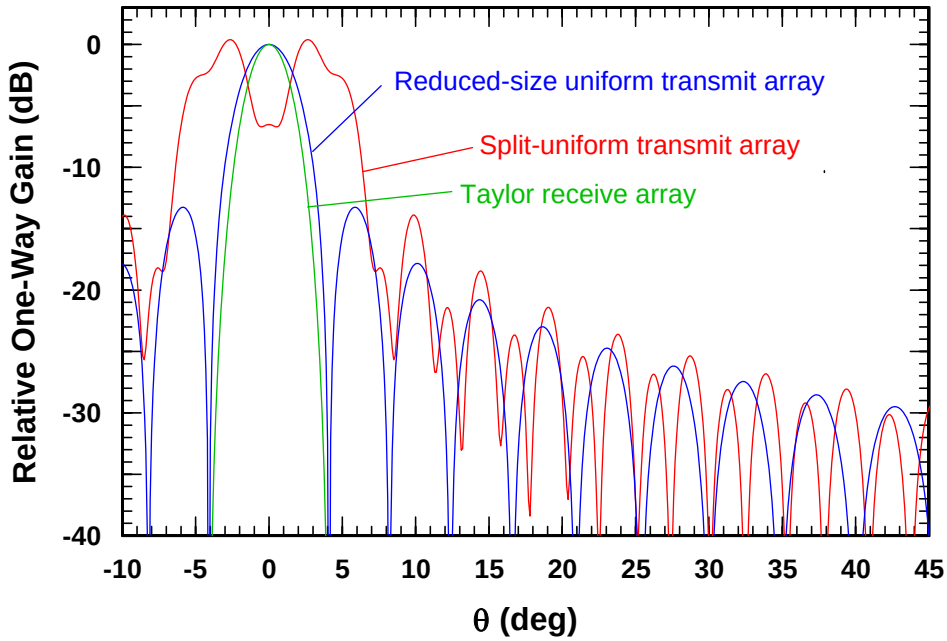

Figure 59 Comparison of one-way patterns of the split-uniform transmit array and the reduced-size transmit array.

8.2.1.2 Sinusoidal phase adjustment

The normalized array factor for a uniformly illuminated linear array extending from $x=-a$ to $x=a$ is

$$S_{uniform}=\frac{1}{2a}\int_{-a}^{a}e^{j\left(\frac{2\pi}{\lambda}x\sin\theta\right)}dx=\frac{\sin\left(\frac{2\pi}{\lambda}a\sin\theta\right)}{\frac{2\pi}{\lambda}a\sin\theta}. \tag{8.23}$$

Consider modifying this illumination by applying sinusoidal adjustment of the phase,

$$S_{Anger}=\frac{1}{2a}\int_{-a}^{a}e^{j\left(\frac{2\pi}{\lambda}x\sin\theta-\zeta\sin\left(\frac{\pi}{a}s\right)\right)}dx=\mathbf{J}_{\frac{2a}{\lambda}\sin\theta}(\zeta), \tag{8.24}$$

where $\mathbf{J}_{\nu}(\zeta)$ is the Anger function [3, 10], plotted in Figure 60 as a function of ν for several values of ζ. The Anger function is related to Bessel's function of the first kind

$$\mathbf{J}_n(\zeta)=J_n(\zeta) \text{ for } n \text{ an integer}. \tag{8.25}$$

The parameter ζ determines the amount of the sinusoidal phase adjustment, with the size of the adjustment proportional to the magnitude of ζ. The Anger function can be approximated with a series in ζ

$$\mathbf{J}_{\nu}(\zeta)=\left(1+\frac{\nu\zeta}{1-\nu^2}-\frac{\zeta^2}{4-\nu^2}-\frac{\nu\zeta^3}{9-10\nu^2+\nu^4}+\mathrm{O}\left(\zeta^4\right)\right)\frac{\sin(\pi\nu)}{\pi\nu}. \tag{8.26}$$

Using the first four terms of the series (8.26) gives 1% or better accuracy when $\zeta<0.9$. For $\zeta\le 0.5$, the accuracy is better than 0.1%. The accuracy improves as ν becomes larger (away from the main lobe).

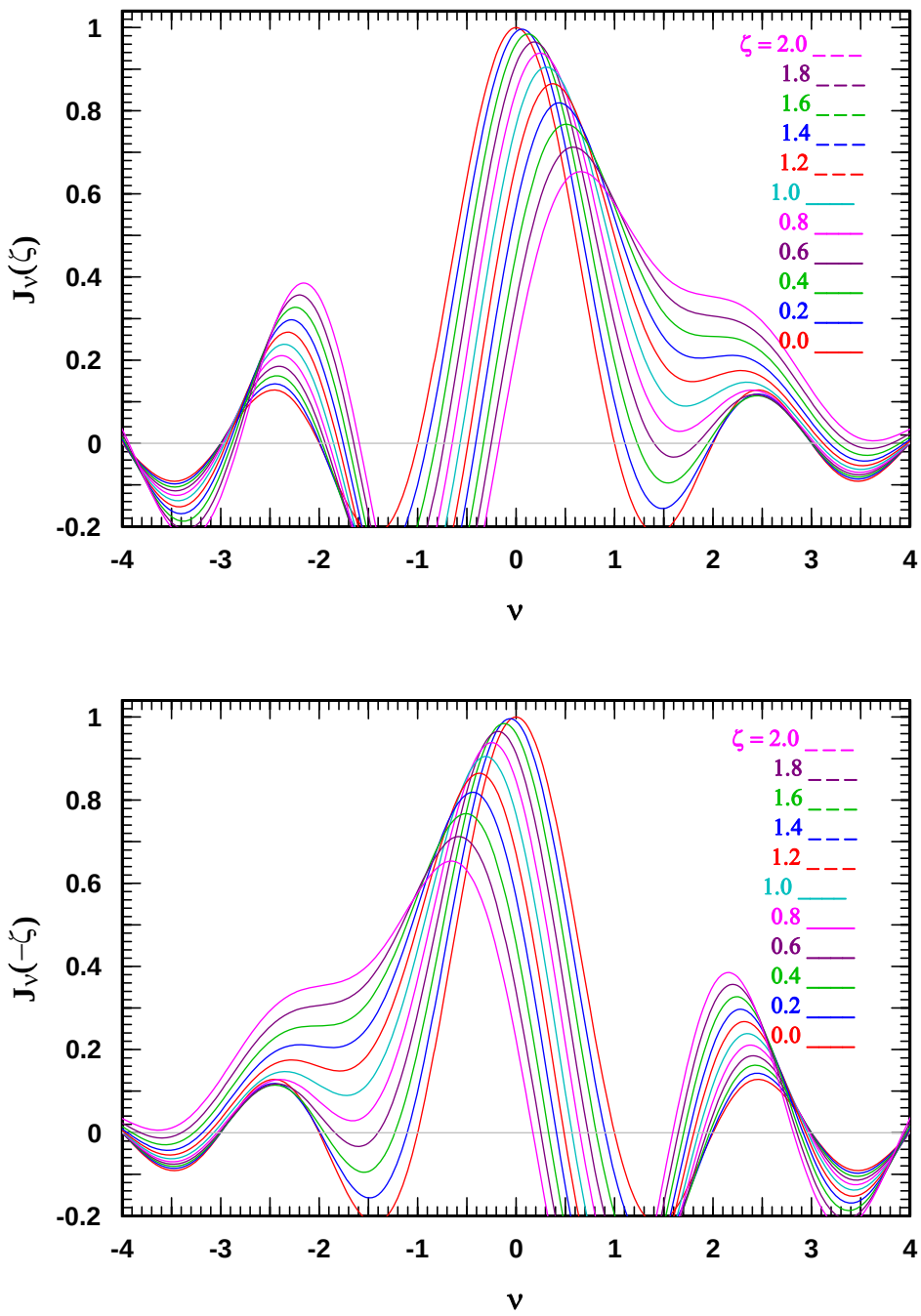

Figure 60 The Anger function, both $\mathbf{J}_\nu(\zeta)$ *and* $\mathbf{J}_\nu(-\zeta)$ *as functions of* ν *, for several values of* ζ *.*

As can be seen from (8.26), $\mathbf{J}_\nu(\zeta)$ is similar to $\operatorname{sinc}(\nu) = \sin(\pi\nu)/\pi\nu$, but the zero at $\nu = \pm 1$, in addition to others, has been cancelled. It is desirable to cancel the zero at $\nu = \pm 1$ in order to move the

first sidelobe further from the center of the main lobe. The first sidelobe of the Anger function occurs approximately at

$$\nu_{sidelobe} \approx 1.42799 + 0.316572\zeta - 0.0788377\zeta^2 + 0.0569093\zeta^3, \text{ for } 0 \le \zeta \le 1.5 \tag{8.27}$$

Note that as $\zeta > 0$ increases, the first sidelobe becomes more like a shoulder on the main lobe. Unfortunately, while the zero is cancelled at both $\nu = +1$ and $\nu = -1$, $\mathbf{J}_\nu(\zeta)$ is not symmetric with respect to ν, as can be seen in Figure 60. In fact, $\mathbf{J}_\nu(-\zeta)$ is the mirror image of $\mathbf{J}_\nu(\zeta)$,

$$\mathbf{J}_\nu(-\zeta) = \mathbf{J}_{-\nu}(\zeta). \tag{8.28}$$

Using the Anger function for the transmit pattern, the two-way antenna pattern for the linear array is

$$S_{\substack{two-way \\ Anger}}(\theta,\zeta) = \mathbf{J}_{\frac{2a}{\lambda}\sin\theta}(\zeta) \sum_{m=-(\bar{n}-1)}^{\bar{n}-1} F_m \frac{\sin\pi\left(\frac{2a}{\lambda}\sin\theta + m\right)}{\pi\left(\frac{2a}{\lambda}\sin\theta + m\right)}. \tag{8.29}$$

The parameter ζ that places the first sidelobe of the transmit pattern, for $\theta > 0$, at the location of the first null of the receive pattern is obtained from the solution of

$$1.42799 + 0.316572\zeta - 0.0788377\zeta^2 + 0.0569093\zeta^3 = \bar{n}\sqrt{\frac{A^2 + \frac{1}{4}}{A^2 + \left(\bar{n} - \frac{1}{2}\right)^2}}, \tag{8.30}$$

where (7.32)

$$\bar{n} = \text{rnd}\left(\left(\frac{SLL_{dB}}{22.8}\right)^2 - \frac{SLL_{dB}}{36.3} + 0.759\right).$$

A convenient fit to this solution is

$$\zeta_{opt}(SLL_{dB}) = -5.94543 - 6.14214\frac{SLL_{dB}}{20} - 1.55552\left(\frac{SLL_{dB}}{20}\right)^2 - 0.145312\left(\frac{SLL_{dB}}{20}\right)^3 \tag{8.31}$$

For example, when $SLL_{dB} = -30$ dB, the minimum Taylor order is $\bar{n} = 3$, and (8.31) gives $\zeta_{opt} = 0.258$ for the Anger transmit pattern. The two-way pattern is plotted in Figure 61. The pattern is not symmetric around $u = 0$, and the sidelobes for $u < 0$ are higher than when $u > 0$. The peak of the main lobe is skewed slightly to $u_{peak} = 0.0477$.

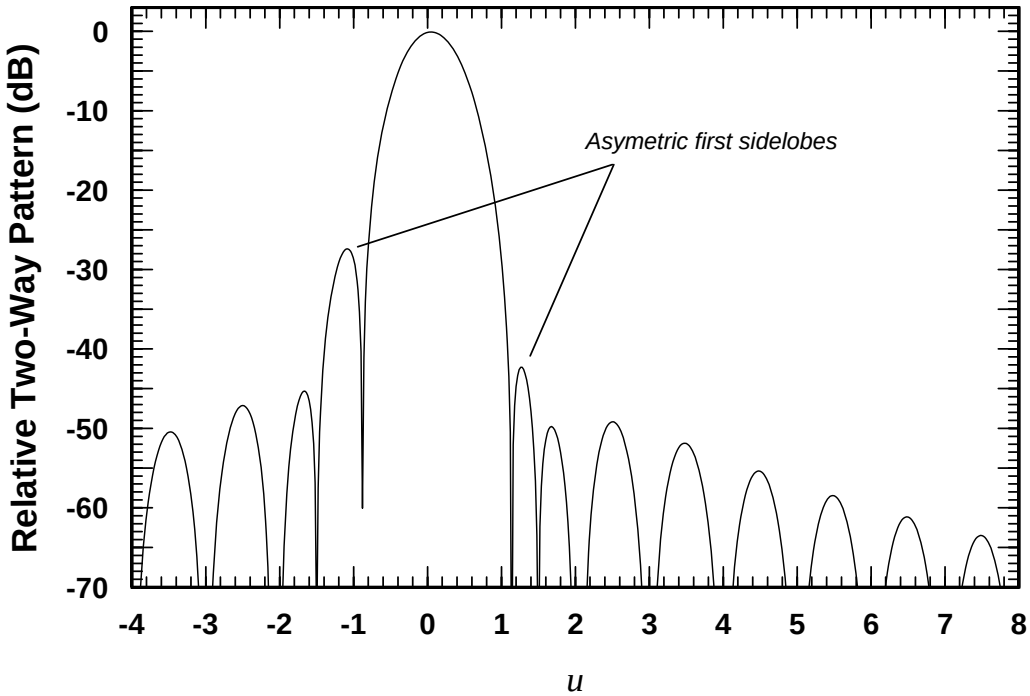

Figure 61 Normalized two-way antenna pattern when the transmit array has sinusoidal phase adjustment with $\zeta = 0.258$*, and the receive array uses a Taylor distribtution with* $\overline{n} = 2$ *and* $SLL = -30$ dB*.*

Note that $u = \frac{2a}{\lambda}\sin\theta$*.*

It is tempting to modify the transmit phase function so that

$$\begin{aligned} S_{Anger} &= \frac{1}{2a}\int_{-a}^{0} e^{j\left(\frac{2\pi}{\lambda}x\sin\theta+\zeta\sin\left(\frac{\pi}{a}s\right)\right)}dx + \frac{1}{2a}\int_{0}^{a} e^{j\left(\frac{2\pi}{\lambda}x\sin\theta-\zeta\sin\left(\frac{\pi}{a}s\right)\right)}dx \\ &= \frac{1}{2}\mathbf{J}_{\frac{2a}{\lambda}\sin\theta}\left(-\zeta\right) + \frac{1}{2}\mathbf{J}_{\frac{2a}{\lambda}\sin\theta}\left(\zeta\right) \end{aligned}, \tag{8.32}$$

which restores the symmetry. Unfortunately, as can be seen from (8.26) and in Figure 62, the cancellation of the zeros at $\nu = \pm 1$ is undone, and the transmit pattern's main lobe is not broadened. Thus, there is no benefit to this approach.

The sinusoidal phase adjustment can utilize the full aperture with uniform illumination for the transmit pattern, while reducing the first sidelobe on one side. However, the two-way pattern is not symmetric, and good sidelobe reduction is only available in a limited region. This method is not recommended for general use.

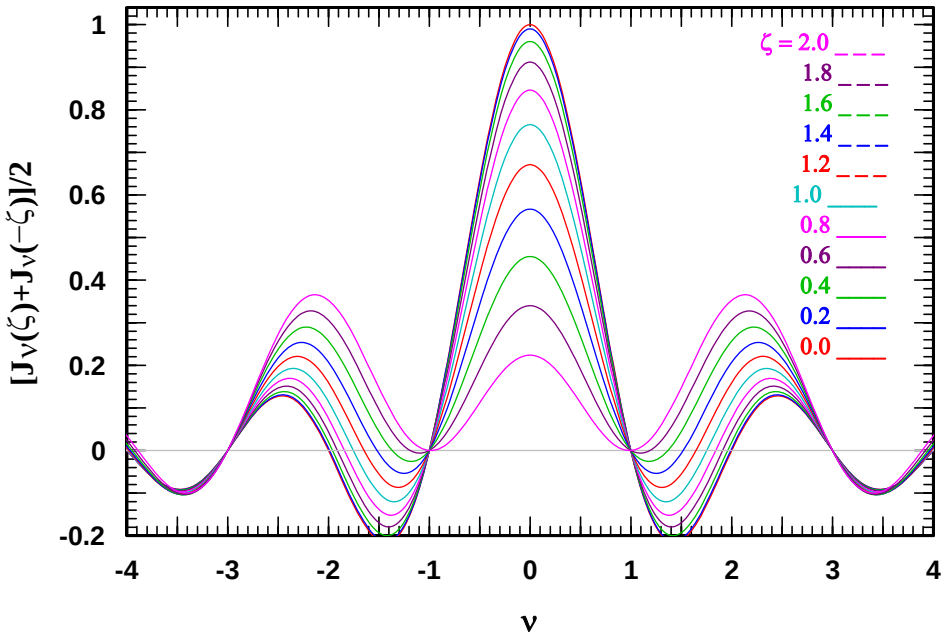

Figure 62 A symmetric linear combination of two Anger functions, $\frac{1}{2}\mathbf{J}_\nu(-\zeta)+\frac{1}{2}\mathbf{J}_\nu(\zeta)$.

8.2.1.3 Quadratic phase adjustment

Consider modifying the uniform illumination by applying quadratic adjustment of the phase, using the parameter ζ as follows,

$$S_q=\frac{1}{2a}\int_{-a}^{a}e^{j\left(\frac{2\pi}{\lambda}x\sin\theta-\zeta^2x^2\right)}dx=\frac{1}{2a}e^{j\frac{\pi^2\sin^2\theta}{\lambda^2\zeta^2}}\int_{-a}^{a}e^{-j\left(\zeta x-\frac{\pi}{\lambda\zeta}\sin\theta\right)^2}dx\,, \tag{8.33}$$

which can be written in terms of Fresnel Integrals,

$$S_q=\frac{1}{2a}\frac{1}{\zeta}\sqrt{\frac{\pi}{2}}e^{j\frac{\pi^2\sin^2\theta}{\lambda^2\zeta^2}}\left(\begin{array}{l}C_1\left(\zeta a+\frac{\pi}{\lambda\zeta}\sin\theta\right)+C_1\left(\zeta a-\frac{\pi}{\lambda\zeta}\sin\theta\right)\\-j\left(S_1\left(\zeta a+\frac{\pi}{\lambda\zeta}\sin\theta\right)+S_1\left(\zeta a-\frac{\pi}{\lambda\zeta}\sin\theta\right)\right)\end{array}\right). \tag{8.34}$$

The Fresnel Integrals are [3]

$$C(x)=\int_0^x\cos\left(\frac{\pi}{2}t^2\right)dt\,, \tag{8.35}$$

$$S(x)=\int_0^x\sin\left(\frac{\pi}{2}t^2\right)dt\,, \tag{8.36}$$

$$C_1(x)=C\left(\sqrt{\frac{2}{\pi}}x\right)=\sqrt{\frac{2}{\pi}}\int_0^x\cos\left(t^2\right)dt\,, \tag{8.37}$$

and

$$S_1(x) = S\left(\sqrt{\frac{2}{\pi}}x\right) = \sqrt{\frac{2}{\pi}}\int_0^x \sin\left(t^2\right)dt\,. \tag{8.38}$$

Writing (8.34) in terms of $u = \frac{2a}{\lambda}\sin\theta$ and $\xi = \zeta a$

$$S_q(u) = \frac{1}{2\xi}\sqrt{\frac{\pi}{2}}e^{j\frac{u^2}{\xi^2}}\left(\begin{array}{l} C_1\left(\xi + \frac{1}{\xi}\frac{\pi}{2}u\right) + C_1\left(\xi - \frac{1}{\xi}\frac{\pi}{2}u\right) \\ -j\left(S_1\left(\xi + \frac{1}{\xi}\frac{\pi}{2}u\right) + S_1\left(\xi - \frac{1}{\xi}\frac{\pi}{2}u\right)\right)\end{array}\right). \tag{8.39}$$

The normalized uniformly illuminated array factor with quadratic phase adjustment is plotted in Figure 63 for several values of the parameter ξ. As ξ increases, the first null is filled in, and the radiation is spread over a larger space. However, the main lobe of the pattern begins to become indistinguishable for the larger values. While the quadratic phase adjustment introduces no loss in the array factor, the peak directivity is reduced considerably as the nulls are filled, and the sidelobe level is increased. Eventually, the sidelobes and the main lobes merge, becoming indistinguishable. The two-way array factor, when the receive array has a –40 dB Taylor illumination, is plotted in Figure 64. For the larger values of the parameter ξ, the two-way pattern has a low first sidelobe, with the sidelobe ratio essentially the same as the receive (Taylor) array factor alone. Much of the transmit energy falls outside the main lobe of the receive pattern.

The quadratic phase adjustment can be used to produce a flat two-way array factor in the main lobe region, as illustrated in Figure 65, for parameter $\xi = \sqrt{6} \simeq 2.45$. This comes at high cost, as the normalized array factor is down about 10 dB from the equivalent array without phase adjustment. A large portion of the transmit energy is radiated to the space outside the main lobe. The first sidelobe is slightly higher than the first sidelobe of the receive array factor alone. An additional problem with this antenna pattern is the phase response across the main lobe, which is plotted in Figure 66. This nonlinear phase response is undesirable for some applications.

As with the other phase adjustment approaches, the quadratic phase adjustment is not very attractive from the point of view of efficiency. When the adjustment parameter ξ is large enough to eliminate the large first sidelobe, much of the transmit energy falls outside the main lobe of the receiver. In addition, the phase response of the two-way pattern is nonlinear. For these reasons, the quadratic phase adjustment is not recommended.

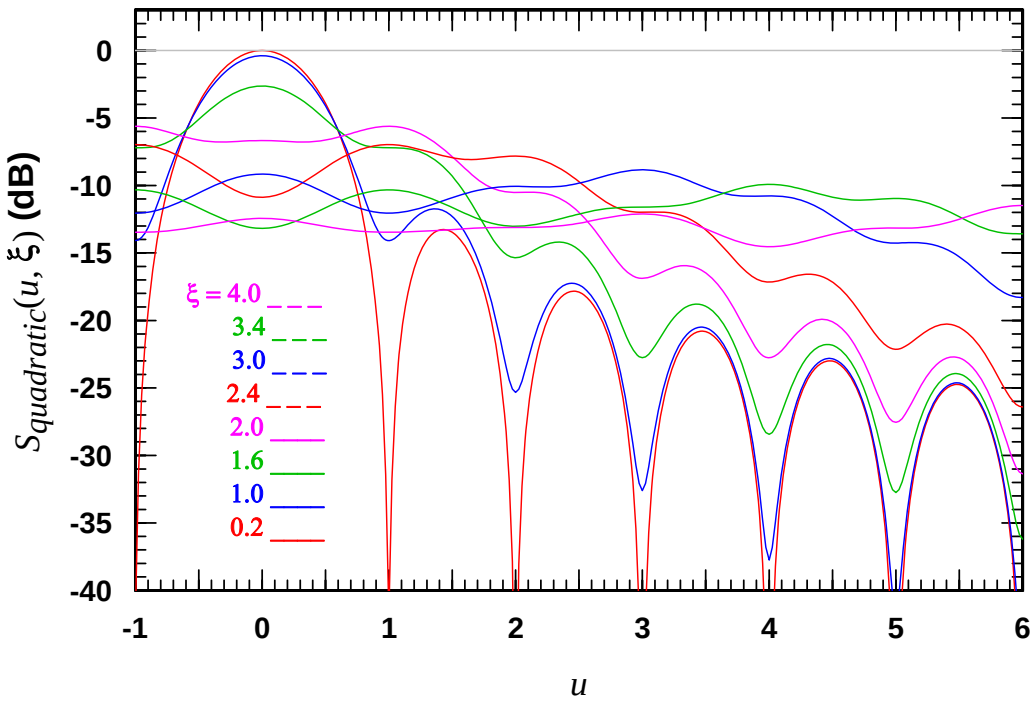

Figure 63 One-way array factor with uniform illumination and quadratic phase adjustment for several values of parameter ξ *.*

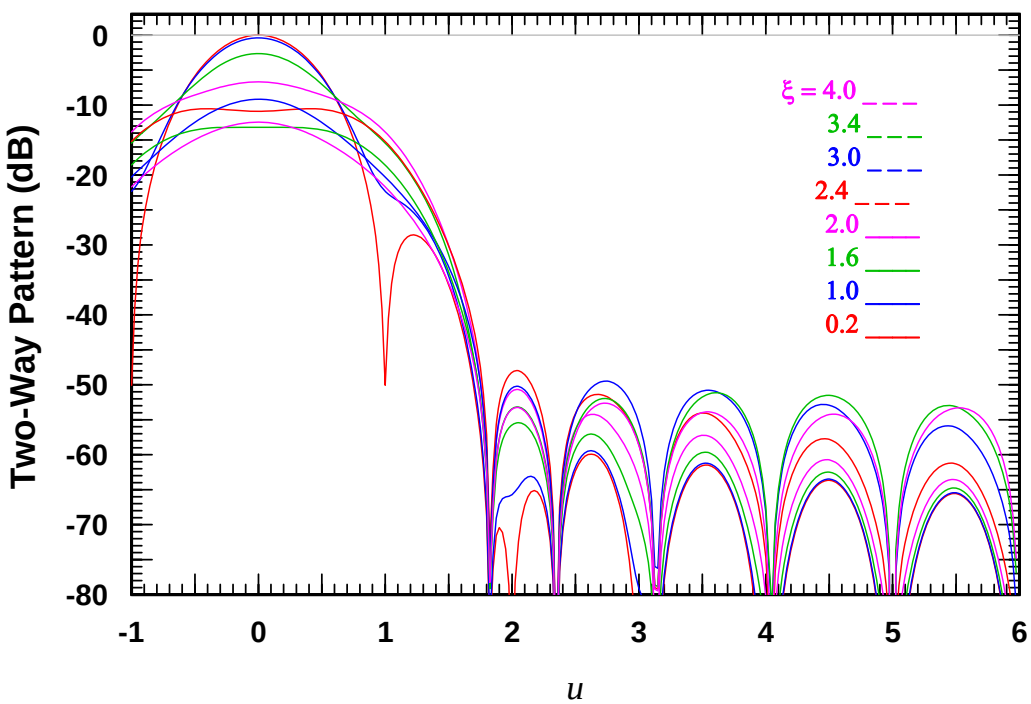

Figure 64 Two-way antenna pattern with uniform illumination and quadratic phase adjustment for several values of ξ *for the transmit array, and a –40 dB sidelobe Taylor illumination for the receive array.*

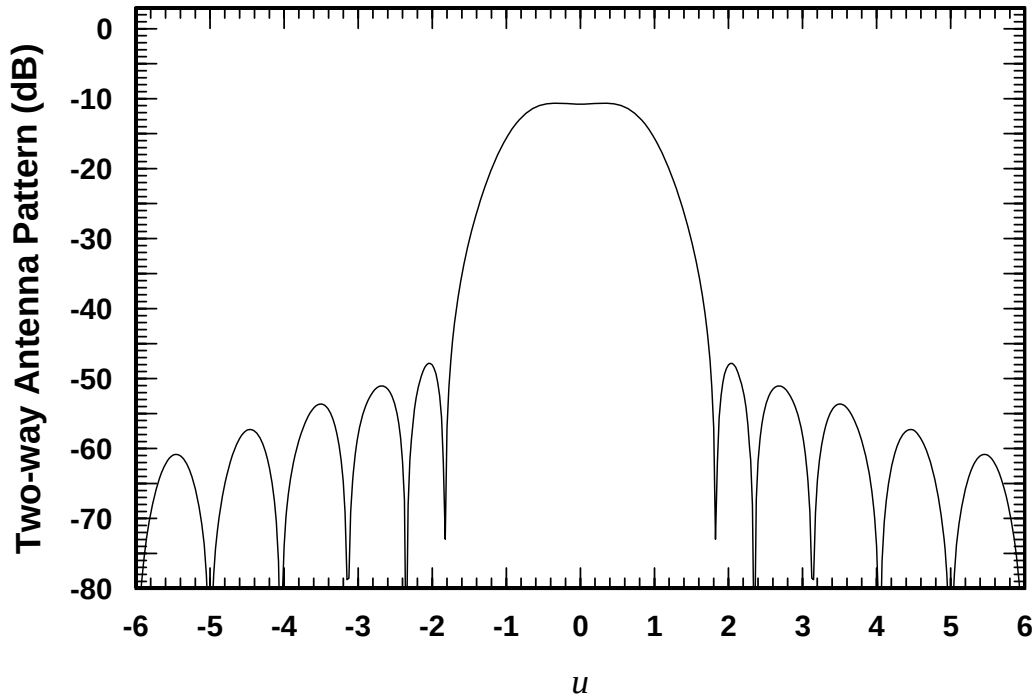

Figure 65 Two-way array factor with quadratic-phase-adjustment parameter $\xi = \sqrt{6} \simeq 2.45$.

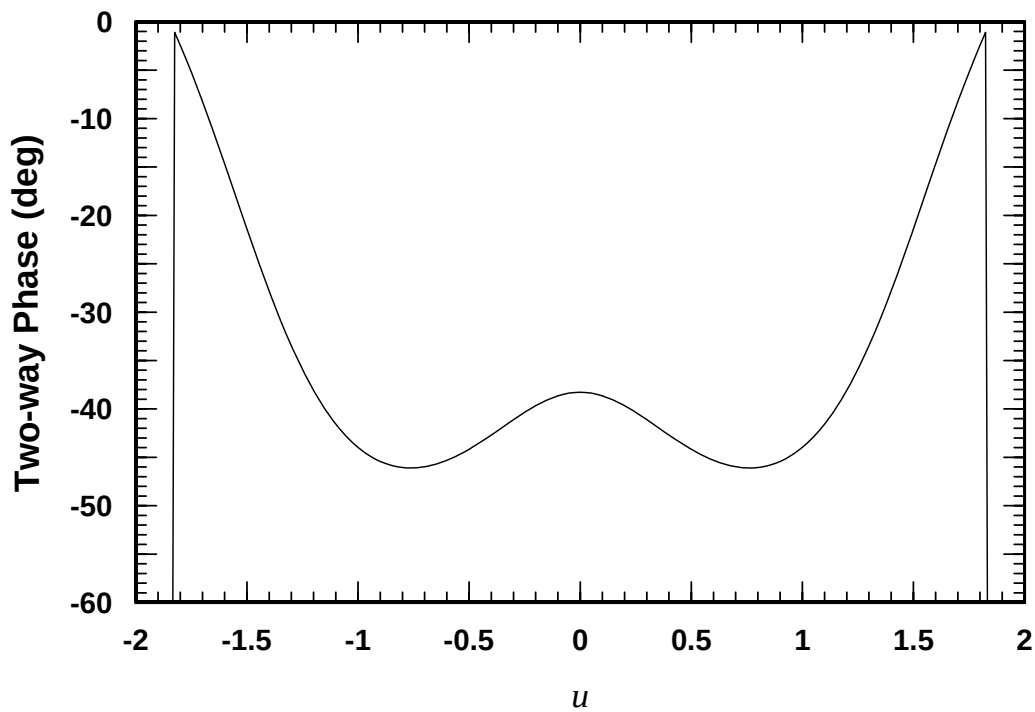

Figure 66 Relative phase of the two-way array factor with quadratic-phase-adjustment parameter $\xi = \sqrt{6} \simeq 2.45$.

8.2.2 Circular aperture

If the uniformly illuminated transmit array is made circular, then the main lobe will be broadened slightly, and the first sidelobe will be reduced. It is useful to examine the array factor for a uniformly illuminated circular aperture of radius *a*, given by

$$\begin{aligned} S_{uniform,\,circular} &= \frac{1}{\pi a^2}\int_0^a\int_0^{2\pi} e^{j\frac{2\pi}{\lambda}r(\cos\phi\cos\phi'+\sin\phi\sin\phi')\sin\theta}\, r d\phi' dr \\ &= \frac{2}{a^2}\int_0^a J_0\left(\frac{2\pi}{\lambda}r\sin\theta\right) r dr \\ &= \frac{J_1\left(\frac{2\pi}{\lambda}a\sin\theta\right)}{\frac{\pi}{\lambda}a\sin\theta} = 2\frac{J_1\left(\pi\sqrt{u^2+v^2}\right)}{\pi\sqrt{u^2+v^2}} \end{aligned} \tag{8.40}$$

where

$$u = \frac{2a}{\lambda}\sin\theta\cos\phi\,,$$

and

$$v = \frac{2a}{\lambda}\sin\theta\sin\phi\,.$$

This is a circularly symmetric pattern, and has its first sidelobe at

$$\sqrt{u^2+v^2} = \frac{\lambda_{2,1}}{\pi} = 1.63471935\cdots \tag{8.41}$$

where $\lambda_{n,1}$ is the first nontrivial zero of

$$J_n(\lambda) = 0\,. \tag{8.42}$$

The peak of the first sidelobe is -17.6 dB below the main lobe, nearly 4 dB better than the -13.5 dB level from the uniform rectangular aperture. In addition, the first null occurs at

$$\sqrt{u^2+v^2} = \frac{\lambda_{1,1}}{\pi} = 1.21966989\ldots, \tag{8.43}$$

compared to $u = 1$ for the rectangular aperture. The normalized array factors for the uniformly illuminated rectangular and circular apertures are illustrated along a principal plane in Figure 67.

Two examples are considered. The first example is based on the truncated Taylor receive array with the *nearly* circular aperture illustrated in Figure 49, and one-way receive array factor illustrated in Figure 50. The one-way transmit array factor of the nearly circular array is plotted in Figure 68, when the transmit illumination is uniform. The first sidelobe is nearly –18 dB from the main peak. When this uniform circular array factor is used with the Taylor receive array, the two-way pattern plotted in Figure 69 is obtained. The parameters of the receive array are $N_{row} = N_{col} = 50$, $SLL = -45$ dB, $\bar{n} = 5$, with the aperture truncated to a nearly circular array at $w_{n,m} \le -12$ dB. The first sidelobe in the two-way pattern is about -36 dB below the peak, and the next large sidelobe is about -60 dB down. Notice that the first sidelobe of the transmit pattern is within the main lobe of the receiver pattern.

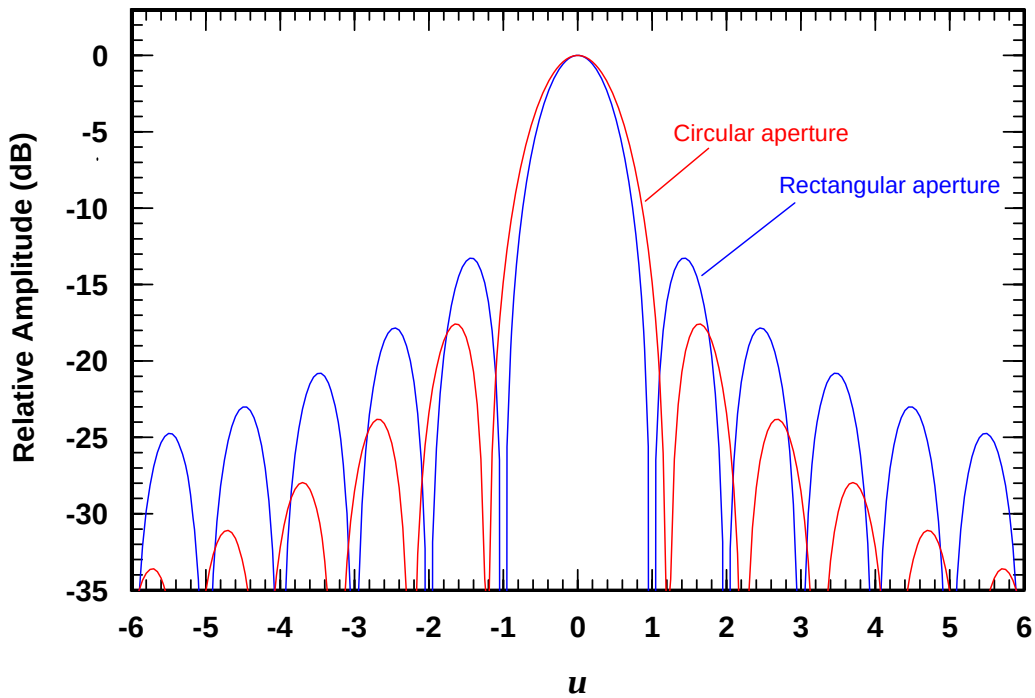

Figure 67 Comparison of normalized array factor for uniform illumination in full rectangular aperture and circular apertures (along a primary axis of the array).

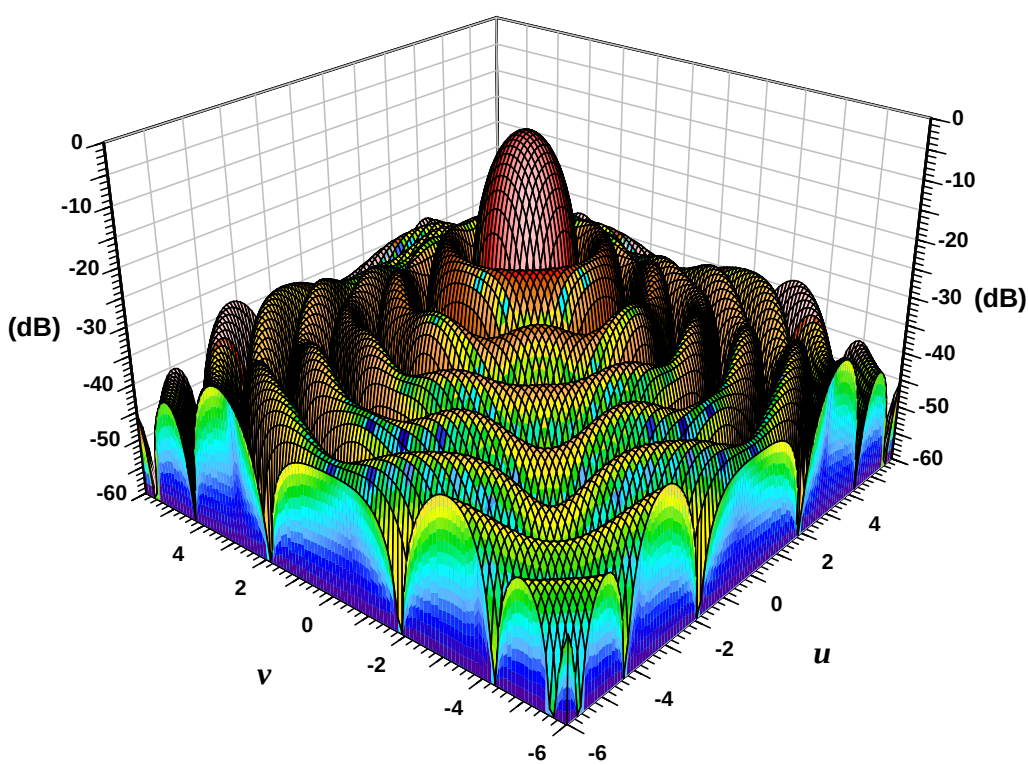

Figure 68 Normalized array factor for a two-dimensional odd array with a uniform illumination in a truncated, nearly circular aperture corresponding to the example in Figure 49.

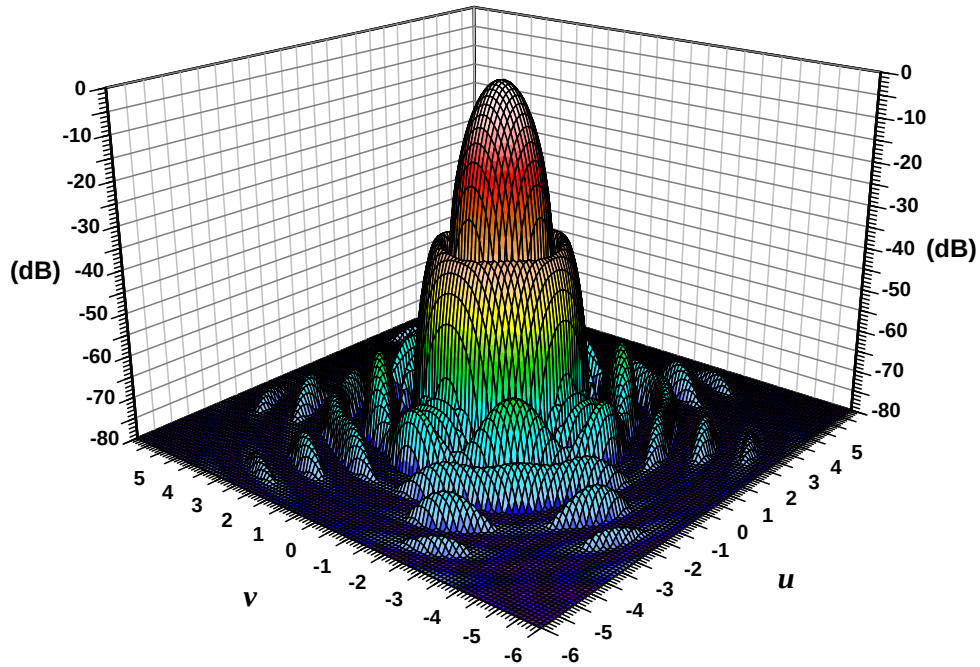

.

Figure 69 Normalized two-way array factor for a two-dimensional, odd array with a uniform illumination for transmit, and Taylor illumination for receive, $SLL = -45$ dB, $\bar{n} = 5$, *with the aperture truncated at* -12 dB *(nearly circular).*

For the second example, consider a smaller array with the Taylor parameters $N_{row} = N_{col} = 13$, $SLL = -20$ dB, $\bar{n} = 2$ for the receive array, while the transmit array is uniform. The aperture is truncated with a "circular" truncation so that

$$n^2 + m^2 \le 13^2 .$$

This is a small array, and the truncation does not really result in a circular array, as indicated in Figure 70. The two-way array factor is plotted in Figure 71. The first sidelobe in the two-way pattern is about -41 dB below the peak, and the next sidelobe is about -47 dB. This array uses only 529 out of the 729 elements contained in the full array, for a reduction of 73%.

Suppose the first lobe of the transmit array is placed at the first zero of the full Taylor receive array, before truncation. Using (8.41), (7.4), and (7.9), the design sidelobe level and Taylor order for the receive array are related by

$$SLL_{dB} \cong -20\log\left(\cosh\left(\pi\sqrt{\frac{\left(\bar{n}-\frac{1}{2}\right)^2\left(\frac{\lambda_{2,1}}{\pi}\right)^2 - \frac{1}{4}^2\bar{n}^2}{\bar{n}^2 - \left(\frac{\lambda_{2,1}}{\pi}\right)^2}}\right)\right). \tag{8.44}$$

Note that (8.44) is based on a *circular* uniform transmit array, having a radius of $N_{row} = N_{col}$ elements, and a *rectangular* Taylor receive array. When the receive array is truncated to a circular array, the first null will be moved slightly. However, the array factor for a circular Taylor array cannot be written as a simple analytic expression, so there is not an expression analogous to (8.44) when both arrays are circular. Nevertheless, the condition (8.44) will be used as a basis for the design when both arrays are truncated.

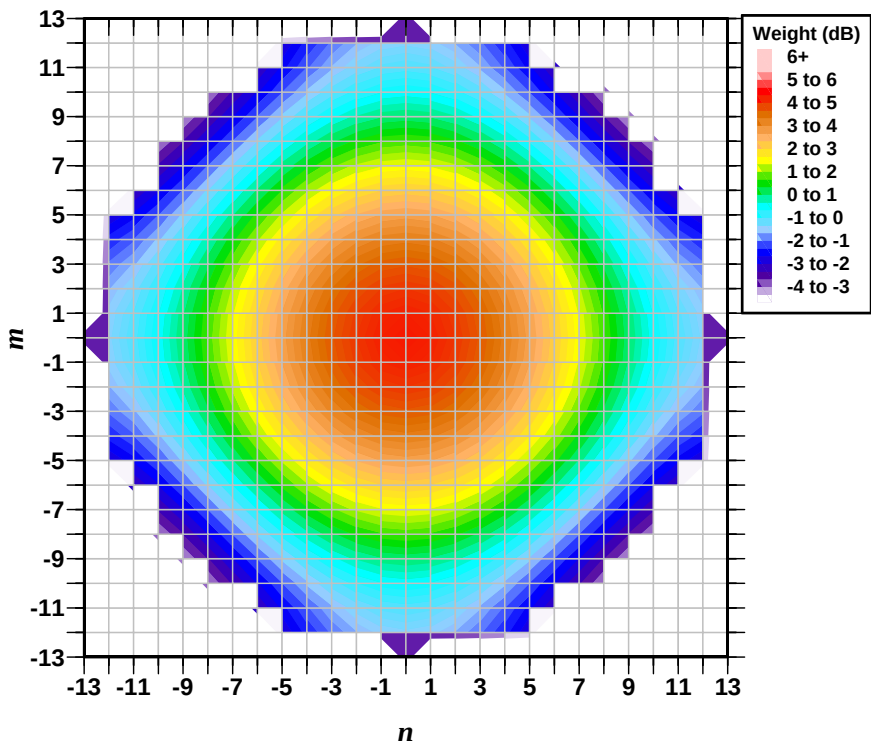

Figure 70 Weights and aperture shape for the truncated odd array with $N_{rwo} = N_{col} = 13$, $\bar{n} = 2$, *and* $SLL = -20$ dB.

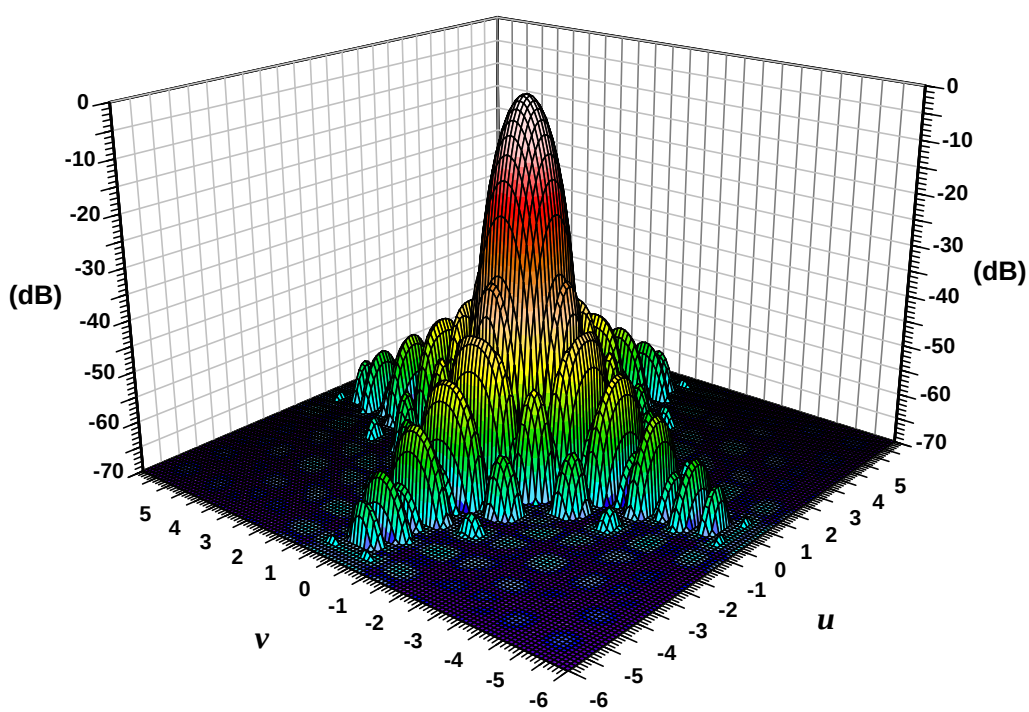

Figure 71 Normalized two-way array factor for a two-dimensional, truncated, odd array with a uniform illumination for transmit, and Taylor illumination for receive, $SLL = -20$ dB, $\bar{n} = 2$.

Table 2 shows the design sidelobe level given by (8.44) for several values of $\bar{n}$. When these values are matched to the recommended range of $\bar{n}$ and sidelobe level given in Figure 35, only one pair of parameters is seen to be appropriate. Thus, to place the first sidelobe of the uniformly illuminated transmit array into the first null of the receive array, the Taylor parameters are $\bar{n} = 4$, $SLL = -34 \text{ dB}$. The receive aperture illumination for this array is plotted in Figure 72, for $N_{row} = N_{col} = 50$. The two-way antenna pattern, assuming uniform illumination for the transmit array is plotted in Figure 73. The first sidelobe is down about -39.7 dB from the main lobe peak, and the next sidelobe is nearly -53 dB down. This array has 7845 elements out of the 10201 that would be in the full rectangular array (77% of the elements in the rectangular array).

Table 2 Taylor parameters to place the first uniform transmit sidelobe in first null of Taylor array .

$\bar{n}$	Sidelobe level (dB)
2	–47.0
3	–35.2
4	–34.0
5	–33.9

Even though the $\bar{n} = 2$, $SLL = -47 \text{ dB}$ pair of Table 2 are not within the recommended range given in Figure 35, it is still a viable design option. For example, the array is truncated to a circular aperture with a diameter of 101 elements along the two center rows, as illustrated in Figure 74. The two-way antenna pattern achieves good performance with a uniform transmit array, with a first sidelobe down by about -40 dB, and the second sidelobe at –52 dB. The two-way pattern is plotted in Figure 75. The circular array has 7845 elements, 77% of the number in the rectangular array.

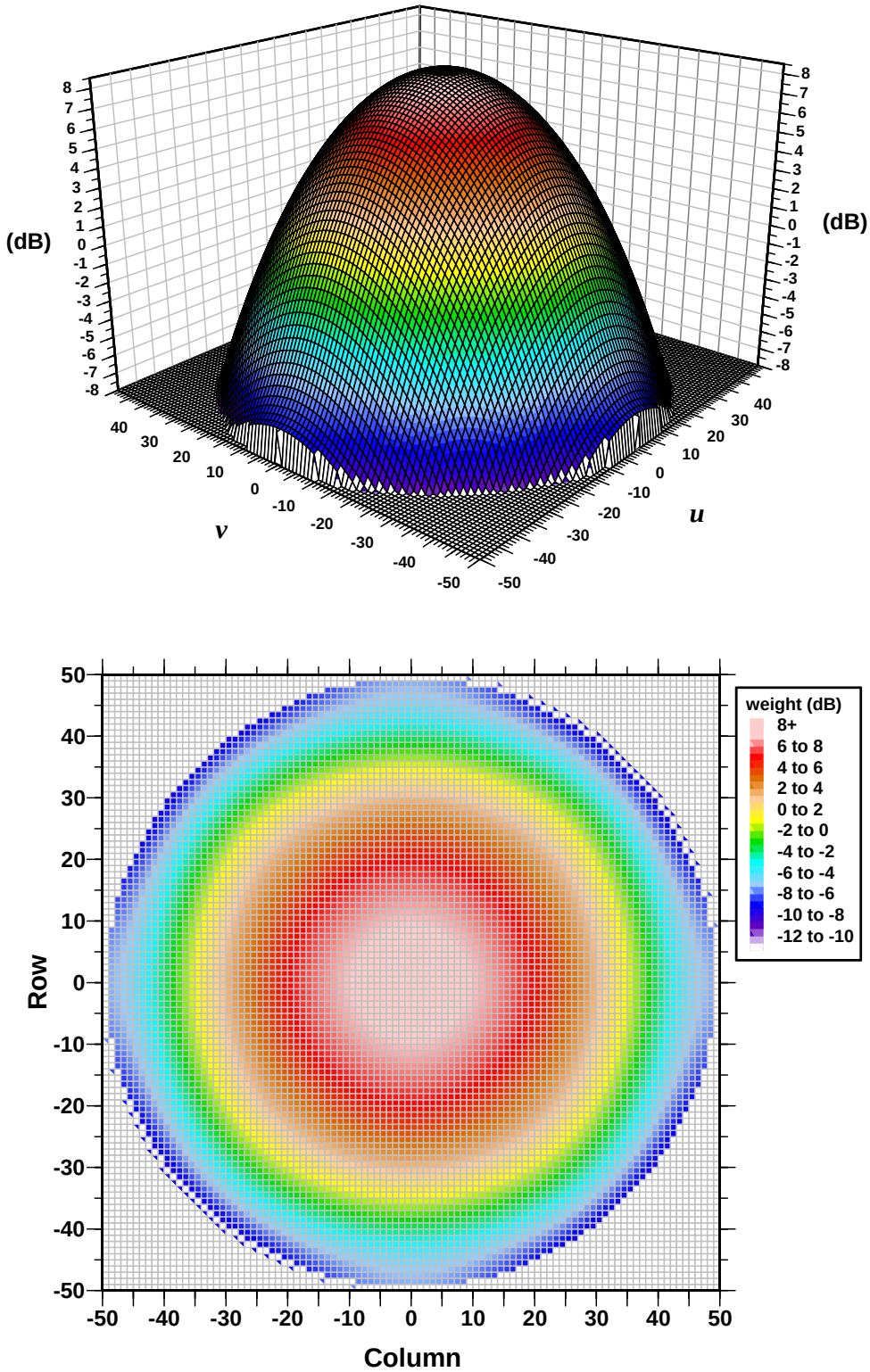

Figure 72 Weights for a two-dimensional odd array with a Taylor illumination, $SLL = -34$ dB, $\bar{n} = 4$, *truncated to a circular aperture.*

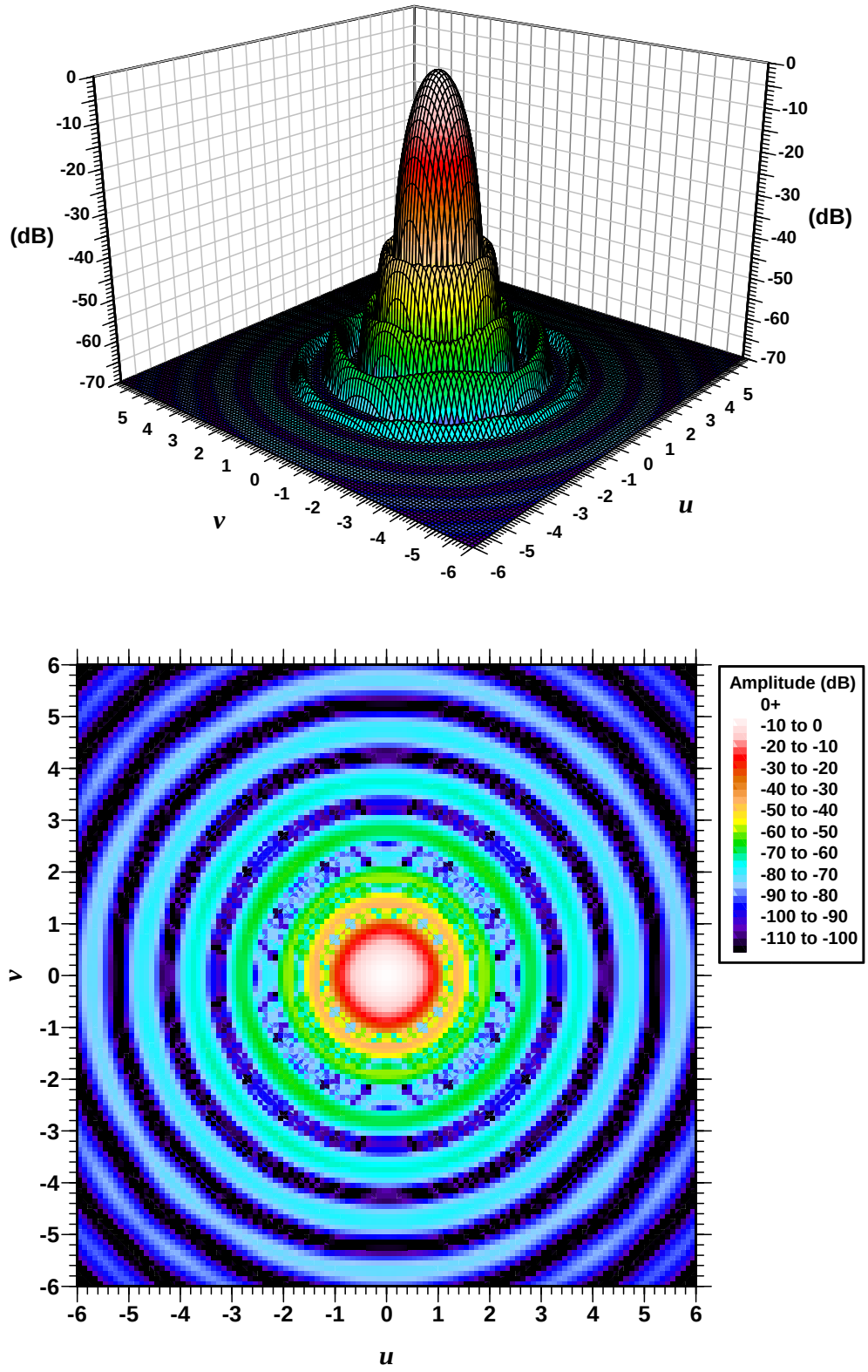

Figure 73 Normalized two-way array factor for a two-dimensional, circular, odd array with a uniform illumination for transmit, and Taylor illumination for receive, $SLL = -34$ dB , $\bar{n} = 4$.

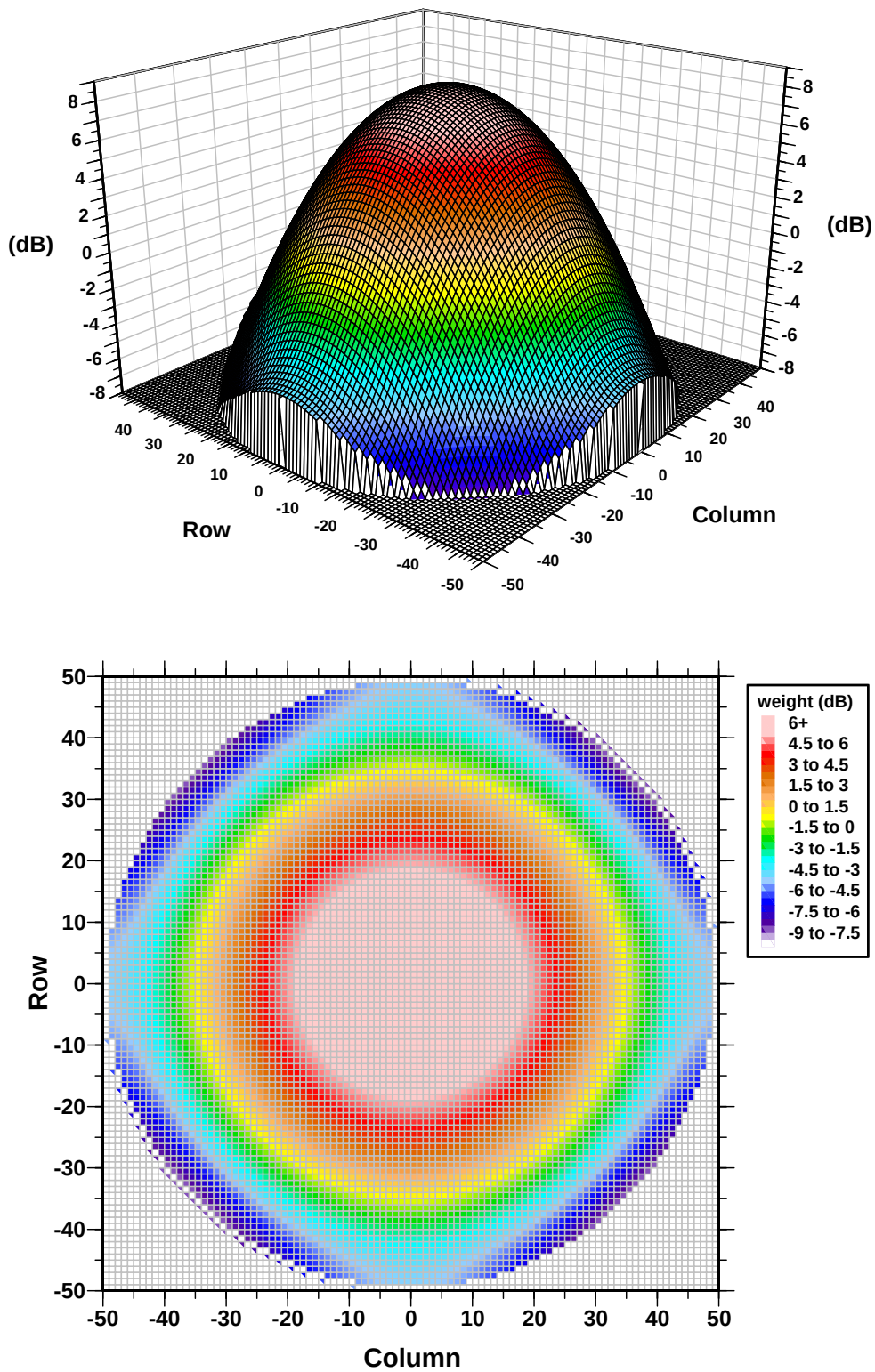

Figure 74 Weights for a two-dimensional odd array with a Taylor illumination, $SLL = -47$ dB, $\bar{n} = 2$, *truncated to a circular aperture.*

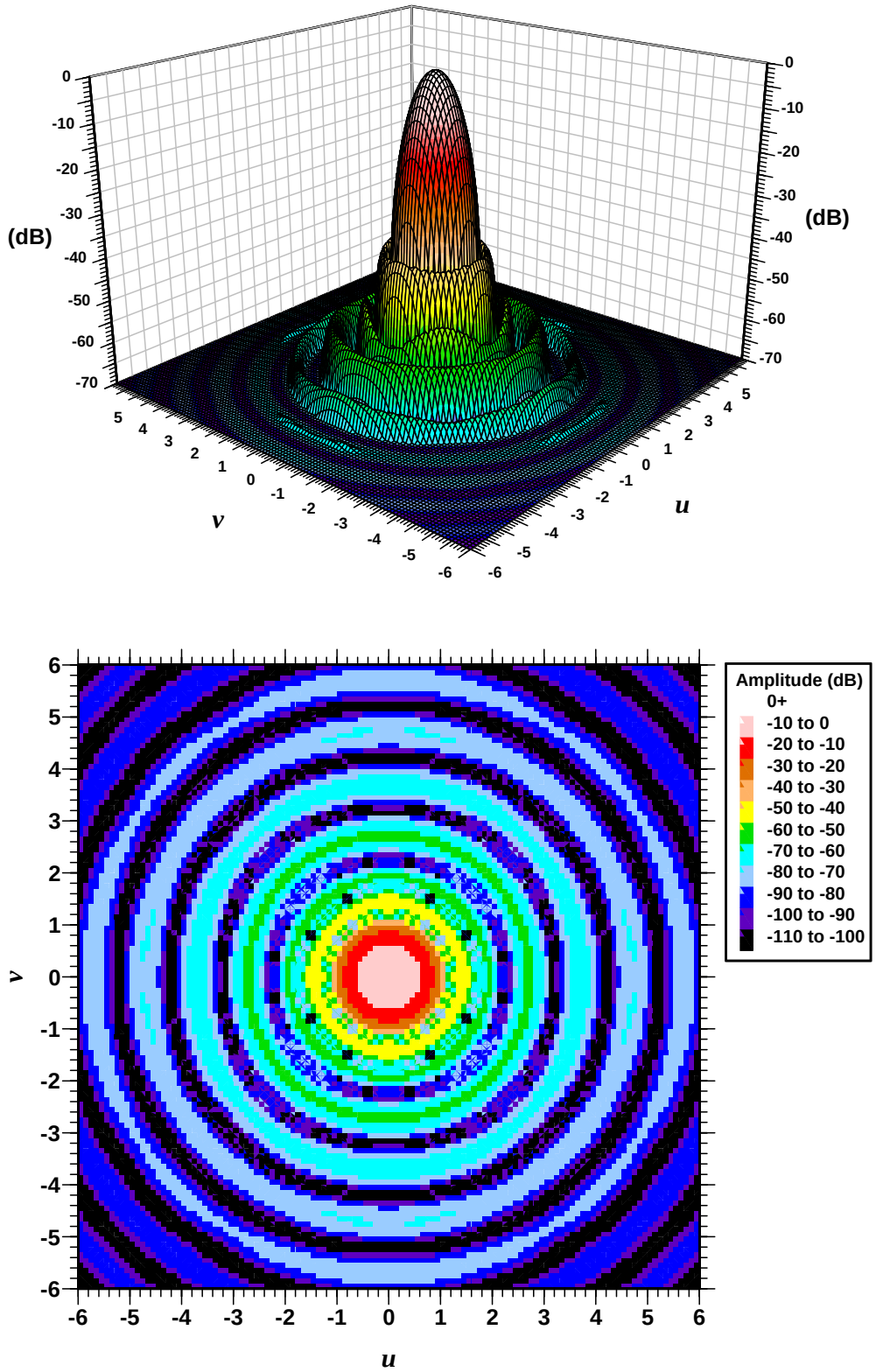

Figure 75 Normalized two-way array factor for a two-dimensional, circular, odd array with a uniform illumination for transmit, and Taylor illumination for receive, $SLL = -47$ dB, $\bar{n} = 2$.

This Page Intentionally Blank

9. References

[1] T. T. Taylor, "Design of Line-Source Antennas for Narrow Beamwidths and Low Sidelobes", *IRE Transactions on Antennas and Propagation*, AP-3, January, 1955, pp 16-28.

[2] B. C. Brock, *The Frequency Response of Phased-Array Antennas*, Sandia Laboratories Report, SAND88-2667, printed February 1989.

[3] M. Abramowitz and I. A. Stegun, ed., *Handbook of Mathematical Functions with Formulas, Graphs, and Mathematical Tables*, Dover Publications, Inc., New York, 1965, (ninth Dover printing, 1972).

[4] S. Wolfram, *Mathematica Book, 3rd edition*, Cambridge University Press, New York, 1996.

[5] G. A. Korn and T. M. Korn, *Mathematical Handbook for Scientists and Engineers*, McGraw-Hill Book Company, New York, 1968.

[6] Warren L. Stutzman, Gary A. Thiele, *Antenna Theory and Design*, John Wiley & Sons, New York, 1981.

[7] Robert S. Elliot, *Antenna Theory and Design*, Prentice-Hall, Inc., Englewood Cliffs, 1981.

[8] Ronald N. Bracewell, *The Fourier Transform and Its Applications, 2nd edition*, McGraw-Hill Book Company, New York, 1978.

[9] Armin W. Doerry, *Synthetic Aperture Radar Processing with Tiered Subapertures*, doctorial dissertation, College of Engineering, University of New Mexico, Albuquerque, May, 1995.

[10] I. S. Gradshteyn, I. M Ryzhik, *Table of Integrals, Series, and Products*, Academic Press, New York, 1965 (originally published as *Tablitsy Integralov, Summ, Ryadov I Proievedeniy*, Gosudarstvennoe Izdatel'stvo Fiziko-Matematicheskoy Literatury, Moscow, 1963.).

[11] George Arfken, *Mathematical Methods for Physicists*, Academic Press, New York, 1968.

This Page Intentionally Blank

Appendix I – Jacobi's Theta Functions

The theta functions [3, 4, 5],

$$\vartheta_n(z,q);\ n \in \{1,2,3,4\},$$

can be computed with very rapidly converging series [5]. Note that Abramowitz and Stegun [3] and *Mathematica* [4] agree on the notation for the theta function given above, but Korn and Korn [5] uses

$$\vartheta_n(\nu \mid \tau),$$

where $\nu = z/\pi$ and $q = \exp(j\pi\tau)$, so

$$\vartheta_n(z,q) = \vartheta_n(\nu \mid \tau);\ n \in \{1,2,3,4\}.$$

The theta functions are computed by

$$\vartheta_1(z,q) = 2q^{1/4}\sum_{n=0}^{\infty}(-1)^n q^{n(n+1)}\sin(2n+1)z,$$

$$\vartheta_2(z,q) = 2q^{1/4}\sum_{n=0}^{\infty} q^{n(n+1)}\cos(2n+1)z,$$

$$\vartheta_3(z,q) = 1 + 2\sum_{n=1}^{\infty} q^{n^2}\cos 2nz,$$

and

$$\vartheta_4(z,q) = 1 + 2\sum_{n=1}^{\infty}(-1)^n q^{n^2}\cos 2nz.$$

The theta functions are related to the Jacobi elliptic functions [3].

This Page Intentionally Blank

Appendix II – Directivity of the array factor

The peak directivity of an antenna is

$$D_{antenna} = 4\pi/\Omega_{antenna} \,, \tag{II-1}$$

where $\Omega_{antenna}$ is the beam solid angle [6]. The beam solid angle for a general antenna is obtained by integrating the square of the *normalized* amplitude pattern, $S(\theta,\phi)$, over all solid angles,

$$\Omega_{antenna} = \int_0^{2\pi}\int_0^{\pi} \left|S(\theta,\phi)\right|^2 \sin\theta d\theta d\phi \,. \tag{II-2}$$

For a planar array, an array factor is defined, which effectively models an array of isotropic radiators. However, it is probably more realistic to assume a semi-isotropic radiator, i.e. a radiator that radiates uniformly only into one half space. Thus, for the planar arrays considered here, the beam solid angle is redefined

$$\Omega_{array} = \int_0^{2\pi}\int_0^{\pi/2} \left|S_{array}(\theta,\phi)\right|^2 \sin\theta d\theta d\phi \,, \tag{II-3}$$

where the integration over θ stops at $\pi/2$ rather than π, and the normalized array factor is substituted for the normalized amplitude pattern. Using this definition, the array directivity pattern is

$$D(\hat{\mathbf{r}},[\xi]) \equiv \frac{4\pi}{\Omega_{array}} \left|S_{array}(\hat{\mathbf{r}},[\xi])\right|^2 \,. \tag{II-4}$$

In general, the array factor is

$$S_{array}(\hat{\mathbf{r}},[\xi]) = \sum_{n,m} A_{n,m} e^{j(\psi_{n,m}-\xi_{n,m})} \,, \tag{II-5}$$

where $A_{n,m}$ is the amplitude weight of each element, $\psi_{n,m}$ is the propagation phase term, and $\xi_{n,m}$ is the steering phase term. The details of the explicit form of the double summation depends on whether the array is an odd array or an even array, as defined in Section 5, *Two-dimensional planar array factor*.

For the odd array, the array factor is

$$S_{array} = \sum_{n=-N}^{N}\sum_{m=-M}^{M} A_{n,m} e^{j(\psi_{n,m}-\xi_{n,m})} \,, \tag{II-6}$$

where the propagation phase is

$$\psi_{n,m} = \begin{cases} 2\pi\dfrac{f}{c}\left[n\Delta x\sin\theta\cos\phi + m\Delta y\sin\theta\sin\phi\right], \; m \text{ even} \\ 2\pi\dfrac{f}{c}\left[\left(x_b - x_a + n\Delta x\right)\sin\theta\cos\phi + m\Delta y\sin\theta\sin\phi\right], \; m \text{ odd} \end{cases} \,, \tag{II-7}$$

and

$$\Delta x = \Delta x_{odd} = \frac{L_x}{2N} \,, \tag{II-8}$$

$$\Delta y = \Delta y_{odd} = \frac{L_y}{2M} \,. \tag{II-9}$$

For the even array, the array factor is

$$S_{array} = \sum_{n=1}^{N}\sum_{m=1}^{M}\left[A_{n,m}e^{j\left(\psi_{n,m}-\xi_{n,m}\right)} + A_{-n,m}e^{j\left(\psi_{-n,m}-\xi_{-n,m}\right)} + A_{n,-m}e^{j\left(\psi_{n,-m}-\xi_{n,-m}\right)} + A_{-n,-m}e^{j\left(\psi_{-n,-m}-\xi_{-n,-m}\right)}\right], \quad \text{(II-10)}$$

and the propagation phase is

$$\psi_{n,m} = \begin{cases} 2\pi\dfrac{f}{c}\left[\sin\theta\cos\phi\left(x_a + \left(n-\tfrac{1}{2}\operatorname{sgn}(n)\right)\Delta x\right) + \sin\theta\sin\phi\left(m-\tfrac{1}{2}\operatorname{sgn}(m)\right)\Delta y\right], & m \text{ even} \\ 2\pi\dfrac{f}{c}\left[\sin\theta\cos\phi\left(x_b + \left(n-\tfrac{1}{2}\operatorname{sgn}(n)\right)\Delta x\right) + \sin\theta\sin\phi\left(m-\tfrac{1}{2}\operatorname{sgn}(m)\right)\Delta y\right], & m \text{ odd} \end{cases}, \quad \text{(II-11)}$$

where the $\pm$ signs are correlated with the sign of *n* and *m* respectively, and

$$\Delta x = \Delta x_{even} = \frac{L_x}{2N-1}, \quad \text{(II-12)}$$

$$\Delta y = \Delta y_{even} = \frac{L_y}{2M-1}. \quad \text{(II-13)}$$

The excitation phase for the *n*, *m* element in the odd array is

$$\xi_{n,m} \equiv \begin{cases} n\xi_x + m\xi_y, & m \text{ even} \\ \left(\dfrac{x_b - x_a}{\Delta x} + n\right)\xi_x + m\xi_y, & m \text{ odd} \end{cases}. \quad \text{(II-14)}$$

In the even array, the excitation phase for the *n*, *m* element is

$$\xi_{n,m} = \begin{cases} \left(\dfrac{x_a}{\Delta x} + \left(n-\tfrac{1}{2}\operatorname{sgn}(n)\right)\right)\xi_x + \left(m-\tfrac{1}{2}\operatorname{sgn}(m)\right)\xi_y, & m \text{ even} \\ \left(\dfrac{x_b}{\Delta x} + \left(n-\tfrac{1}{2}\operatorname{sgn}(n)\right)\right)\xi_x + \left(m-\tfrac{1}{2}\operatorname{sgn}(m)\right)\xi_y, & m \text{ odd} \end{cases}. \quad \text{(II-15)}$$

In (II-14) and (II-15), the incremental steering phases are

$$\begin{aligned} \xi_x &= k_0\Delta x\sin\theta_\xi\cos\phi_\xi \\ \xi_y &= k_0\Delta y\sin\theta_\xi\sin\phi_\xi \end{aligned}, \quad \text{(II-16)}$$

where

$$k_0 = 2\pi\frac{f}{c}. \quad \text{(II-17)}$$

The beam solid angle for the planar array is

$$\Omega_{array} = \int_0^{2\pi}\int_0^{\pi/2}\sum_{n,m}A_{n,m}e^{j\left(\psi_{n,m}-\xi_{n,m}\right)}\sum_{n',m'}A^*_{n',m'}e^{-j\left(\psi_{n',m'}-\xi_{n',m'}\right)}\sin\theta d\theta d\phi. \quad \text{(II-18)}$$

Recall that the integration over θ stops at $\pi/2$ rather than π, because the elements are assumed to radiate into only one half space. The order of the integration and summation can be interchanged, so the integrals are of the form

$$\mathcal{I}_{n,m,n',m'} = A_{n,m}A^*_{n',m'}e^{-j\left(\xi_{n,m}-\xi_{n',m'}\right)}\int_0^{2\pi}\int_0^{\pi/2}e^{j\left(\psi_{n,m}-\psi_{n',m'}\right)}\sin\theta d\theta d\phi \quad \text{(II-19)}$$

From (II-7) and (II-11), the form of $\psi_{n,m}$ is

$$\psi_{n,m} = 2\pi \frac{f}{c}\left(\beta_{x,n}\sin\theta\cos\phi + \beta_{y,m}\sin\theta\sin\phi\right). \tag{2.20}$$

For the odd array,

$$\beta_{x,n} = \begin{cases} n\Delta x, \ m \text{ even} \\ \\ \left(x_b - x_a + n\Delta x\right), \ m \text{ odd} \end{cases}, \tag{II-21}$$

and

$$\beta_{y,m} = m\Delta y\,. \tag{II-22}$$

For the even array

$$\beta_{x,n} = \begin{cases} x_a + \left(n - \tfrac{1}{2}\operatorname{sgn}(n)\right)\Delta x, \ m \text{ even} \\ \\ \left(x_b + \left(n - \tfrac{1}{2}\operatorname{sgn}(n)\right)\Delta x\right), \ m \text{ odd} \end{cases}, \tag{II-23}$$

and

$$\beta_{y,m} = \left(m - \tfrac{1}{2}\operatorname{sgn}(m)\right)\Delta y\,. \tag{II-24}$$

Because of the offsets included to allow a triangular lattice, the values of $\beta_{x,n}$ depend on the row index, *m*, even though the dependence is not explicitly contained in the subscript.

The order of integration can be interchanged, so first consider the integration over ϕ. We have

$$\int_0^{2\pi} e^{j2\pi\frac{f}{c}\left(\left(\beta_{x,n}-\beta_{x,n'}\right)\cos\phi-\left(\beta_{y,m}-\beta_{y,m'}\right)\sin\phi\right)\sin\theta} d\phi = \int_0^{2\pi} e^{j2\pi\frac{f}{c}\sqrt{\left(\beta_{x,n}-\beta_{x,n'}\right)^2+\left(\beta_{y,m}-\beta_{y,m'}\right)^2}\sin\theta\cos\left(\phi-\alpha_{n,m,n',m'}\right)} d\phi\,, \tag{II-25}$$

where

$$\alpha_{n,m,n',m'} = \tan^{-1}\left(\frac{\left(\beta_{y,m}-\beta_{y,m'}\right)}{\left(\beta_{x,n}-\beta_{x,n'}\right)}\right). \tag{II-26}$$

Let $\varsigma = \phi - \alpha_{n,m,n',m'}$, so that $d\phi = d\varsigma$ and the interval $0 \le \phi \le 2\pi$ becomes $-\alpha_{n,m,n',m'} \le \varsigma \le 2\pi - \alpha_{n,m,n',m'}$. However, the integration is still over a full period of the integrand, and the integral can be written in closed form as [3, 11]

$$\begin{aligned}\int_0^{2\pi} e^{j2\pi\frac{f}{c}\sin\theta\left(\left(\beta_{x,n}-\beta_{x,n'}\right)\cos\phi-\left(\beta_{y,m}-\beta_{y,m'}\right)\sin\phi\right)} d\phi &= \int_0^{2\pi} e^{j2\pi\frac{f}{c}\sqrt{\left(\beta_{x,n}-\beta_{x,n'}\right)^2+\left(\beta_{y,m}-\beta_{y,m'}\right)^2}\sin\theta\cos(\varsigma)} d\varsigma \\ &= 2\pi J_0\left(2\pi\frac{f}{c}\sqrt{\left(\beta_{x,n}-\beta_{x,n'}\right)^2+\left(\beta_{y,m}-\beta_{y,m'}\right)^2}\sin\theta\right)\end{aligned} \tag{II-27}$$

In (II-27), $J_0(x)$ is the zeroth-order cylindrical Bessel's function of the first kind.

The remaining integration over θ gives (see 6.683-8 in [10])

$$\begin{aligned}\mathcal{I}_{n,m,n',m'} &= A_{n,m}A^*_{n',m'}e^{-j\left(\xi_{n,m}-\xi_{n',m'}\right)}\int_0^{\pi/2} 2\pi J_0\left(2\pi\frac{f}{c}\sqrt{\left(\beta_{x,n}-\beta_{x,n'}\right)^2+\left(\beta_{y,m}-\beta_{y,m'}\right)^2}\sin\theta\right)\sin\theta d\theta \\ &= 2\pi A_{n,m}A^*_{n',m'}e^{-j\left(\xi_{n,m}-\xi_{n',m'}\right)}\operatorname{sinc}\left(2\pi\frac{f}{c}\sqrt{\left(\beta_{x,n}-\beta_{x,n'}\right)^2+\left(\beta_{y,m}-\beta_{y,m'}\right)^2}\right)\end{aligned} \tag{2.28}$$

where

$$\operatorname{sinc}(x) \equiv \begin{cases} 1 & \text{for } x = 0 \\ \sin x / x & \text{for } x > 0 \end{cases}. \tag{2.29}$$

Thus, the beam solid angle for the planar array is

$$\Omega_{array} = 2\pi \sum_{n,m} \sum_{n',m'} e^{-j\left(\xi_{n,m} - \xi_{n',m'}\right)} A_{n,m} A_{n',m'}^{*} \operatorname{sinc}\left(2\pi \frac{f}{c} \sqrt{\left(\beta_{x,n} - \beta_{x,n'}\right)^2 + \left(\beta_{y,m} - \beta_{y,m'}\right)^2} \right). \tag{II-30}$$

For the odd array,

$$\xi_{n,m} - \xi_{n',m'} = \begin{cases} (n-n')\xi_x + (m-m')\xi_y, & m \text{ even and } m' \text{ even} \\ \left(n - n' + \dfrac{x_a - x_b}{\Delta x}\right)\xi_x + (m-m')\xi_y, & m \text{ even and } m' \text{ odd} \\ \left(n - n' - \dfrac{x_a - x_b}{\Delta x}\right)\xi_x + (m-m')\xi_y, & m \text{ odd and } m' \text{ even} \\ (n-n')\xi_x + (m-m')\xi_y, & m \text{ odd and } m' \text{ odd} \end{cases}. \tag{II-31}$$

and for the even array,

$$\xi_{n,m} - \xi_{n',m'} = \begin{cases} \left(n - n' - \dfrac{\operatorname{sgn}(n) - \operatorname{sgn}(n')}{2}\right)\xi_x + \left(m - m' - \dfrac{\operatorname{sgn}(m) - \operatorname{sgn}(m')}{2}\right)\xi_y, & m \text{ even and } m' \text{ even} \\ \left(n - n' - \dfrac{\operatorname{sgn}(n) - \operatorname{sgn}(n')}{2} + \dfrac{x_a - x_b}{\Delta x}\right)\xi_x + \left(m - m' - \dfrac{\operatorname{sgn}(m) - \operatorname{sgn}(m')}{2}\right)\xi_y, & m \text{ even and } m' \text{ odd} \\ \left(n - n' - \dfrac{\operatorname{sgn}(n) - \operatorname{sgn}(n')}{2} - \dfrac{x_a - x_b}{\Delta x}\right)\xi_x + \left(m - m' - \dfrac{\operatorname{sgn}(m) - \operatorname{sgn}(m')}{2}\right)\xi_y, & m \text{ odd and } m' \text{ even} \\ \left(n - n' - \dfrac{\operatorname{sgn}(n) - \operatorname{sgn}(n')}{2}\right)\xi_x + \left(m - m' - \dfrac{\operatorname{sgn}(m) - \operatorname{sgn}(m')}{2}\right)\xi_y, & m \text{ odd and } m' \text{ odd} \end{cases}. \tag{II-32}$$

The symmetry of the summations causes the cancellation of the imaginary part of the sum, so replacing $e^{-j\left(\xi_{n,m} - \xi_{n',m'}\right)}$ with $\cos\left(\xi_{n,m} - \xi_{n',m'}\right)$. The beam solid angle becomes

$$\Omega_{array} = 2\pi \sum_{n,m} \sum_{n',m'} A_{n,m} A_{n',m'}^{*} \cos\left(\xi_{n,m} - \xi_{n',m'}\right) \operatorname{sinc}\left(2\pi \frac{f}{c} \sqrt{\left(\beta_{x,n} - \beta_{x,n'}\right)^2 + \left(\beta_{y,m} - \beta_{y,m'}\right)^2} \right), \tag{II-33}$$

and the directivity is

$$D(\theta, \phi, [\xi]) = \frac{2\left|S_{array}\left(\hat{\mathbf{r}}, [\xi]\right)\right|^2}{\sum_{n,m} \sum_{n',m'} A_{n,m} A_{n',m'}^{*} \cos\left(\xi_{n,m} - \xi_{n',m'}\right) \operatorname{sinc}\left(2\pi \frac{f}{c} \sqrt{\left(\beta_{x,n} - \beta_{x,n'}\right)^2 + \left(\beta_{y,m} - \beta_{y,m'}\right)^2} \right)}. \tag{II-34}$$

Incorporating the explicit details of the summation,

$$\Omega_{odd\ array} = 2\pi \sum_{n=-N}^{N} \sum_{n'=-N}^{N} \sum_{m=-M}^{M} \sum_{m'=-M}^{M} A_{n,m} A_{n',m'}^{*} \cos\left(\xi_{n,m} - \xi_{n',m'}\right) \operatorname{sinc}\left(2\pi \frac{f}{c} \sqrt{\left(\beta_{x,n} - \beta_{x,n'}\right)^2 + \left(\beta_{y,m} - \beta_{y,m'}\right)^2} \right), \tag{II-35}$$

for the odd array, and

$$\Omega_{even\ array} = 2\pi \sum_{\substack{n=-N \\ n\neq 0}}^{N} \sum_{\substack{n'=-N \\ n'\neq 0}}^{N} \sum_{\substack{m=-M \\ m\neq 0}}^{M} \sum_{\substack{m'=-M \\ m'\neq 0}}^{M} A_{n,m} A_{n',m'}^{*} \cos\left(\xi_{n,m} - \xi_{n',m'}\right) \mathrm{sinc}\left(2\pi \frac{f}{c} \sqrt{\left(\beta_{x,n} - \beta_{x,n'}\right)^2 + \left(\beta_{y,m} - \beta_{y,m'}\right)^2}\right),$$

(II-36)

for the even array.

For the special case $x_a = x_b$,

$$\begin{aligned} \beta_{x,n} - \beta_{x,n'} &= \left(n - n'\right)\Delta x \\ \beta_{y,m} - \beta_{y,m'} &= \left(m - m'\right)\Delta y \\ \xi_{n,m} - \xi_{n',m'} &= \left(n - n'\right)\xi_x + \left(m - m'\right)\xi_y \end{aligned} \quad . \qquad \text{(II-37)}$$

for the odd array, and

$$\begin{aligned} \beta_{x,n} - \beta_{x,n'} &= \left(n - n' - \frac{\mathrm{sgn}\left(n\right) - \mathrm{sgn}\left(n'\right)}{2}\right)\Delta x \\ \beta_{y,m} - \beta_{y,m'} &= \left(m - m' - \frac{\mathrm{sgn}\left(m\right) - \mathrm{sgn}\left(m'\right)}{2}\right)\Delta y \\ \xi_{n,m} - \xi_{n',m'} &= \left(n - n' - \frac{\mathrm{sgn}\left(n\right) - \mathrm{sgn}\left(n'\right)}{2}\right)\xi_x + \left(m - m' - \frac{\mathrm{sgn}\left(m\right) - \mathrm{sgn}\left(m'\right)}{2}\right)\xi_y \end{aligned} \quad . \qquad \text{(II-38)}$$

for the even array. When the array is also symmetric, so that $A_{n,m} = A_{\pm n,\pm m}$, then

$$\Omega_{odd\ array} = 2\pi \sum_{n=-N}^{N} \sum_{n'=-N}^{N} \sum_{m=-M}^{M} \sum_{m'=-M}^{M} A_{n,m} A_{n',m'}^{*} \cos\left(\left(n - n'\right)\xi_x + \left(m - m'\right)\xi_y\right) \mathrm{sinc}\left(2\pi \frac{f}{c} \sqrt{\left(n - n'\right)^2 \Delta x^2 + \left(m - m'\right)^2 \Delta y^2}\right), \qquad \text{(II-39)}$$

for the odd array, and

$$\Omega_{even\ array} = 8\pi \sum_{n=1}^{N} \sum_{n'=1}^{N} \sum_{m=1}^{M} \sum_{m'=1}^{M} A_{n,m} A_{n',m'} \left(\begin{aligned} &\cos\left(\left(n - n'\right)\xi_x\right)\cos\left(\left(m - m'\right)\xi_y\right)\mathrm{sinc}\left(2\pi \frac{f}{c} \sqrt{\left(n - n'\right)^2 \Delta x^2 + \left(m - m'\right)^2 \Delta y^2}\right) \\ &+\cos\left(\left(n - n'\right)\xi_x\right)\cos\left(\left(m + m' - 1\right)\xi_y\right)\mathrm{sinc}\left(2\pi \frac{f}{c} \sqrt{\left(n - n'\right)^2 \Delta x^2 + \left(m + m' - 1\right)^2 \Delta y^2}\right) \\ &+\cos\left(\left(n + n' - 1\right)\xi_x\right)\cos\left(\left(m - m'\right)\xi_y\right)\mathrm{sinc}\left(2\pi \frac{f}{c} \sqrt{\left(n + n' - 1\right)^2 \Delta x^2 + \left(m - m'\right)^2 \Delta y^2}\right) \\ &+\cos\left(\left(n + n' - 1\right)\xi_x\right)\cos\left(\left(m + m' - 1\right)\xi_y\right)\mathrm{sinc}\left(2\pi \frac{f}{c} \sqrt{\left(n + n' - 1\right)^2 \Delta x^2 + \left(m + m' - 1\right)^2 \Delta y^2}\right) \end{aligned}\right) \qquad \text{(II-40)}$$

for the even array.

This Page Intentionally Blank

Appendix III – Definition of beamwidth for off-normal scan

It is commonplace to measure the beamwidth of an antenna in two orthogonal planes. For example, when the antenna boresight is aligned with the $\hat{\mathbf{z}}$ axis, a common choice is to measure the beamwidth in the $\hat{\mathbf{x}},\hat{\mathbf{z}}$ plane and the $\hat{\mathbf{y}},\hat{\mathbf{z}}$ plane. These two planes correspond to the $\hat{\mathbf{r}},\hat{\boldsymbol{\theta}}$ and $\hat{\mathbf{r}},\hat{\boldsymbol{\phi}}$ planes, respectively, when $\theta=\phi=0$. When the antenna is a phased array, the main lobe of the radiation pattern is steered away from the normal to the array ($\hat{\mathbf{z}}$ axis), and the question of how to define the planes for defining the beamwidth arises. The definition and procedure described here is a logical generalization of the beamwidth definition for a fixed-beam antenna.

Consider a phased-array antenna with the beam steered in direction $\hat{\mathbf{r}}_\xi$, defined by the spherical angles θ_ξ and ϕ_ξ, as illustrated in Figure 76. The following vectors, illustrated in Figure 76, can be defined

$$\vec{\mathbf{r}}_{+\theta}=\hat{\mathbf{r}}_\xi+\hat{\boldsymbol{\theta}}\delta_{+\theta}, \tag{2.41}$$

$$\vec{\mathbf{r}}_{-\theta}=\hat{\mathbf{r}}_\xi-\hat{\boldsymbol{\theta}}\delta_{-\theta}, \tag{2.42}$$

$$\vec{\mathbf{r}}_{+\phi}=\hat{\mathbf{r}}_\xi+\hat{\boldsymbol{\phi}}\delta_{+\phi}, \tag{2.43}$$

and

$$\vec{\mathbf{r}}_{-\phi}=\hat{\mathbf{r}}_\xi-\hat{\boldsymbol{\phi}}\delta_{-\phi}. \tag{2.44}$$

The unit vectors in (2.41) through (2.44) are

$$\hat{\mathbf{r}}_\xi=\hat{\mathbf{x}}\sin\theta_\xi\cos\phi_\xi+\hat{\mathbf{y}}\sin\theta_\xi\sin\phi_\xi+\hat{\mathbf{z}}\cos\theta_\xi, \tag{2.45}$$

$$\hat{\boldsymbol{\theta}}=\hat{\mathbf{x}}\cos\theta_\xi\cos\phi_\xi+\hat{\mathbf{y}}\cos\theta_\xi\sin\phi_\xi-\hat{\mathbf{z}}\sin\theta_\xi, \tag{2.46}$$

and

$$\hat{\boldsymbol{\phi}}=-\hat{\mathbf{x}}\sin\phi_\xi+\hat{\mathbf{y}}\cos\phi_\xi. \tag{2.47}$$

Clearly, $\vec{\mathbf{r}}_{\pm\theta}$, $\left(\vec{\mathbf{r}}_{+\theta}-\vec{\mathbf{r}}_{-\theta}\right)$, and $\hat{\mathbf{r}}_\xi$ lie in one plane, and $\vec{\mathbf{r}}_{\pm\phi}$, $\left(\vec{\mathbf{r}}_{+\phi}-\vec{\mathbf{r}}_{-\phi}\right)$, and $\hat{\mathbf{r}}_\xi$ lie in a second plane. Since

$$\left(\vec{\mathbf{r}}_{+\theta}-\vec{\mathbf{r}}_{-\theta}\right)\cdot\left(\vec{\mathbf{r}}_{+\phi}-\vec{\mathbf{r}}_{-\phi}\right)=\left(\delta_{+\theta}+\delta_{-\theta}\right)\left(\delta_{+\phi}+\delta_{-\phi}\right)\hat{\boldsymbol{\theta}}\cdot\hat{\boldsymbol{\phi}}=0,$$

it is clear that the two planes are orthogonal. These two planes are ideal for measuring the beamwidth. Conveniently, they coincide with the $\hat{\mathbf{x}},\hat{\mathbf{z}}$ plane and the $\hat{\mathbf{y}},\hat{\mathbf{z}}$ plane respectively, when $\theta=\phi=0$.

Once the definition of the beamwidth (3-dB points, first nulls, etc.) has been chosen, it is simply a matter of determining $\delta_{\pm\theta}$ and $\delta_{\pm\phi}$ such that the following unit vectors point in the direction of the appropriate value on the beam,

$$\hat{\vec{\mathbf{r}}}_{\pm\theta}=\frac{\hat{\mathbf{r}}_\xi\pm\hat{\boldsymbol{\theta}}\delta_{\pm\theta}}{\sqrt{1+\delta_{\pm\theta}^2}}, \tag{2.48}$$

and

$$\hat{\mathbf{r}}_{\pm\phi} = \frac{\hat{\mathbf{r}}_{\xi} \pm \hat{\boldsymbol{\theta}}\delta_{\pm\phi}}{\sqrt{1+\delta_{\pm\phi}^2}} . \tag{2.49}$$

Since the antenna pattern is usually given as a function of the spherical angles θ, ϕ, the variables $\delta_{\pm\theta}$ and $\delta_{\pm\phi}$ provide a simple parameterization for the spherical angles locating the beam edges in each plane

$$\theta\left(\delta_{\pm\theta}\right) = \cos^{-1}\left(\hat{\mathbf{z}} \cdot \hat{\mathbf{r}}_{\pm\theta}\right) \text{ and } \phi\left(\delta_{\pm\theta}\right) = \tan^{-1}\left(\frac{\hat{\mathbf{y}} \cdot \hat{\mathbf{r}}_{\pm\theta}}{\hat{\mathbf{x}} \cdot \hat{\mathbf{r}}_{\pm\theta}}\right), \tag{2.50}$$

and

$$\theta\left(\delta_{\pm\phi}\right) = \cos^{-1}\left(\hat{\mathbf{z}} \cdot \hat{\mathbf{r}}_{\pm\phi}\right) \text{ and } \phi\left(\delta_{\pm\phi}\right) = \tan^{-1}\left(\frac{\hat{\mathbf{y}} \cdot \hat{\mathbf{r}}_{\pm\phi}}{\hat{\mathbf{x}} \cdot \hat{\mathbf{r}}_{\pm\phi}}\right), \tag{2.51}$$

which satisfy the beamwidth definition.

An iterative method can be applied to search over the simple parameters $\delta_{\pm\theta}$ and $\delta_{\pm\phi}$ to locate the appropriate edges of the beam in the two planes, and thus determine $\hat{\vec{\mathbf{r}}}_{\pm\theta}$ and $\hat{\vec{\mathbf{r}}}_{\pm\phi}$. The beamwidth in the $\hat{\mathbf{r}}_{\xi}, \hat{\boldsymbol{\theta}}$ plane is

$$BW_{\theta} = \cos^{-1}\left(\hat{\mathbf{r}}_{\xi} \cdot \hat{\mathbf{r}}_{+\theta}\right) - \cos^{-1}\left(\hat{\mathbf{r}}_{\xi} \cdot \hat{\mathbf{r}}_{-\theta}\right), \tag{2.52}$$

and in the $\hat{\mathbf{r}}_{\xi}, \hat{\boldsymbol{\phi}}$ plane is

$$BW_{\phi} = \cos^{-1}\left(\hat{\mathbf{r}}_{\xi} \cdot \hat{\mathbf{r}}_{+\phi}\right) - \cos^{-1}\left(\hat{\mathbf{r}}_{\xi} \cdot \hat{\mathbf{r}}_{-\phi}\right). \tag{2.53}$$

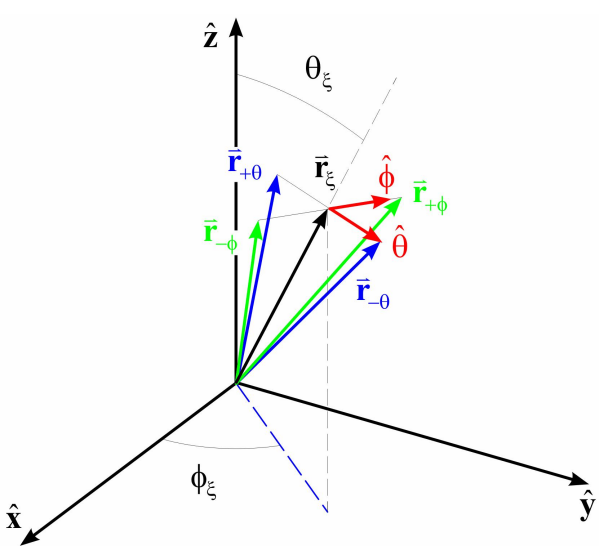

Figure 76 Diagram showing the planes in which the beamwidth can be measured when the beam is scanned away from the normal vector.

This Page Intentionally Blank

Distribution

1	MS 1330	S. C. Holswade	5340	
1	MS 1330	A. W. Doerry	5344	
1	MS 1330	W. H. Hensley	5344	
1	MS 1330	K. W. Sorensen	5345	
1	MS 1332	B. L. Burns	5340	
1	MS 0529	S. E. Allen	5345	
1	MS 0529	K. Coperich Branch	5345	
5	MS 0529	B. C. Brock	5345	
1	MS 0529	G. K. Froehlich	5345	
1	MS 0529	H. Loui	5345	
1	MS 0529	T. V. Satterthwait	5345	
1	MS 0529	M. D. Sena	5345	
1	MS 1330	G. R. Sloan	5345	
1	MS 0529	B. Strassner	5345	
1	MS 0529	M. B. Murphy	5356	
1	MS 0529	C. W. Ottesen	5356	
1	MS 0529	W. E. Patitz	5345	
1	MS 0519	L. M. Wells	5354	
1	MS 0519	D. L. Bickel	5354	
1	MS 0899	Technical Library	9536	(electronic copy)